Civil Engineering ETDs   Engineering ETDs

2-9-2010

Optimal sensor placement in structural health monitoring (SHM) with a field application on a RC bridge

Mohammad Azarbayejani

Follow this and additional works at: https://digitalrepository.unm.edu/ce_etds

www.manaraa.com

Mohammad Azarbayejani
Candidate

Civil Engineering
Department

This dissertation is approved, and it is acceptable in quality
and form for publication:

Approved by the Dissertation Committee:

_____ Reda 09/30/09 _____ , Chairperson

_____ 9/30/2009 _____

_____ 09/30/2009 _____

_____ 09/30/2009 _____

_____ 9/30/09 _____

_____

_____

_____

OPTIMAL SENSOR PLACEMENT IN STRUCTURAL HEALTH MONITORING (SHM) WITH A FIELD APPLICATION ON A RC BRIDGE

BY

MOHAMMAD AZARBAYEJANI

B.S., Civil Engineering, University of Tehran, IRAN, 2002
M.S., Civil (Structural) Engineering, University of Tehran, IRAN, 2005

DISSERTATION

Submitted in Partial Fulfillment of the
Requirements for the Degree of

Doctor of Philosophy

Engineering

The University of New Mexico
Albuquerque, New Mexico

December, 2009

iii

DEDICATION

This dissertation is dedicated to my mother (Tayebeh) and my father (Abbasali).

iv

ACKNOWLEDGMENTS

OPTIMAL SENSOR PLACEMENT IN STRUCTURAL HEALTH MONITORING (SHM) WITH A FIELD APPLICATION ON A RC BRIDGE

BY

MOHAMMAD AZARBAYEJANI

ABSTRACT OF DISSERTATION

Submitted in Partial Fulfillment of the
Requirements for the Degree of

Doctor of Philosophy

Engineering

The University of New Mexico
Albuquerque, New Mexico

December, 2009

OPTIMAL SENSOR PLACEMENT IN STRUCTURAL HEALTH MONITORING (SHM) WITH A FIELD APPLICATION ON A RC BRIDGE

by

Mohammad Azarbayejani

B.S., Civil Engineering, University of Tehran, IRAN, 2002
M.S., Civil (Structural) Engineering, University of Tehran, IRAN, 2005
Ph.D., Engineering, University of New Mexico, 2009

ABSTRACT

Structural health monitoring (SHM) is a research field that targets detecting and locating damage in structures. The main objective of SHM is to detect damage at its onset and inform authorities about the type, nature and location of the damage in the structure. Successful SHM requires deploying optimal sensor networks. We present a probabilistic approach to identify optimal location of sensors based on *a priori* knowledge on damage locations while considering the need for redundancy in sensor networks. The optimal number of sensors is identified using a multi-objective optimization approach incorporating information entropy and cost of the sensor network. As the size of the structure grows, the advantage of the optimal sensor network in damage detection becomes obvious.

We also present an innovative field application of SHM using Field Programmable Gate Array (FPGA) and wireless communication technologies. The new SHM system was

installed to monitor a reinforced concrete (RC) bridge on interstate I-40 in Tucumcari, New Mexico. The new monitoring system is powered with renewable solar energy. The integration of FPGA and photovoltaic technologies make it possible to remotely monitor infrastructure with limited access to power. Using calibrated finite element (FE) model of the bridge with real data collected from the sensors installed on the bridge, we establish fuzzy sets describing different damage states of the bridge. Unknown states of the bridge performance are then identified using degree of similarity between these fuzzy sets. The proposed SHM system will reduce human intervention significantly and can save millions of dollars currently spent on prescheduled inspection by enabling performance based monitoring.

Preface

This dissertation is the result of research conducted during August 2005 – September 2009 in the Department of Civil Engineering at University of New Mexico.

Azarbayejani, M., El-Osery, A., Reda Taha, M. M. (2009). "Entropy-based optimal sensor networks for structural health monitoring of a cable-stayed bridge", *Smart Structures and Systems*, 5 (4) : 369-379.

Azarbayejani, M., El-Osery, A., Choi, K. –K, Reda Taha, M. M. (2008). "Probabilistic approach for optimal sensor allocation in structural health monitoring", *Smart Materials and Structures*, 17 (5), paper # 055019, 2008.

Azarbayejani, M., Reda Taha, M. M., Ross, T. J. (2008). "An inductive fuzzy damage classification approach for structural health monitoring", *International Journal of Materials and Structural Integrity*, 2 (3) : 193-206.

Azarbayejani, M., Foley, E., El-Osery, A., Reda Taha, M. M. (2009). "Structural health monitoring of a prototype bridge", *CD Proc. of SEM Annual Conference and Exposition on Experimental and Applied Mechanics*, Albuquerque, New Mexico.

Azarbayejani, M., Reda Taha, M. M. (2008). "Optimal sensor placement on a long cable-stayed bridge", *Proc. of 5th ASCE International Engineering and Construction Conference (IECC'5),* Irvine, CA, pp. 907-914.

Azarbayejani, M., Reda Taha, M. M., Ross, T. J. (2007). "An inductive reasoning approach for fuzzy damage detection in structures", *Proc. of the 12th International Colloquium on Structural and Geotechnical Engineering*, Cairo, Egypt.

Azarbayejani, M., El-Osery, A., Choi, K. –K, Reda Taha, M. M. (2007). "Optimal sensor placement for efficient structural health monitoring", *Proc. of International Workshop on Structural Health Monitoring*, Stanford, USA, Chang, Fu-Kuo, Ed., pp. 451-458.

TABLE OF CONTENTS

LIST OF FIGURES

xiv

xvii

xviii

LIST OF TABLES

CHAPTER 1 INTRODUCTION

1.1 Introduction

A recent report in *USA Today* (July 25, 2008) shared with the public the current state of the nation's infrastructure. *USA Today*'s report stated "*Billions needed to shore up bridges*". The current status of the nation's infrastructure reflects the need for reliable and efficient monitoring strategies and techniques. Deploying efficient monitoring systems on bridges can provide early warning about potential damage. Moreover, continuous monitoring of bridges and critical infrastructure may enable us to move from the current schedule-based maintenance to condition-based maintenance. This should save millions of dollars and allow for the focusing of resources. Furthermore, by using new advances in sensing technology and wireless communication systems, remote monitoring of the nation's infrastructure will become a reality.

Structural health monitoring (SHM) is the field of study that targets detecting and locating damage in structures. The main aim of SHM is to enhance safety and reliability in mechanical, civil and aerospace infrastructure by recognizing damage before it becomes perilous. SHM is divided into four main subjects: <u>data acquisition</u> including identifying effective sensor type and network, <u>damage feature extraction</u>, which aims at selecting a feature that is sensitive to presence of damage based on sensor observations, <u>statistical modeling and pattern recognition</u> that allows the realization of damage severity

1

based on known healthy performance (reference) and damage conditions, and finally <u>damage prognosis</u> where the remaining life of the structure can be estimated. In the past decade, most research efforts were directed to damage feature extraction through signal processing, while little effort had been directed toward designing sensor networks.

Deploying different kinds of sensors including accelerometers, strain gages, fiber optic sensors and piezoelectric sensors, etc., most current SHM systems measure the dynamic response of structures. Vibration-based SHM is developed with the assumption that if stiffness reduction of the structure takes place as a result of damage occurrence, the vibration response of the structure will be significantly altered. Structural dynamic signals can be used to compute damage metrics such as energy of signals, mode shapes, curvature of mode shapes and natural frequency components in time domain, frequency domain or wavelet domain. Using proper domain for different damage metrics, researchers have shown that one can differentiate between healthy and damage status of bridges. The damage state of the structure can then be identified by considering theory of probability or other information theories for classifying these damage features. The use of reference performance to classify the structural health proved helpful to determine the need for maintenance or repair of bridges.

Advances in sensing technology have enabled the use of large numbers of sensors for structural health monitoring; therefore, designing efficient sensor networks becomes necessary. Design of the sensor network includes identifying the number, location and types of sensors. Moreover, reliability, economy, robustness and redundancy of the sensor network are major requirements that should be taken into account. An efficient sensor network should help detecting all possible damages and their locations in a

2

reliable and economical manner and should maintain system stability and effectiveness if one or more sensors in the network fail. Due to uncertainties that exist in damage locations and damage severities, finding a robust sensor network that can provide useful information to identify possible damage locations and severities of damage is a challenging task.

Most of previous methods in the literature relied heavily on theoretical frameworks and did not address critical issues such as sensor network robustness. These methods also relied heavily on assumptions directly related to the damage feature used for detecting damage. For example, many methods depend on detecting damage using mode shape changes. This limits the usefulness of these methods if such damage feature can not be used for detecting damage in other structures.

1.2 Dissertation Contributions

This dissertation introduces three major contributions to existing SHM knowledge:

(1) A methodology to identify optimal locations of a given number of sensors for sensor networks using probabilistic assumptions is introduced. The proposed method also considers redundancy in sensor networks that will result in designing robust sensor networks. The efficiency of the proposed method is examined based on the definition of probability of detection (POD) and is verified by example implementation of a prestressed concrete bridge.

(2) Using principles of information entropy along with probabilistic assumptions, an innovative method is introduced to identify the optimal number and location of sensors in any sensor network. Redundancy of the sensor network to achieve network robustness is

also included. The proposed method is based on solving a multi-objective optimization problem with different constraints. The efficiency of the proposed method in enhancing the damage detection process is examined and verified on a cable-stayed bridge passing over the Mississippi River. As the size of the structure grows, the advantage of the proposed method becomes obvious.

(3) Finally, a field implementation of Field Programmable Gate Array (FPGA) technology for monitoring the performance of a reinforced concrete (RC) bridge at Interstate 40 (I-40) near the city of Tucumcari, New Mexico is developed and presented. Integrating this technology with wireless communication, a robust and effective SHM system was designed and installed. The new SHM system allows continuous remote monitoring of a critical infrastructure that is 200 miles away from the monitoring office. Moreover, using solar panels as a power supplier for the SHM system, the system can be deployed on infrastructure with limited access to sources of power. By implementing such a SHM system on any aged infrastructure, artificial intelligence can be added to the monitoring systems that will reduce the human intervention. This automation process not only can save millions of dollars currently spend on prescheduled inspection, but will also lead to performance based monitoring.

1.3 Dissertation Layout

After the introduction chapter, Chapter 2 presents a literature review on SHM systems. Work done by different researchers in different categories of SHM is discussed. The necessity of the investigation made in this dissertation is also presented.

In Chapter 3, a method to identify the optimal sensor network is presented. This method determines the optimal location of a given number of sensors to enhance the damage detection process. The proposed method is based on a probabilistic approach to identify the optimal sensor network. We establish the probability distribution functions (PDFs) that describe the importance of each sensor. These PDFs are established based on the weights extracted from training an artificial neural network (ANN). To evaluate a sensor network, the probability of detection (POD) is evaluated. Furthermore, an approach based on leave one sensor out analysis is introduced to evaluate sensor network redundancy. A prestressed concrete bridge is chosen as a case study and the optimal sensor network is determined and the network ability to identify damage is evaluated.

In Chapter 4, an entropy-based method to find the optimal number of sensors using information entropy is introduced. A case study using the Luling Bridge, a cable-stayed bridge over the Mississippi River, demonstrates the ability of the proposed method to successfully identify the optimal number and location of sensors necessary to effectively monitor the bridge. An entropy-based probabilistic method can address the uncertainties existing in sensor allocation without the need to prior assumptions on the damage feature. The proposed methodology and approach paves the road for design of robust sensor networks for efficient SHM. While in Chapter 3, the optimal location of sensors for any given number of sensors is identified, in this chapter both the optimal number and location of sensors are identified. This extension allows implementation of optimal sensor network on medium and long-span bridges.

In Chapter 5, an innovative SHM system using FPGA technology with minimum human intervention is described. The SHM system was calibrated on a model bridge in

5

the SHM laboratory at the University of New Mexico (UNM). The SHM system was then installed and tested to monitor a RC bridge on I-40 passing through the City of Tucumcari in New Mexico. The system operates wirelessly and is powered with a solar system. System efficiency to detect damage is verified.

Finally, in Chapter 6, the conclusions of this work are summarized and recommendations for future work are suggested.

CHAPTER 2 LITERATURE REVIEW

2.1 Introduction

Structural health monitoring (SHM) is the term used to describe the technical activities necessary to keep an eye on infrastructures. SHM incorporates the necessary work to deploy sensors on the structures and to communicate and analyze data acquired by these sensors to detect damage and provide reliable and efficient strategies for structural maintenance and repair. In the past three decades, many researchers have examined aspects of SHM. These efforts originated from the need to lengthen the service life of critical infrastructure such as bridges, dams, pipelines, airplanes and space shuttles by providing efficient means of maintenance. Safety and reliability of these structures were examined to realize that how long these structures can stay in service. Many recent reports examine the status of the nation's infrastructure and the subsequent need for investment upgrades to the current system. An article in USA Today (July 25, 2008) stated, "*Billions needed to shore up bridges*". This cost covers not only the shoring up of bridges, but also includes keeping a watchful eye on bridges with degrading performance, thereby helping the U.S. Departments of Transportation (DOTs) to make efficient decisions on future maintenance, repair or full replacement of the nation's bridge infrastructure. Mufti (2004) indicated that only in the United States, there are more than

7

200,000 deficient bridges that are needed to be taken care of immediately due to inadequate maintenance, excessive loading in addition to natural and man made adverse environmental conditions. A similar estimate was also given by Wang et al. (1997) who indicated that Federal Highway Administration (FHWA) estimated that almost 35% of all bridges in the United States (236,000 out of 576,000) are either structurally or functionally deficient. In this regard, Helmicki et al. (1999) stated that the U.S. DOT needs around $100 billion for bridge repair and concluded the great opportunities to implement SHM systems to civil infrastructures are now open for researchers. It became obvious to the public that if simple monitoring system was installed on I-35 Bridge in Minneapolis, the significance of the disaster of total failure of this bridge would have been lessened or prevented.

Deploying efficient SHM systems on bridges can provide early warning about potential damage. Moreover, continuous monitoring of bridges might enable the DOTs to move from the current classical schedule-based maintenance to condition-based maintenance where maintenance is tied to structural performance which can result in saving millions of dollars (Adams 2007). On the other hand, a great number of civil infrastructures under construction can incorporate SHM systems. During its construction, Li et al. (2006) implemented a SHM system on a cable-stayed bridge in Shandong Province in China called Binzhou Yellow River Highway Bridge. The system consists of a sensor module, a data acquisition module, a wired and wireless data transmitted module, a structural analysis module, a database module and a warning module. Such system can monitor the structure from its birth to observe its degradation.

The basic components of SHM include data acquisition, data processing, damage detection, damage pattern recognition and structural prognosis to evaluate the remaining structural life. One important aspect in data processing is the need for efficient signal de-noising technique. While many researchers have described SHM systems in the context of anomaly detection (Bukkapatnam et al. 1999, Worden and Dulieu-Barton 2004), major SHM research was focused on feature extraction and pattern recognition. A hierarchical structure of SHM systems was described by Worden and Dulieu-Barton (2004). Moreover, Farrar et al (2004) provided in-depth analysis of the status and needs for damage prognosis as an estimate of a system's remaining useful life. Essential damage prognosis research demonstrated that a critical issue to sensing and data acquisition is the need to capture response on varying length and time scales. A detailed analysis tying damage prognosis to bridge maintenance strategy has been suggested by Frangopol et al. (2004).

While defining damage is a challenging task, researchers agreed that damage cannot be measured but its influence on the structure's response might be sensed/observed (Lemaitre and Desmorat 2002). Farrar et al. (2005) defined damage as "*Intentional or unintentional changes to the boundary conditions and system connectivity, which adversely affect the current or future performance of that system.*" Other definitions of damage considering other view points including stiffness, crack growth and strain thresholds exist in the literature (Broek 1986, Worden and Dulieu-Barton 2004 and Lemaitre and Desmorat 2002).

Much effort has been done to probe damage in a structure, before it reaches a critical state. Damage reduces the structure stiffness and hence affects the performance of the

structure. Identifying a proper feature that can be observed to realize changes that occur in the structural response due to presence of damage has been the focus of most research efforts. Most current damage features rely on dynamic characteristics of the structure such as natural frequency, modes shapes, etc., because vibration characteristics demonstrate the degradation in stiffness and are relatively easy to measure in the time domain (Neild et al. 2003). Using vibration signals, it has been shown that some damage features can be identified in the frequency domain or the wavelet domain (Chang and Chen 2004 and Reda Taha et al. 2004). However, damage location detection proved to be more challenging than damage occurrence detection due to the complex interaction between the different parts of the structure and their influence on the dynamic response (Staszewski et al. 2003). The size and complexity of civil infrastructure play a major role in developing efficient SHM systems. For some structures, the measurements of interest might not be limited to strain and vibration measurements (Ansari 2004). For instance, in cable-stayed bridges, measuring force and the condition of strands are a major focus in monitoring the health of the cables. In pipeline structures, corrosion of pipelines is of major interest for its health monitoring (Thien 2006). Four important questions need to be considered in SHM: First, is there any damage existing in the structure? This issue is related to damage detection. Second, what is the level of this damage? Is the structure severely damaged or just a little damaged? Third, where are the locations of damage in the structure? Fourth and finally, how long will the structure remain intact before it requires maintenance? The fourth question addresses what is called damage prognosis.

In recent years, a change in the direction of SHM research has lead to designing smart structures. Smart structure is a term used to describe structures that can sense changes in

their environment and respond accordingly (Staszewski et al. 2003). This issue contains the integration of sensors, actuators, controllers and signal processors. The performance of smart structures basically relies on the quality of information that can be extracted from the sensed data. This quality depends on type, number and location of sensors chosen for the structure. In most cases, intuition and engineering judgment are the basis of sensor location selection (Parker et al. 2006); however, recently, analytically based judgment to identify optimal sensor networks has gained good interest (Raich and Liszkai 2003, Swann and Chattopadhyay 2005 and Guratzsch and Mahadevan 2005). The need for optimization method is associated with gathering reliable and useful information from a robust sensor network while constrained by economical issues. In the past few years, different methods have been suggested by researchers when considering sensor networks to achieve optimal sensor placement.

It should be noted that there are two types of SHM systems: <u>Active SHM</u> system that has the sensors with the capability of both emitting waves and sensing waves and <u>Passive SHM</u> system where sensors are only used for data acquisition. In passive SHM system useful information from a sensor can only be guaranteed when the signal to noise ratio is above a certain threshold. A classical classification of SHM systems is to separate between active and passive monitoring. In active monitoring, the structural response due to an active (*a priori* known) force applied to the structure is determined. Active monitoring is typically used with seismic evaluation (Adams 2007). In such case, the monitoring system tries to solve the inverse problem and determine the structural stiffness matrix. Damage can then be identified by detecting losses in the stiffness matrix elements (Zhu and Law 2007). However, the more dominant class of SHM is the passive

monitoring system where monitoring is performed to structural response under random loadings without measuring the applied load (Giurgiutiu 2007).

Chang and Markmiller (2006) introduced probability of detection (POD) as a general measurement for quantifying the reliability of a sensor network. They showed that sensor functionality, number and location of sensors, which are case dependent, can significantly influence the POD. It is important that the sensor configuration can achieve an acceptable POD. The problem was defined to determine the sensor network and validate its performance for a specific structure, whose configuration, materials and design limit loads were known. The objective was to find the sensor network that reaches the target probability of detection. A simulation model or experimental data can generate the data necessary for calibration. A composite plate was used as the case study and the method was implemented for a certain number of sensors. The locations that resulted in the maximum POD was found by using genetic algorithms (GA) (Baker 1987).

Similarly, Rus et al. (2006) established an optimization criterion for optimal sensor networks using GA and based on minimizing an objective function that was established considering the residual error between experimental data and modeling data. To establish this objective function *(f)*, a metric to describe the state of structure Φ is defined as

$$\Phi = \frac{\psi - \psi^0}{RMS(\psi^0)} \tag{2-1}$$

In this Equation ψ^0 is a measurement vector (e.g. acceleration or strain vector) for the undamaged state to help calibration of data and *RMS* is root mean square of

12

measurements and ψ is the measurement vector of synthetic damaged case. The vector of residuals (γ) is defined as

$$\gamma = \Phi^* - \Phi \qquad (2.2)$$

Where Φ and Φ^* are computed using Equation (2.1). Φ^* denotes the metric for the structural state based on experimental data and Φ denotes for the structural state based on simulation data. The objective function f can then be established as

$$f = \frac{1}{2}|\gamma|^2 = \frac{1}{2}\frac{1}{N_i}\sum_{i=1}^{N_i}\gamma_i^2 \qquad (2.3)$$

where N_i is the size of γ vector. The goal was to minimize the objective function. Then, the variation of the objective function due to damage with a magnitude of damage p (defined as damage area and extent) is calculated as

$$f_{,p} = \frac{\partial f}{\partial p} = \lim_{\Delta p \to 0}\frac{f(p,0) - f(0,0)}{\Delta p} \qquad (2.4)$$

Considering $\Delta p = p - 0$ then $\Delta p = p$. In this Equation $f(p,0)$ describes the objective function based on damage p without noise in measurements and $f(0,0)$ describes objective function for undamaged case without noise in measurements. Now, the rate of the variation of the objective function due to p can be calculated by considering second derivative as

$$f_{,pp} = \frac{\partial^2 f}{\partial p^2} = \lim_{p \to 0}\frac{f(p,0) - f(0,0)}{p^2} \qquad (2.5)$$

Similarly, the objective function can be differentiated with respect to noise effects σ_n were thus $f_{,nn}$ can be computed as

13

$$f_{,nn} = \frac{\partial^2 f}{\partial \sigma_n^2} = \lim_{\sigma_n \to 0} \frac{f(0, \sigma_n) - f(0,0)}{\sigma_n^2} \tag{2.6}$$

In both Equations (2.5) and (2.6) the variation without defect and without noise ($f_{,p}(0,0)$ and $f_{,n}(0,0)$) is assumed to be zero for being evaluated for a healthy case. Thus, the ratio between two objective functions can be calculated as

$$\frac{f^n}{f^p} \approx \frac{f_{,nn}}{f_{,pp}} \left(\frac{\sigma_n}{p} \right)^2 \tag{2.7}$$

Now the POD can be defined as the probability that the change of the objective function due to noise is less than the change of objective function due to damage and can be described as

$$POD = P(\frac{f^n}{f^p} \leq 1) \tag{2.8}$$

The optimization process targeted maximizing POD. The method was applied successfully to a steel plate under impact loads and the goal was to enhance the damage detection probability.

Parker et al. (2006) developed another optimization algorithm that used essential elements of linear, finite dimensional, time invariant dynamical systems to find the optimal locations of the sensors. In other words, while damage develops in the structure, the algorithm targeted maximizing the change in the output signal. The suggested method was applied to a wing spar structure that was 1.7 m long by 101 mm wide by 203 mm thick. The spar was modeled using shell elements with 22128 degrees of freedom (DOF). The model was reduced to 29 DOFs to be simulated on personal computer for modal

14

analysis. It is obvious that such assumption could greatly affect the simulation results. The work by Parker et al. (2006) showed the importance of considering Finite Element (FE) model resolution as a factor in the analysis. Moreover, Schulte et al. (2006) examined the use of the information content in measurement data. One method aimed at maximizing the determinant of the Fisher information matrix. The Fisher information matrix relies on the eigenvectors of the sensitivity matrix derived by work by Fritzen and Bihle (2001). The partial derivatives of the mode shapes can be used to indicate how sensitive a particular element of the mode shape ϕ_{ji} is to damage, where j represents the *j*th element in the *i*th mode shape. Damage was discussed using parameter x_l that is used to represent percentage of reduction in member stiffness matrix *ΔK* as

$$\Delta K = \sum_{l=1}^{k} K_l . \Delta x_l \tag{2.9}$$

Where *K* is the stiffness matrix, *ΔK* is the reduction in stiffness matrix due to damage. Based on Taylor series, the changes in natural frequency ω and mode shapes ϕ can be described as a function of the damage parameter (x_l)

$$\Delta\omega_i^2 = \sum_{l=1}^{k} \frac{\partial\omega_i^2}{\partial x_i}\Delta x_l \quad \text{and} \quad \Delta\phi_{ji} = \sum_{l=1}^{k} \frac{\partial\phi_{ji}}{\partial x_l}\Delta x_l \tag{2.10}$$

Now, the sensitivity matrix can be written as

15

$$S_\phi = \begin{bmatrix} \dfrac{\partial \phi_{11}}{\partial x_1} & \dfrac{\partial \phi_{11}}{\partial x_2} & \cdots & \dfrac{\partial \phi_{11}}{\partial x_k} \\ \dfrac{\partial \phi_{21}}{\partial x_1} & \dfrac{\partial \phi_{21}}{\partial x_2} & \cdots & \dfrac{\partial \phi_{21}}{\partial x_k} \\ \vdots & \vdots & \vdots & \vdots \\ \dfrac{\partial \phi_{ji}}{\partial x_1} & \dfrac{\partial \phi_{ji}}{\partial x_2} & & \dfrac{\partial \phi_{ji}}{\partial x_k} \\ \vdots & & & \\ \dfrac{\partial \phi_{nm}}{\partial x_1} & \dfrac{\partial \phi_{nm}}{\partial x_2} & \cdots & \dfrac{\partial \phi_{nm}}{\partial x_k} \end{bmatrix} \qquad (2.11)$$

The Fisher information matrix (F) can be established by considering the sensitivity matrix (S_ϕ and a diagonal covariance matrix Σ that has the variances and covariances of the measurement channels, which can be considered as $\sigma^2 I$ with σ^2 are the variances of the channel measurements and I is the identity matrix. The Fisher information matrix F can be describes as Equation (2.12)

$$F = S_\phi{}^T \Sigma^{-1} S_\phi \qquad (2.12)$$

The objective of the sensor placement in this method was to find those rows of the sensitivity matrix that maximize the Fisher information matrix determinant. The determinant maximization of the Fisher information matrix is an indicator of reduction of uncertainty. Because of the computational expenses to solve this optimization problem, a new forward-backward selection algorithm for locating sensors was used to determine the optimal sensor positions. Fisher information matrix was also used by Kwon et al. (2003). They used maximum likelihood approach as a mathematical basis formulating Fisher information matrix in terms of mode shape sensitivity with respect to structural parameters to design an optimal accelerometer layout for a two-span multi-girder bridge. Furthermore, the use of information-entropy for sensor networks was introduced by

16

Papadimitriou et al. (2000). Information entropy is a measurement of uncertainty based on probability theory. Ntotsios et al. (2006) selected the information entropy norm to measure the performance of a sensor set-up. It was argued that the information entropy norm is a measure that corresponds to uncertainty in the model parameter estimation. It was demonstrated that using the information entropy enabled comparing between sensor configurations with different number of sensors. Two empirical methods were used to identify the optimal sensor location. Both methods were implemented on a 180 m long, 13 m wide and four-span bridge located at Kavala (Greece) to identify the optimal locations of accelerometer sensors (Papadimitriou 2004 and Metallidis et al. 2003). While both methods were less computationally expensive compared to classical optimization, they did not guarantee finding an optimal sensor configuration. Nevertheless, it was shown that upper and lower bounds of the information entropy can be identified as a function of sensor numbers. Guratzsch and Mahadevan (2006) defined a methodology to design optimum sensor layout in SHM systems under uncertainty. The optimal sensor locations of SHM sensors were defined to maximize the probability of damage detection.

Numerous methods are suggested to monitor structures including monitoring structural deformations and strains. Cardini and Dewolf (2009) used strain data from a multi-girder composite steel bridge in the state of Connecticut for long-term monitoring. The strain data were collected from normal truck traffic with known loads and a finite element analysis was maid to verify the field data. Using strain data seemed to be appealing in other researchers work. Chacon et al. (2009) used strain measurements taken with conventional pre-wired gauges and compared them to a newly developed wirelessly

17

connected strain-measuring system. A hybrid steel plate girder subjected to concentrated loads at the end of an unstiffened panel to produce a typical reaction of the piers while launching steel girders in bridges was considered as experimental setup for this work. Using strain measurements as a metric for long-term monitoring of bridges under heavy vehicle traffic was also reported by Liu et al. (2009). However, significant limitations of using strain measurements have been reported (Shrive et al. 2009). The significantly low strains under service loads make strain measurements due to traffic very small as compared to strain measurements due to environmental effects (e.g. temperature variation). Also, noise effects in signals play a major role in relatively low measurements of strain. Kim and Paik (1997) used fiber-optic strain gauges for monitoring bridges and stated that Fabry-Perot optical fiber sensors showed a high resolution of approximately 0.12 microstrain. Todd et al. (2000) also developed a strain sensing system for a clamped plate where damage is induced by loosening the clamping bolts. They used fiber bragg grating (FBG) sensors to measure strains at 16 locations to provide high resolution and low-noise data. Iranmanesh et al. (2009) also used fiber optic Bragg grating (FBG) sensors to monitor the column curvature of a bridge and took advantage of high resolution and high signal to noise ratio of this kind of sensors. As mentioned by Ansari (2007) shifting in the central wavelength of the Bragg gratings is the strain transduction mechanism in FBG sensors. Recently, fiber Bragg grating (FBG) accelerometers were used for structural health monitoring of bridges. Talebinejad et al. (2009) describe a methodology to develop a fiber optic accelerometer based on the shift in wavelength of FBG as a result of change in acceleration and utilized a low frequency version of this

accelerometer to monitor a reinforced concrete (RC) bridge located at western suburb of Chicago.

However, significant efforts have been directed to examining vibration-based damage detection methods in bridges. The premise of vibration-based SHM is that dynamic characteristics of a structure are a function of its mechanical properties. Thus changes in these mechanical properties as a result of localized structural damage will result in observable changes in the dynamic characteristics vibrations of the structure. Research on vibration-based damage identification goes back to the late 1970s in the study of offshore oil and gas platforms, as well as in the aerospace industry. A review of vibration-based SHM techniques for damage detection can be found elsewhere (Doebling et al. 1998, Yong 2002).

Acoustic monitoring is an alternative approach from vibration-based damage detection that was introduced to the SHM community (Ohtsu et al. 1996). Tozser and Elliott (2000) showed the possible use of this method to monitor cable stayed bridges and post-tensioning cables in bridges and also in high rise buildings. The concept is that fracture of these cables result in acoustic events that can be monitored. Assessment of the rate of detecting acoustic events can provide an efficient health monitoring devices. Damage detection using acoustic emission has been suggested by many researchers. For instance, Carpinteri et al. (2005 and 2009) showed the use of acoustic emission for structural damage detection and prognosis of historical masonry structures.

2.2 Vibration-based SHM

Several damage metrics (sometimes also referred to as damage features) have been suggested by many researchers for vibration-based SHM. These metrics included natural frequency (Natke and Cempel 1997, Zak et al. 1999 and Williams and Messina 1999), mode shapes (Stanbridge et al. 1997, Doebling and Farrar 1996 and Ahmadian et al. 1997) and curvature of mode shapes (Maeck and De Roeck 1999, Ho and Ewins 2000, and Chandrashekhar and Gangul 2009). These damage metrics can be extracted by performing digital signal processing of acceleration signals received from the bridge structure (Neild et al. 2003, Reda Taha et al. 2004). Time and frequency analysis methods have been the most dominant techniques. In frequency analysis Fast Fourier Transform (FFT) is usually used to identify the major frequency components and the major mode shapes and observe changes in these components as damage happens in the structure. More information on FFT can be found elsewhere (Agneni et al. 2000 and Humar 2002). A time representation of an acceleration signal observed using accelerometers installed on a reinforced concrete bridge is shown in Figure 2-1. The high acceleration amplitude at 40 seconds is attributed to a heavy truck passing over the bridge at that time.
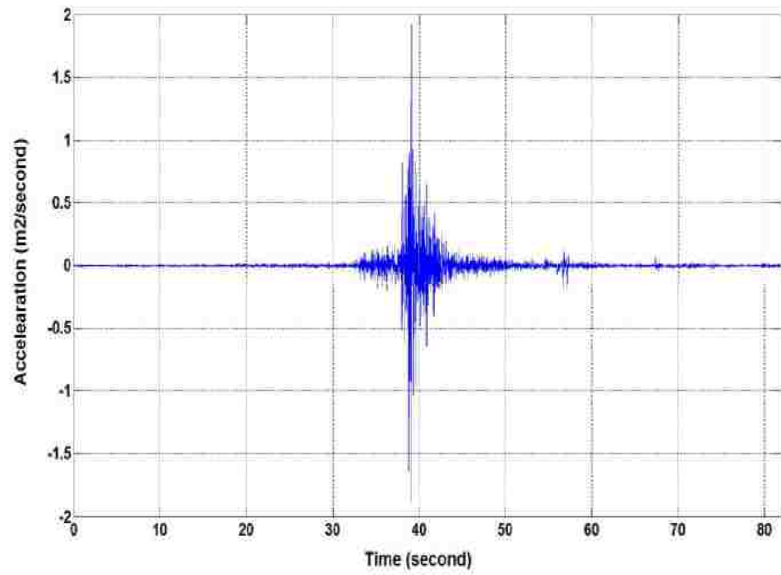
Figure 2-1 Acceleration of reinforced concrete (RC) bridge in the time domain.

Figure 2-2 shows the frequency analysis of the same signal shown in Figure 2-1. The figure signal shows the ability of frequency based analysis to identify basic frequency components. However, it is obvious that the frequency analysis completely misses all time information.
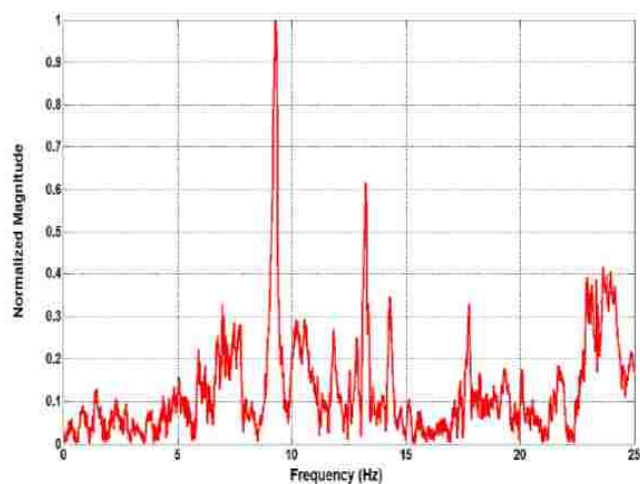
Figure 2-2 Acceleration of RC bridge observed in the frequency domain.

21

Modal analysis has been also suggested by researchers for identifying damage. Damage detection algorithms from modal analysis depend on observing signals from sensors distributed over the structure and developing accurate structural models (e.g. finite element (FE) models) to identify observable mode shapes. Problems associated with FE modeling such as discretization, configuration errors and modeling errors, as discussed by Yang et al. (2003), proved that modal testing might not be sufficiently practical. Moreover, experimental verification of damage detection algorithms using modal data from relatively large structures showed that modal characteristics might be insensitive to localized damage (Friswell and Penny 1997). Zhang et al. (1998) utilized modal strain energy as a structural damage identification method which uses mode shapes and modal frequencies from both damaged and undamaged structures to locate damage. To locate and quantify damage within a space truss model, Carrasco et al. (1997) proposed using changes in modal strain energy. Kim et al. (2003) suggested using modal strain energy to estimate the severity of damage and pointed out that changes in the natural frequencies are difficult to measure due to the limited change in frequencies caused by the uneven mass distribution in large structures. Using changes in modal strain energy is also used in the work done by Choi and Stubbs (1997). Ren and De Roeck (2002) examined the effect of noise on the reliability of damage identification from modal analysis and reported that the effect of noise is highly dependent on damage severity such that limited damage states will be more challenging to detect at high levels of noise than severe ones.

Critique was directed to frequency based methods for being heavily dependent on the structural mass (Shrive et al. 2003 and 2009). While many laboratory experiments

showed the ability of frequency metrics to detect damage in small lightweight structures in laboratory settings, field experiments showed very little success in detecting damage in large reinforced concrete bridges using frequency based metrics. The inability to replicate laboratory experiments to field observations for SHM systems is a major challenge in SHM design due to the significant effect of scale on structural response (Shrive et al. 2009). Despite all the facts that natural frequencies could be insensitive to local and small parameter variations (damages) in the structure, the frequency shift based is used as a popular structural damage detection method in field applications. Jiang and Wang (2009) attempted to address this problem in frequency shift methods by developing the concept of sensitivity-enhancing control using eigenstructure (dual eigenvalue-eigenvector) assignment-based approach.

Such challenge suggested the use of alternative signal analysis methods such as Short Time Fast Fourier Transform (STFT), wavelets (Hubbard 1998) and principal component analysis (PCA) (Browne et al. 2002) for analysis of structural dynamics observations. STFT showed the ability to provide good time and frequency localization as STFT utilizes a window function that is multiplied by the input signal before computing the FFT (Robertson et al. 1996). Although STFT provides a time-frequency representation of a signal, there is a major drawback with respect to utilizing STFT in SHM applications; namely that the width of the window is fixed. Thus, there remains a need for multiple resolution analysis that can provide fine time resolution for long duration signals and fine frequency resolution for high frequency signals (Strang and Nguyen 1997). A thorough review of various time-frequency techniques for structural vibration analysis is provided by Neild et al. (2003). Strengths and weakness of each technique were examined through

23

examining a group of synthetic signals representing possible structural dynamics. Although the review did not address the issue of damage diagnosis it shed light on similarities between these techniques.

On the other hand, wavelet transform (WT) was suggested as an efficient method for digital signal processing that can provide time and frequency information. WT can be used to obtain vibration signal wavelet coefficients establishing what is known as the wavelet scalogram. Moreover, wavelet multi-resolution analysis (WMRA) can be used to decompose the structural vibration signal into its basic component signals. We discuss both methods here for our major use of these methods in SHM. The structural acceleration signal presented in Figure 2-1 is analyzed here first using WT. Figure 2-3 presents typical scalograms of the wavelet transform of the dynamic response acceleration signal of the bridge.
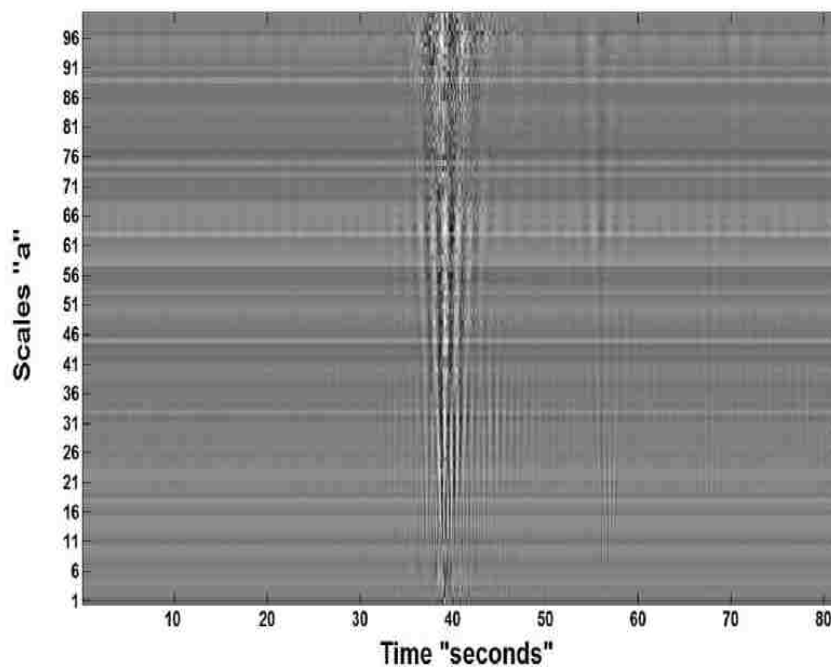
Figure 2-3 Acceleration of RC Bridge observed in the wavelet domain.

The WT is performed using the Morlet mother wavelet showing the variation of the amplitude of wavelet coefficients as variation of the gray color intensities with respect to both time and scale. It is obvious that Figure 2-3 is more capable of describing the changes in the system dynamics in both time and frequency domains than Figure 2-1 and Figure 2-2 individually. While a peak acceleration in the structural response is indicated close to 40 seconds, this peak intensifies at relatively high scale values (relatively stretched wavelets) indicating the existence of high frequency components at that time.

Figure 2-4 demonstrates a schematic representation of the wavelet multi-resolution decomposition of a signal. An example analysis of the acceleration signal using WMRA is shown in Figure 2-5. The dynamic response of the reinforced concrete (RC) bridge that was previously shown in Figure 2-1 is decomposed here using the Morlet wavelet at three decomposition levels. Figure 2-5 presents the components that constitute this decomposition, including the third level approximation (A3) and the first, second, and third level details (D1, D2 and D3). This process of decomposition can be useful for de-noising or for damage detection in SHM systems. However, this analysis in not limited to one form of WT technology.
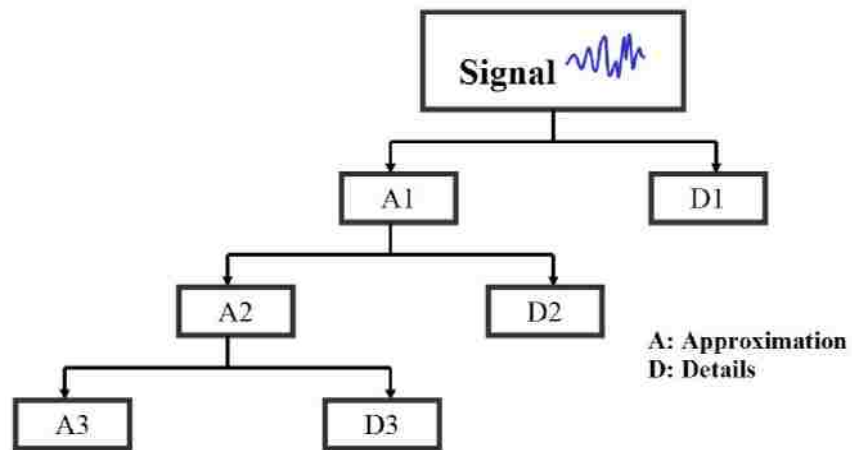
Figure 2-4 Schematic representation of wavelet multi-resolution analysis (WMRA) of a signal.

It is important to note that wavelet analysis of the acceleration signal can make use of the wavelet packet decomposition. Figure 2-6 demonstrates a schematic representation of the wavelet packet decomposition of a signal. Figure 2-7 presents the wavelet packet decomposition of the same structural dynamic signal presented in Figure 2-1 using the Daubechies wavelet and not the Morlet wavelet with WMRA at three levels of decomposition. The flexibility of wavelet analysis avails itself to the more general use of structural damage detection in the civil infrastructure.

26
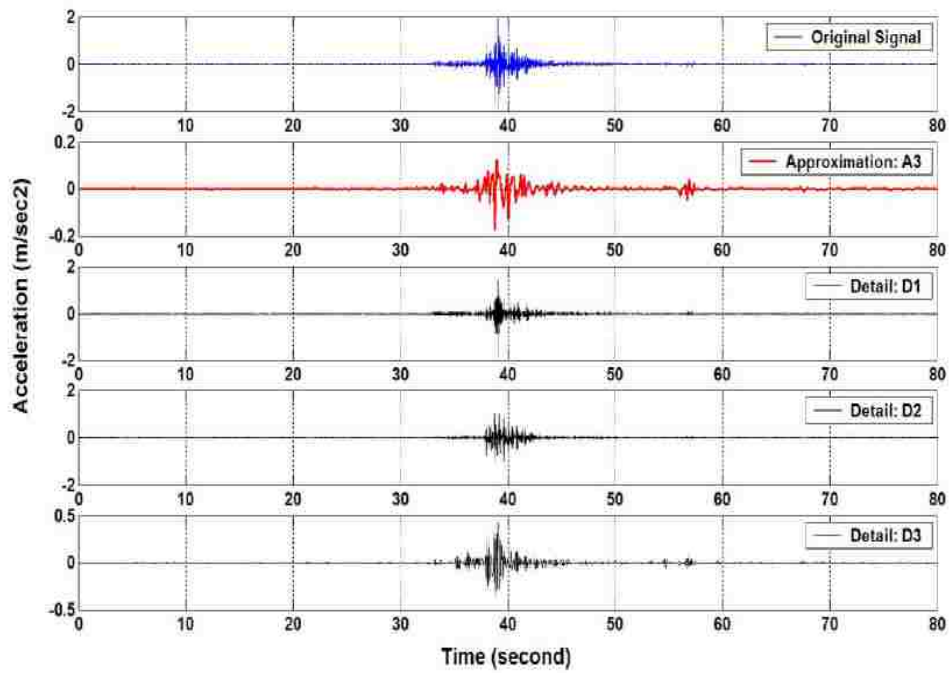
Figure 2-5 Example decomposition of the acceleration signal using WMRA.
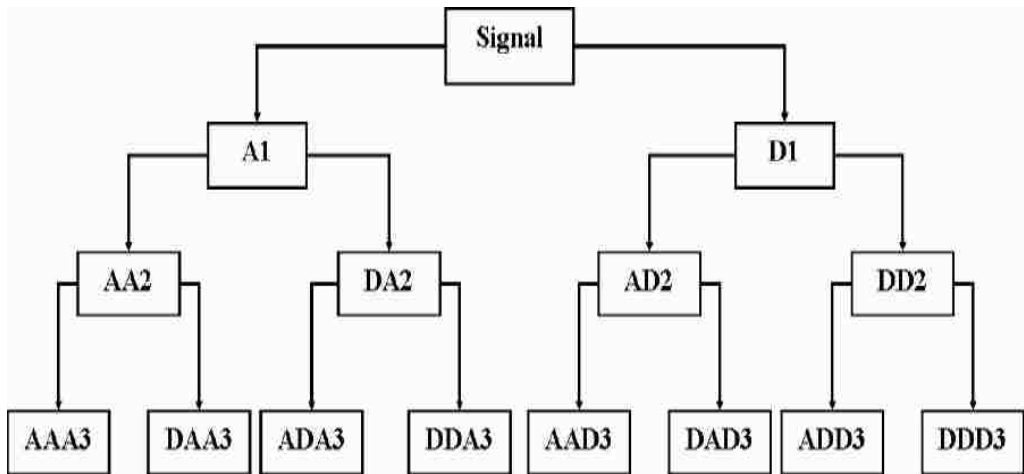
Figure 2-6 Schematic representation of wavelet packet transformation of a signal.

27
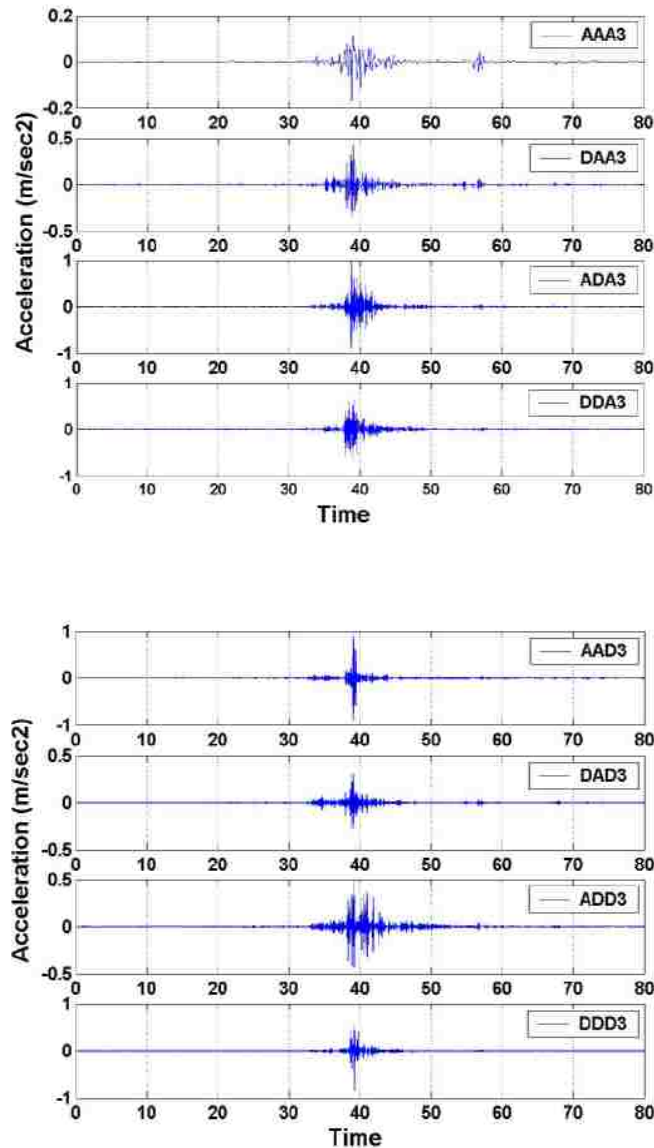
Figure 2-7 Wavelet packet analysis of the acceleration signal shown in Figure 2-1.

As discussed above, wavelets provide an excellent tool for signal processing for damage detection of civil infrastructure. The choice of the wavelet function is an interesting challenge. Many methods have been suggested in the literature to tackle this challenge. Entropy-based criterion has been nominated by a few researchers to be the

28

most successful method for selecting the optimal wavelet function for efficient damage diagnosis (Browne et al. 2002b). Bukkapatnam et al. (1999) explained the basic principles of using entropy-based analysis for signal processing. An entropy-based criterion would try to establish a crisp division between systematic signals and noise using means of Shannon's information theory (Coifman and Wickerhauser 1992). Horton et al. (2005) suggested that the most optimal wavelet function is the one that closely resembles the shape features of the acceleration signals.

Liew and Wang (1998) showed that crack identification of a non-propagating crack in structural systems such as simply supported beams using WT is much more efficient than using PCA. Douka et al. (2003) used WT to determine the location and size of the crack in a beam using the fundamental mode of vibration. The size of the crack was related to the wavelet coefficients. Similar work was also reported by Gentile and Messina (2003) who showed that the WT can detect damage location and crack size from both noisy and clean data. It was argued that damage of machinery parts can be predicted by observing the changes in the wavelet coefficients of the wavelet-transformed vibration signal (Moria et al. 1996 and Masuda et al. 1995). Instead of working in the time domain, the spatial wavelet based approach replaces the time variable with a spatial coordinate allowing for the detection and the positioning of a crack.

Experimental and theoretical investigations by Reda Taha et al. (2004), Horton et al. (2005) and McCuskey et al. (2006) showed the possible use of WMRA for damage detection of bridges. It was suggested that the energy of the third approximation signal decomposed using wavelets can be used as the damage feature (Reda Taha et al. 2004). Other researchers also showed that the energy spectrum in the wavelet packet can be used

29

to detect small structural damage (Yan and Yam 2004). This method is further explained in Chapter 5 of this dissertation and is used for damage detection in the RC frame bridge in Tucumcari.

2.3 SHM for Structural Composites Including FRP

On the other hand, damage detection in FRP composite laminates have been suggested by many researchers (Zhao and Sim 2002, Liang et al. 2004, Yu et al. 2007, Kostopoulos et al. 2009). Guan and Karbhari (2006) implemented a health monitoring system utilizing wireless technology on the Kings Stormwater Channel Bridge located on a major state highway in California. This bridge consists of fiber reinforced polymer (FRP) composite girders and deck panels (Seible et al. 1999). The data collected by different types of sensors are transmitted wirelessly and processed in real-time remotely. A friendly web user interface was made to present the information in a clear and useful manner. The development of the easy to use web interface for this work can be found elsewhere (Karbhari et al. 2003a, 2003b). Strain measurements were considered the most dominant methods for damage detection of FRP. Strain measurement using electrical strain gauges were reported to be useful in detecting fiber debonding (Mehrani et al. 2009). However, methods using fiber optical sensors have gained considerable interest in detecting damage in FRP (Read et al. 2002). Significant efforts have been directed for damage detection using Fiber Bragg Grating (FBG) sensors. The concept of FBG is simple, represented by the change of light reflected wavelength when the fibers are strained. Comparison of FBG wavelength of unstrained fibers provides the needed information to calculate the strain by determining the wavelength shift. Due to its relatively small size, fiber optic

sensors have become the most commonly adopted sensing technology for damage detection of FRP composites. New data integration modules can allow recording data from a large number of sensors. FBG sensors can be mounted on the surface of FRP composites used to strengthen RC structures. Using multiplexed FBG provides a profile of strain changes along the FRP plates. FBG sensors have also been reported efficient in field monitoring of FRP (Mehrani et al. 2009, Shrive et al. 2003). Rizkalla et al. (2000) proposed a method to use FBG sensors to directly measure temperature to calculate thermally induced strains in bridges in order to separate thermally induced strains from the strains caused by possible damage in fiber reinforced polymer reinforcements. Canceling the effects of thermally induced strains in FBG sensors was also recognized by Moerman et al. (1999). Further details on developing FBG thermal strain sensors can be found elsewhere (Foedinger et al. 1999). Taljsten (2005) used optical fiber sensors as well as LVDT crack gauges for monitoring a 400 m long prestressed box bridge called Grondal Bridge in Sweden. This bridge was also strengthened using carbon fiber reinforced polymer (CFRP) laminates to limit the size of cracks that some of them exceeded more than 0.5 mm. Mosallam et al. (2009) also used the concept of optical fiber sensing for wireless monitoring of a composite bridge. In this work, a Diagnostic Prognostic (DPS) Fiber Sensor Interrogator (FSI) system is used to acquire real-time strain and temperature data from an array of multiple FBG sensors along a single channel.

Many researchers have suggested monitoring FRP composites using acoustic sensors. Ultrasonic damage identification methods are common to check damage in composites in the aerospace industry (Gros et al. 1998). On the other hand, acoustic emission (AE)

sensors have been proposed by many researchers (Qi et al. 1997 and Prosser 1996). The concept in using AE sensors is based on the realization of the energy released of a material upon fracture. The scale of damage recognized by the AE techniques is dependent on their sensitivity to energy (Kessler 2002). Advances in micro fabrication of micro-electro-mechanical systems (MEMS) enabled the manufacturing of AE sensors that can be embedded in the material (Schoess and Zook 1998). A group of new investigations suggested that optical fiber sensors can be sensitive to AE (Lee and Tsuda 2005). Other efforts examined Rayleigh, shear and lamb waves, with the latter being the most successful (Wang and Yuan 2005 and Su et al. 2002). Significant effort is currently performed by researchers worldwide to detect damage location and severity using lamb waves and piezoelectric sensor networks (Aberg and Gudmundson 1998). Kessler (2002) suggested the use of piezoelectric sensors to identify AE energies in materials. Furthermore, researchers also showed the ability of AE sensors or surface acoustic sensor to identify damage locations by employing large sensor networks (Zhou and Sim 2002). A major challenge in using AE surface acoustic and piezoelectric sensors for damage detection in composite laminates is the need for complex analysis of the received signals to realize damage occurrence. Using time reversal acoustics (TRA) concept and extending this concept to guided wave propagation within the CFRP strengthened reinforced concrete beam, Kim et al. (2007) proposed a method to continuously monitor the debonding of CFRP from the host structure in real time.

2.4 Damage Diagnosis and Prognosis

Researchers have shown that using proper domain of each damage metrics can differentiate between healthy and damaged cases of bridges (Mehrani et al. 2009). The damage state of the structure can be identified by considering effective damage features and by the use of probabilistic methods for classifying these damage features. The use of reference performance to classify the structural health has proven helpful in determining the need for maintenance repair of bridges.

Researchers have combined all the above methods to provide damage diagnosis and prognosis of structures. While damage diagnosis means providing information for damage reasoning, location and severity, damage prognosis is using this former information to predict the service life of the structure (Frangopol et al. 2004).

Statistical methods have been attractive tools for damage diagnosis. For instance, Staszewski (1998) discussed two approaches for applying statistical pattern recognition in SHM. The first method considered classifying all operating modes of the structures and recognizing any structural response as one of the pre-classified modes. The second method compared any unknown structural response to *a priori*-known healthy response, subsequently, to distinguish the difference between the two responses. While almost all SHM methods utilize one of these two approaches, two major differences between these methods can be recognized. The first is the choice of the feature for building the patterns, and the second is the approach used to aid the damage detection analysis.

Significant research has utilized artificial intelligence (AI) combined with modal analysis to develop the response patterns and to perform efficient feature extraction using

artificial neural networks (ANNs) (Barai and Pandey 1995, Pandy et al. 1991). Browne et al. (2002) demonstrated that cracking introduces a discontinuity to curvatures and deformation time history. Reda Taha and Lucero (2005) introduced the use of Bayesian analysis to establish unknown health patterns in bridges. Yan et al. (2004) examined the use of statistical methods for extracting the modal parameters of the structure response for detecting structural damage.

Many researchers combined wavelets and neural networks for damage detection and damage pattern recognition. For instance, crack growth in structural concrete was detected using neural networks and was used to provide information about the structural health and the residual service life of the structure. Su and Ye (2004) integrated artficail neural network (ANN) and signal processing to extract what is named as "Digital Damage Fingerprints (DDF)" of the structure. This method was successfully used to detect delamination damage in composite structures.

Other researchers have shown the possible use of fuzzy set theory and possibility theory for damage pattern recognition in structures (Reda Taha et al. 2006, Altunok et al. 2007, Carden and Brownjohn 2008). The use of statistical information to establish fuzzy damage sets for a reinforced concrete structure is shown in Figure 2-8. It was found that a fuzzy damage metric can be developed to detect the severity of damage in the reinforced concrete structure.
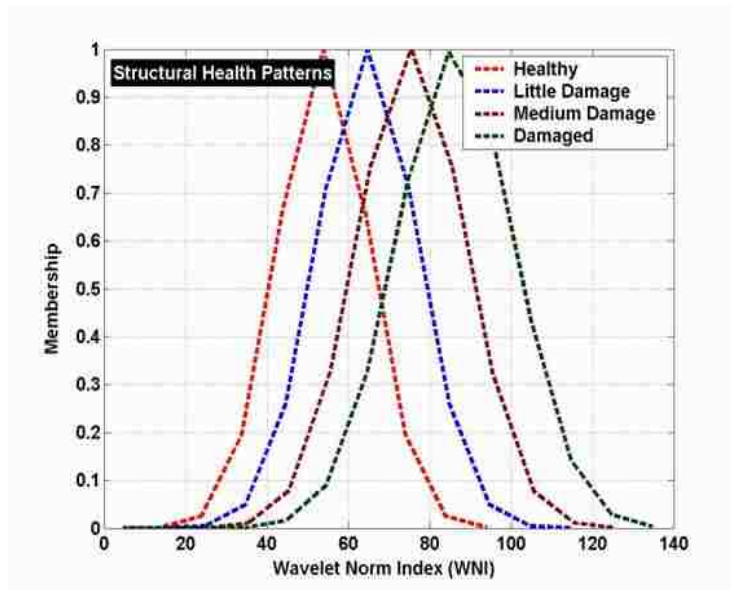
Figure 2-8 Fuzzy damage sets relating the change in damage features to the severity of damage in the structure (Reda Taha et al. 2006).

Moreover, possibility theory was also shown capable of detecting damage when applied to a model bridge and to a pipeline structure. Possibility distributions for damage detection of a model bridge are shown after Altunok et al. (2007) in Figure 2-9.
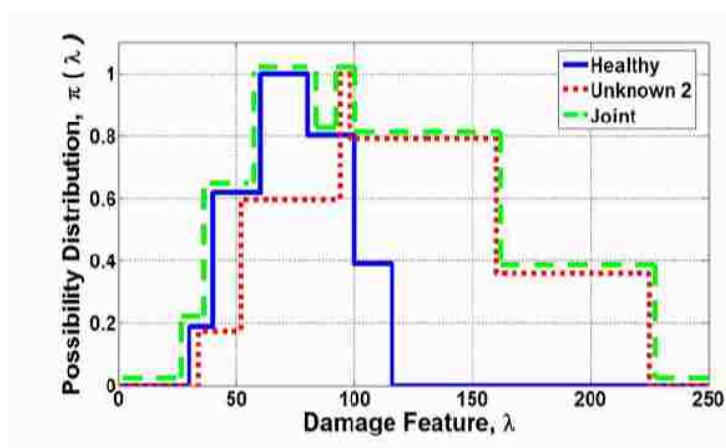
Figure 2-9 Possibility distribution of the damage feature observed in a model bridge (Altunok et al. 2007).

35

The use of evidence and possibility theory has shown an excellent ability to consider non-statistical uncertainty in damage detection. Consideration of uncertainty allowed for establishing damage sets using principles of minimum entropy (Azarbayejani et al. 2008). We discuss this method in Chapter 5 to keep establishing the damage states and to identify the level of damage in the structure. A schematic representation of damage sets in the ASCE benchmark structure (ASCE 2006) is shown in Figure 2-10. The figure also shows how the different severity of damage observations will be located with respect to the damage sets established based on principles of minimum uncertainty.
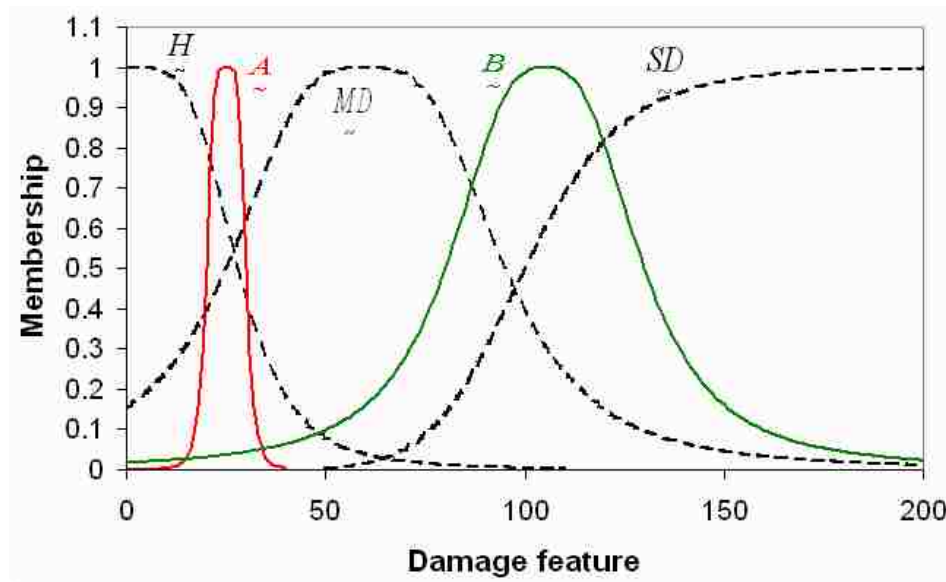
Figure 2-10 Damage fuzzy sets as observed in the ASCE benchmark structure (Azarbayejani et al. 2008).

2.5 Conclusion

This chapter provides a short review of structural health monitoring with focus on the areas pertaining to this dissertation. New advances in sensing technology and wireless communication systems have directed SHM systems to remotely monitor infrastructure.

36

By deploying different kinds of sensors including accelerometers, strain gauges and thermocouples, most current SHM systems are capable of measuring the response of structures. While classical strain gauges can provide a reasonable set of information for structural composites, most recent research suggests the use of FBG fiber optical sensors or acoustic emission for damage detection of FRP composites. Methods to analyze this data for damage feature extraction and to establish domains for damage pattern recognition are also discussed. The findings in the literature relate to the methods used in Chapters 3 and 4 and also are implemented in designing the SHM system to monitor the FRP strengthened RC bridge in Tucumcari, New Mexico.

CHAPTER 3 A PROBABILISTIC APPROACH FOR OPTMAL PLACEMENT OF SENSORS IN SHM SYSTEMS

3.1 Introduction

In this chapter, we describe a probabilistic approach to identify optimal location of any given number of sensors for different structures. Our method aims at identifying optimal locations of sensors in the sensor network such that probability of detection (POD) maximizes all possible combinations of damage locations and damage severities. We define a finite set of damage locations and severities such that damage at any location on the structure can be described as X_i^j where $i = 1, 2, …, K$ and $j = 1, 2, …, D$; K denotes the number of possible damage locations and D denotes the number of possible damage severities. We also define the finite element (FE) modeling resolution (r) as the minimum distance between finite element nodes.

3.1.1 Establishing Probability Distribution Functions

FE analyses of the structure are performed assuming sensors can be located at FE model nodes with predefined resolution (r). The nodes are uniformly placed throughout the structure. Based on *a priori* knowledge of critical damage locations in the structure, damage is induced for various levels of damage severity in the structural model. The dynamic response of the structure is obtained from the structural analyses for both

38

healthy and damaged cases. It is important to note that our intention is to create FE models that incorporate all possible combinations of damage locations and damage levels. The number of FE models required N_m can be calculated as

$$N_m = N_L^{N_d} \tag{3.1}$$

where N_d and N_L = numbers of damage locations and damage levels considered in the FE analysis.

As obvious from Equation (3.1), the total number of FE models N_m required can be significantly high. Therefore, it is important to recognize the fundamental structural behaviors and primary practical issues to obtain the best number of damage locations (N_d) with high possibility of occurrence and a limited number of damage severities (N_L) with significant difference between them. The dynamic response of the structure obtained from each FE model are used to investigate the possible damage features, which is necessary to explain the damage state in the structure in each model. The number of damage feature (N_n) is a function of the number of FE models N_m and the modeling resolution *r*. The selected damage feature shall be able to differentiate between healthy and damaged cases. It is assumed that a specific value of the damage feature can be calculated at each sensor. In this proposed approach, the damage features obtained from FE analyses are used as inputs to an artificial neural network (ANN) with no hidden layers, which is called perceptron (Haykin 1998), and the corresponding damage locations are considered as ANN outputs. The neural network is thus trained to predict damage location by observing the damage feature values at all sensors. Cybenko (1989), Haykin (1998), Bishop (2000) showed that ANN can learn and generalize from example data sets. Ross (2004) demonstrated that ANN could produce reasonable outputs after a

limited training from inputs that were not observed during the training process. In Figure 3-1, the proposed neural network is schematically represented to show system inputs and outputs.
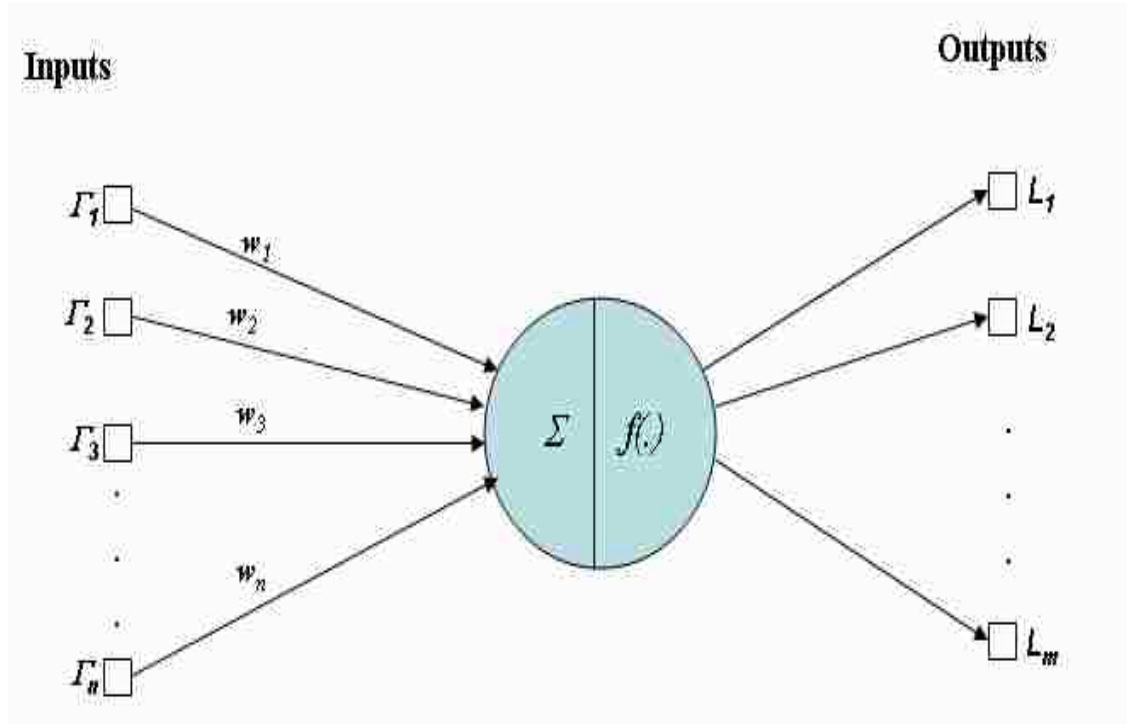
Figure 3-1 Artificial neural network used for extracting weights.

In Figure 3-1 Γ_1 to Γ_n are the damage features used as inputs to the neural network while L_1 to L_m are the damage locations considered as outputs of the neural network. Moreover, w_1 to w_n are the network weights determined during network training and $f(.)$ is the transfer function. The ANN suggested in this process does not have any hidden layers and is used just to make a nonlinear mapping between inputs and outputs. A nonlinear transfer function shall be used. Here we suggest the hyperbolic tangent sigmoid function to be used as the transfer function (Ross 2004). The whole process aims at

40

detecting the weights necessary to relate the damage features and the damage locations. It should be noted that this neural network is just trained as a tool to make the nonlinear mapping between damage features and the locations of damage. The backward error propagation also known as the backpropagation (BP) is used as a learning rule.

3.1.2. Identify Optimal Sensor Location

After the neural network is trained for selected combination of damage locations (N_d) and damage levels (N_L) with a prescribed resolution of sensors (*r*), the weights of the neural network (w_1 to w_n) can be used to represent the importance of these sensors in the damage detection process. A vector of all these weights *h(k)* can be constructed as

$$h(k) = |w_k| \qquad\qquad k = 1, 2 \dots N \qquad\qquad (3.2)$$

where $|w_k|$ is the absolute value of the *k*th weight of ANN associated with the *k*th sensor and *N* is the number of sensors distributed uniformly through the structure with certain spacing between them. If more sensors with less spacing are used for sampling, the above formula shall be modified to give the sensor weight vector for any other resolution as

$$h'(k) = \tau\left[\frac{h(k)}{N'/N} \right] \qquad\qquad k = 1, 2 \dots N' \qquad\qquad (3.3)$$

where N' is any arbitrary number of sensors with a resolution less than *r*. τ is the Finite Impulse Response (FIR) interpolation function used for the discrete nature of the data. Given that the sensors importance weights are determined using Equations (3.2) and (3.3) a discrete probability density function (PDF) can be computed. This PDF represents the probability of the sensor ability to detect damage and thus its probability of being included in the optimal sensor network. To establish the discrete probability distribution

41

function *f(n)* at the locations on the structure *n*, which is a multiplier of prescribed sensor resolution, $h'(k)$ needs to be normalized as:

$$f(n) = \sum_{k=1}^{N'} \frac{h'(k)}{\sum_{m=1}^{N'} h'(m)} \delta(n - kr) \qquad (3.4)$$

In Equation (3.4), δ is a discrete impulse function used to construct the PDF. The PDF represents the sensor probability distribution along the structure assuming the problem is one-dimensional. Based on the discrete PDF, a continuous PDF can be constructed by refining the resolution.

It is important to point out that the above formulation can be developed for a two-dimensional analysis without much complexity with the continuous PDF. Once the continuous PDF is established, it can be sampled for any number of sensors to identify optimal sensor locations. A flow chart explaining the methodology to find the continuous PDF is shown in Figure 3-2.
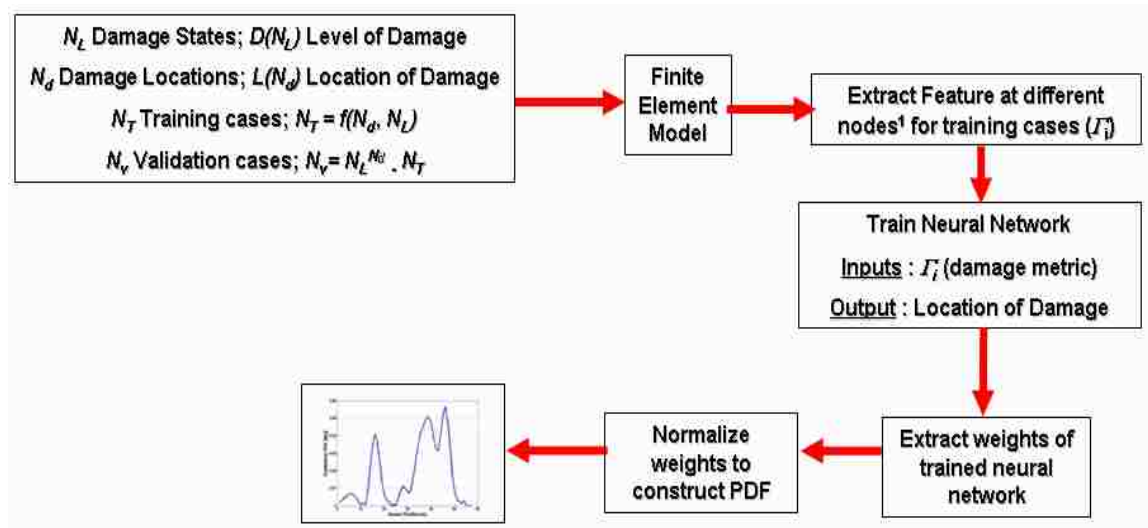
Figure 3-2 Flowchart of establishing continuous PDF on the structure.

42

www.manaraa.com

3.1.3. Validating Optimal Sensor Location

For a given number of sensors, the method allocates the sensors to places that have the highest probability to detect damage in the structure. Distributing any given number of sensors based on sampling of the PDF shall be repeated for large number of iterations (*K* iterations) to ensure considering the effect of randomness on the sampling process (here we consider *K*=1000 iterations). Such large number of sampling iterations will also guarantee the repeatability of the final output (sensors' distribution). The ability of the proposed method to allocate sensors in optimal locations for damage detection can be demonstrated by defining an absolute metric for damage detection efficiency known as the probability of detection (POD). POD is a representation of the probability that a specific flaw in a given structure can be detected by a given monitoring system (Achenbach 2007 and Beard et al. 2007). We define POD as the frequency of the sensor network to identify a specific level of damage accurately. To evaluate POD, we first identify the threshold value (Γ_α) for a given damage level (α). To identify Γ_α, we first extract the damage feature Γ at all sensor locations for the healthy case. The probability distribution function that fits the damage feature data for the healthy case can be identified (Ang and Tang 2006). We suggest here using the normal (Gaussian) probability distribution function for simplicity based on the mean (Γ_H) and the standard deviation (σ_H) of the damage feature values for the healthy case. The probability that the damage feature is less than the damage threshold ($\Gamma \leq \Gamma_\alpha$) can be calculated as

$$p(\Gamma \leq \Gamma_\alpha) = \int_0^{\Gamma_\alpha} \frac{1}{\sigma_H \sqrt{2\pi}} e^{\frac{-(\Gamma - \Gamma_H)^2}{2\sigma_H^2}} \tag{3.5}$$

43

Γ_α is the threshold value that is a function of damage severity level and the probability density function for the damage feature based on the healthy case. Figure 3-3 schematically illustrate the change of Γ_α for moderate and severe damage levels expressed by a probability of damage of 50 and 90% respectively. It is obvious from the figures that the damage feature threshold Γ_α will be higher for a severe damage case, compared to a case with little damage in the structure.
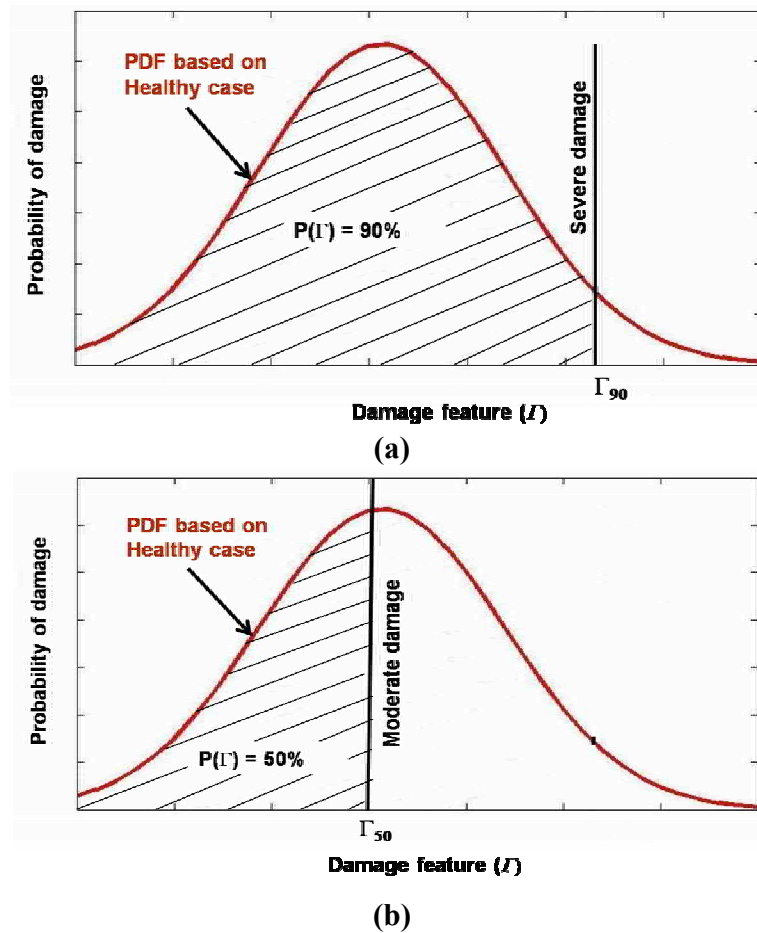
Figure 3-3 Normal distribution of the damage feature based on healthy performance showing (a) damage threshold Γ_{90} for a severe damage represented by 90% probability and (b) damage threshold Γ_{50} for a moderate damage represented by 50% probability (Azarbayejani et al. 2008).

44

The efficiency of the proposed method in detecting different damage levels can be evaluated by computing the frequency of correct classification of the damage level. Correct classification can be identified by using the mean damage features for all sensor locations greater than or equal to the damage threshold (Γ_α) for that damage level. We thus define the POD as

$$POD = \frac{N(\Gamma_{mean} \geq \Gamma_\alpha)}{N_{total}} \tag{3.6}$$

Where $N(\Gamma_{mean} \geq \Gamma_\alpha)$ is the number of simulations where the sensor network using the proposed sensor allocation was capable of identifying the damage class of the structure correctly (i.e. with a mean damage feature higher than the damage threshold). N_{total} is the total number of simulations performed. Figure 3-4 represents a flowchart explaining the above methodology.
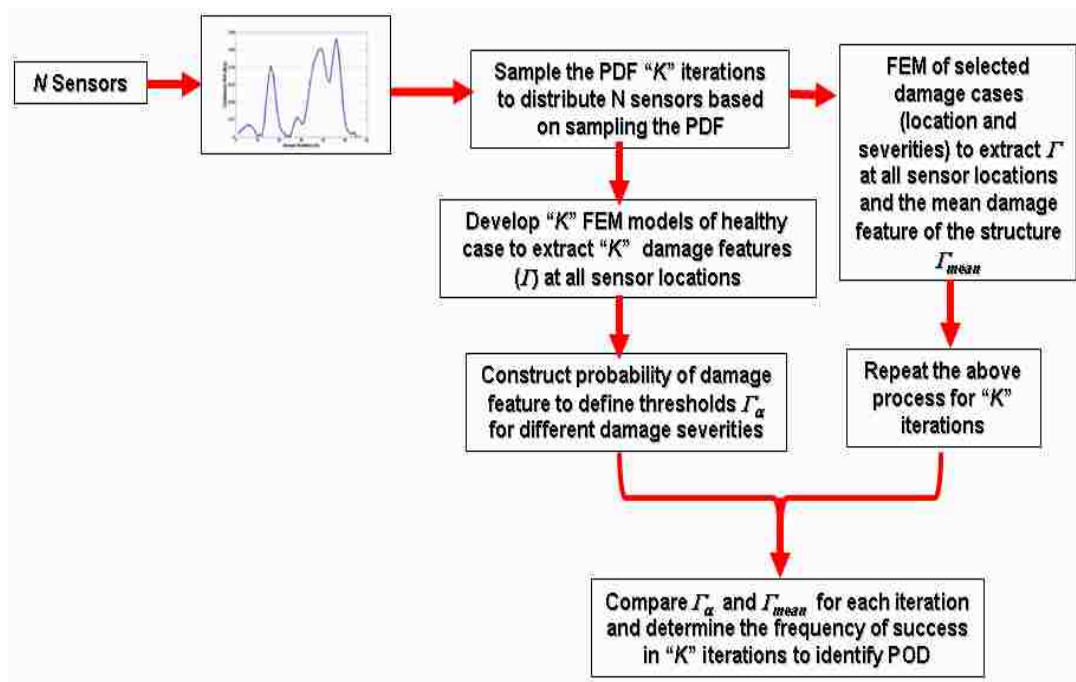
Figure 3-4 Flowchart of calculating POD.

45

3.1.4. Redundancy of Sensor Networks

Finally, an interesting problem in sensor network is to address the issue of network robustness once an optimal network is identified. The objective is to keep the SHM system operating efficiently even if one or more sensors fail or malfunction. This goal can be achieved if additional sensors are used as redundant sensors at the locations of critical sensors. Thus, these locations of critical sensors shall be identified. We suggest such critical locations can be identified after determining the optimal sensor network by performing "leave one sensor out" analysis. Such analysis is well known for examining sensitivity (Saltelli 2000). We thus can compute the significance factor (S_i) for each sensor as

$$S_i = \frac{\left|POD_{opt} - POD_i\right|}{N_{total}} \times 100 \tag{3.7}$$

POD_{opt} is the probability of detection for optimal placement of the sensor network while all sensors work properly and POD_i is the probability of detection of the sensor network when sensor i stops working. Sensors with high magnitude of S_i can be considered critical sensors where redundancy of the monitoring process is needed.

3.2 Case Study

To demonstrate the possible enhancement of damage detection efficiency by optimally allocating the sensors across the structure, a case study to determine the optimal sensor network on a prestressed concrete bridge is considered. A FE model is used to simulate the structural response of the prestressed concrete bridge under healthy and damage conditions. In the absence of experimental data, the use of simulation data for

46

demonstrating the efficiency of new algorithms is a typical methodology that has been widely used by other researchers (Ren and De Roeck 2002 and Sun and Chang 2002).

3.2.1. Description of the Case Study

A three-dimensional (3D) FE model of a two span 57m (27m and 30m spans) prestressed concrete bridge was developed. The FE model included four parallel I-girders modeled as frame elements and the concrete bridge deck slab modeled as shell elements. A schematic representation of the FE model and the different elements used are shown in Figure 3-5. Schematic representation of cross section of the bridge showing the traffic lanes is shown in Figure 3-6.

Figure 3-5 Finite element model of bridge showing damage locations.

47
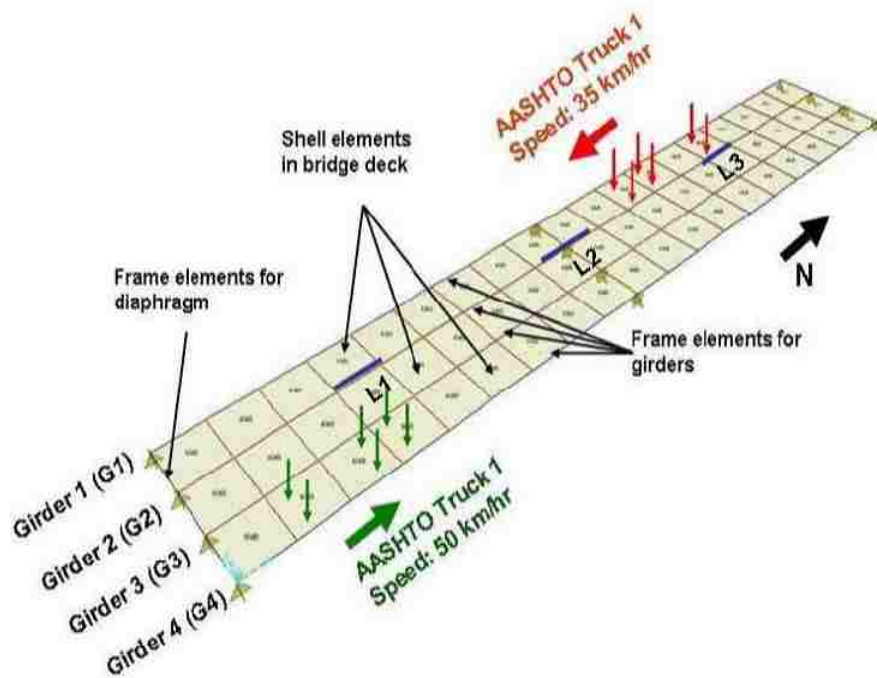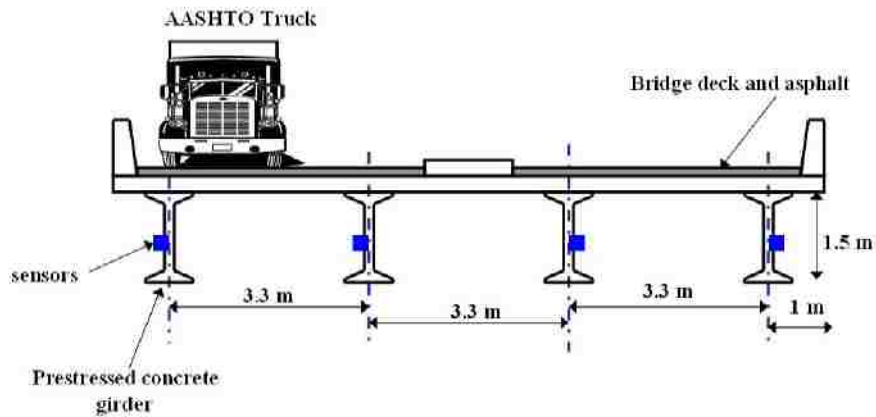
Figure 3-6 Cross section of the prestressed concrete bridge with the location of accelerometers and traffic lanes.

Each bridge girder was assumed to be 1.5 m deep with a distributed mass per unit length of 4800 kg/m. The bridge girders are spaced at 3.3 m as shown in Figure 3-6. The four girders are denoted G_1, G_2, G_3 and G_4 respectively, as schematically presented in Figure 3-5 and Figure 3-6. The concrete has a characteristic compressive strength of 50 MPa and a modulus of elasticity of 37000 GPa. The bridge was loaded using a time-history loading function representing two HL-93 AASHTO (2006) trucks crossing over the bridge from opposite directions at two different speeds (35 km/hr and 50 km/hr) as shown in Figure 3-5. Each girder was modeled using a number of discrete frame elements, each of 3 m in length requiring a total of 19 beam elements per girder. Accelerometers were assumed to be located at the nodes. The beam elements connected 19 nodes, each having three degrees of freedom (DOF). These DOFs included the lateral translations along the longitudinal axis (x axis), the vertical axis (z axis) and rotation about the lateral axis (y

48

axis). Three nodes per girder were used to represent the three support (bridge bearing) locations for each girder creating the 27 m and 30 m spans. The two translations were restrained at bridge bearing locations. The torsion rigidities of both the deck slab and the girders were considered to allow proper load transfer between the girders. End diaphragms were assumed at the bridge bearing lines along the bridge and are also shown in Figure 3-5. The diaphragms were 500 mm wide and 1000 mm deep. The analysis assumed linear elastic behavior of the prestressed concrete, which is usually accepted under service loads (Allbright et al. 1994 and Cai and Shahaway 2004). All the loading and modeling details are represented in Figure 3-5 and Figure 3-6.

The FE modeling process was performed using a group of 19 accelerometers that were assumed to be distributed over each bridge girder and spaced uniformly 3 m to monitor the bridge accelerations due to traffic loading. The accelerometers were assumed to be located on the web of the girders as shown in Figure 3-6. Given this configuration, the bridge vertical accelerations due to the two opposite moving trucks were extracted from the finite element analysis as the z-axis accelerations. The dynamic effect of the traffic loads was measured during the time period when the trucks crossed the bridge. Irregularities in the asphalt layer above the bridge deck slab were randomly distributed along the bridge span and were introduced to the model. A dynamic load effect using a trapezoidal time-step function was used to simulate the load dynamics. Figure 3-7 shows an example acceleration signal for healthy structure. The bridge response due to the dynamic loading was recorded and was then noised with a random signal to simulate the effect of sensing and communication noise. It is worth noting that noise always exists in

real sensor networks. That noise can significantly affect the efficiency of an SHM system. In this study, we considered a 5% constant noise-to-signal ratio in the analysis.
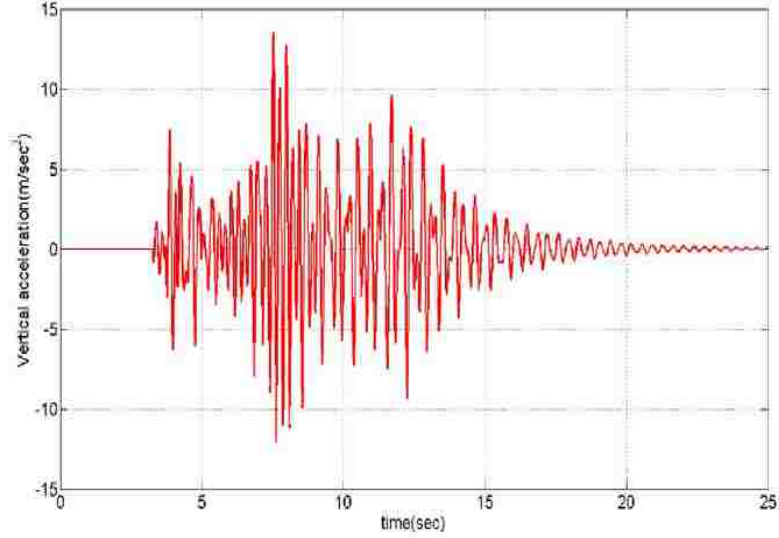
Figure 3-7 Acceleration signal at sensor located at 15 m from South support of Girder G2 for healthy state.

3.2.2. Damage feature extraction

A damage feature Γ based on observing the energy of the monitored acceleration signal was developed. The use of acceleration signal energy has been reported by other researchers to be a feature sensitive to damage (Reda Taha et al. 2004 and Kumara et al. 1999). This energy can be calculated as

$$\Gamma_i = \varepsilon \left[a_{zi}^2(t) \right] + \varepsilon^2 \left[a_{zi}(t) \right] \tag{3.8}$$

where Γ_i is the damage feature representing the energy of the *i*th accelerometer, $a_{zi}(t)$ is the acceleration measured at the *i*th accelerometer in the z-axis direction and ε is the expected value. Other damage features such as the curvature of mode shapes can be used.

50

The only restriction is that it will be possible to evaluate the damage feature value at each sensor location.

3.2.3. Allocating the optimal sensor locations

We start by using *a priori* knowledge on location of critical damage places in the structure. Three locations (L_1, L_2 and L_3) on Girder 2 (G_2) were selected as the critical locations on this girder. These three locations are corresponding to the locations of maximum tensile stresses due to combined dead loads and live loads. These locations are thus more prone to cracking and damage as shown in Figure 3-5. Five different levels of damage, D_1, D_2, D_3, D_4 and D_5 representing 10, 20, 30, 40 and 50 percent loss in stiffness of the girder were considered. These levels of damage severity can be assumed to correspond to a gradually increased probability of damage $P(\Gamma)$ ranging between 50% for D_1 and 90% for D_5. The suggested values of the probability of damage values realize the fact that increasing the level of damage severity shall result in increase in the probability of damage and thus the damage feature threshold Γ_α.

FE models considering all possible combinations of damage locations and damage severities ($5^3 = 125$ models) were developed. The damage feature Γ_i was evaluated at each sensor for each model. The damage features and their locations were used to train the ANN. The training process was repeated 10 times to obtain non-biased weights. The weights were normalized and the continuous PDF was developed as discussed before. A time period of 10 minutes were necessary for performing the 10 training iterations of the ANN on PC with 1.8 GHz processor and 1GB memory. After the continuous PDF was established, the PDF was sampled for any number of sensors distributed over each girder. It is obvious that as the number of sensors for each girder increases, POD will increase.

Hence, the number of sensors that provides acceptable POD can be considered as the optimal number of sensors (Chang et al. 2006). Other considerations such as cost, uncertainty and practical constraints should be taken into account to find the optimal number of sensors that are beyond the scope of this chapter. We demonstrate here the results for distributing 15 to 20 sensors. Once an optimal number is chosen, a sensitivity analysis of significance of the optimal sensors was performed using Equation (3.7) to determine sensor redundancy requirements.

3.3 Results and Discussion

Figure 3-8, Figure 3-9, Figure 3-10 and Figure 3-11 illustrate the process from obtaining the NN weights based on 3 m spacing between sensors, interpolating weights for 1 m spacing between sensors, normalizing weights to get a discrete PDF and finally establishing a continuous PDF of sensor importance in detecting damage along the structure respectively. It is important to note that the values shown on these figures have been randomized by running the training process enough times (10 times) to avoid any bias in the training process. We used Levenberg-Marquardt backpropagation as an optimization algorithm for the NN to map between damage features (energy of acceleration signals) and three damage locations. It is noted that the continuous PDF established here is highly dependent on the locations and levels of damage assumed *a priori*. We argue that this knowledge is almost available for all practical applications for structures using simple structural analysis and the FE modeling.

52
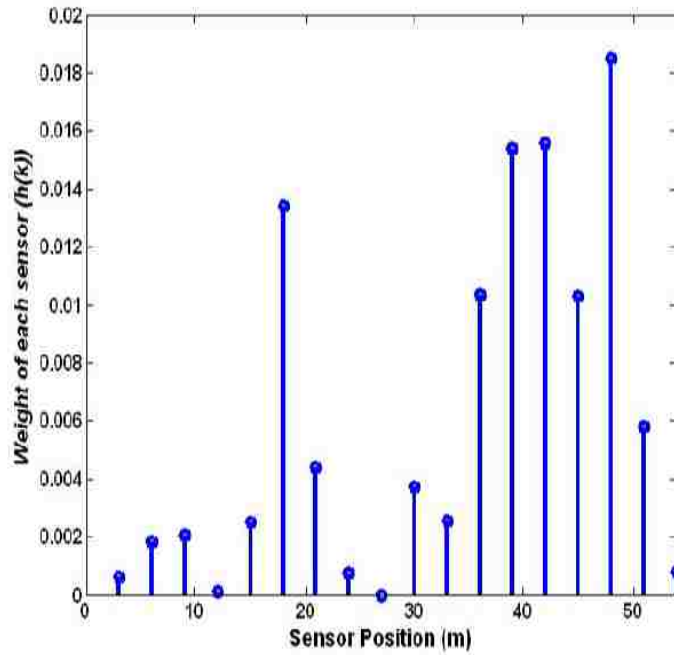
Figure 3-8 Weights of sensors as extracted from artificial neural network (ANN).
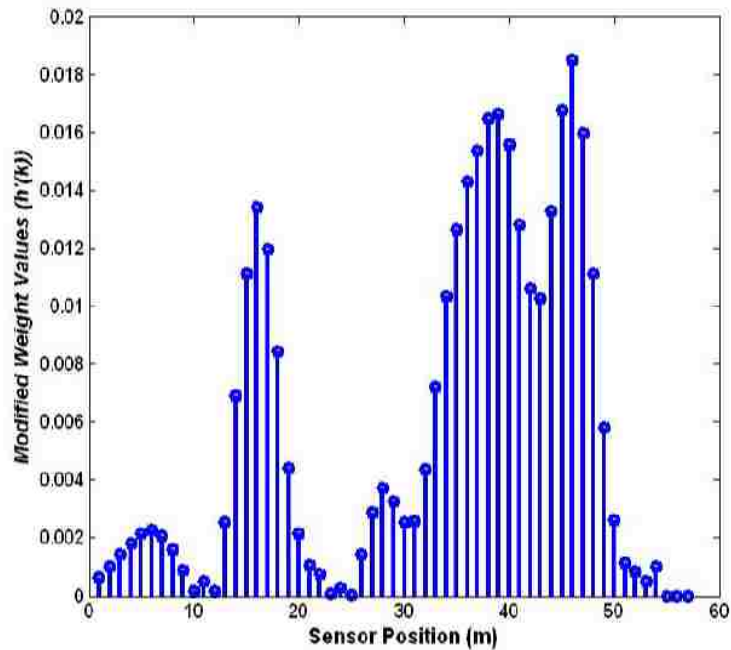
Figure 3-9 Weights of sensors based on prescribed resolution.

53
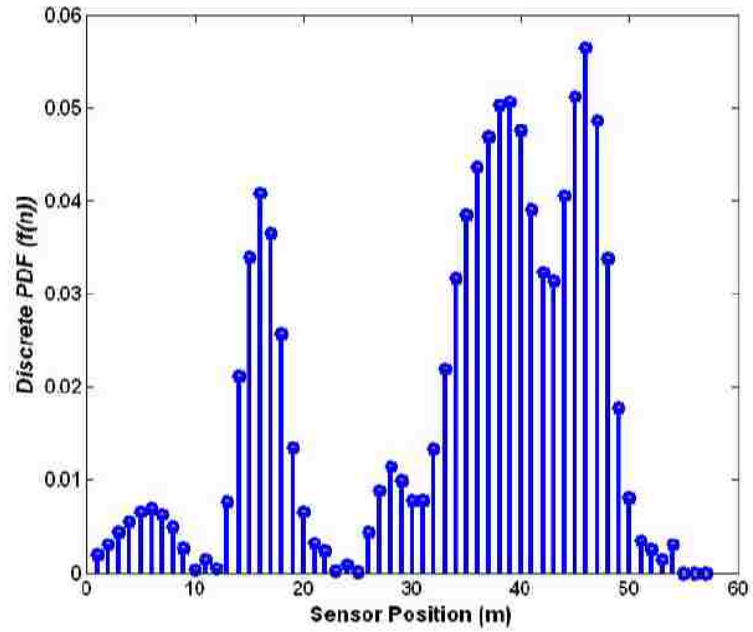
Figure 3-10 Discrete probability density function (PDF) generated along the bridge length.
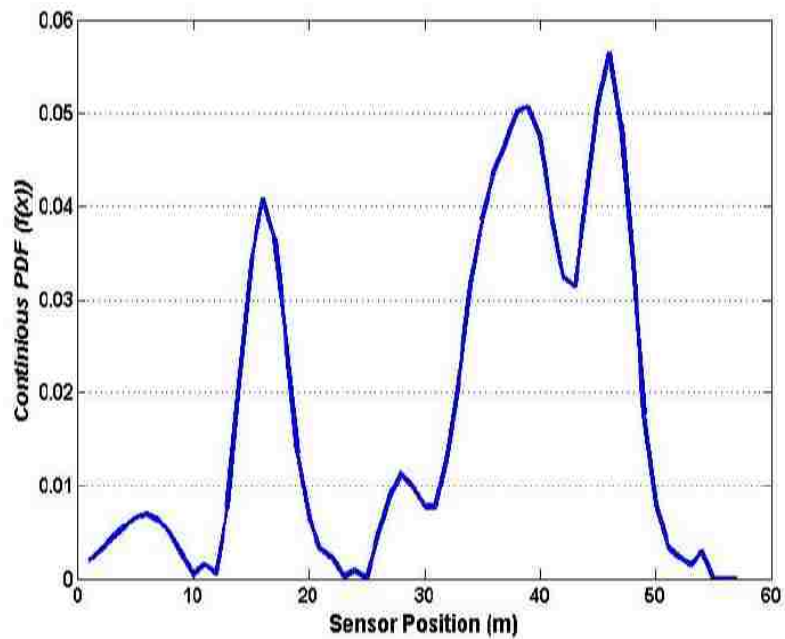
Figure 3-11 Continuous probability density function (PDF).

54

Table 3-1 shows the variability of the damage feature (energy of acceleration signal) values calculated at optimal locations for 20 sensors using 5 sampling iterations for the damage location L_1 and for damage severity D_1.

Table 3-1 Damage features evaluated for 20 sensors allocated using five sampling iterations for damage case L_1 and damage severity D_1.

Sensor #	Iteration 1	Iteration 2	Iteration 3	Iteration 4	Iteration 5
1	4.64	3.1	1.8	4.64	3.1
2	9.89	11.55	14.26	9.89	11.55
3	11.55	13.03	15.01	11.55	13.03
4	13.03	15.07	15.07	13.03	15.07
5	15.00	13.38	13.38	15.01	13.38
6	13.38	9.04	12.08	13.38	9.04
7	10.61	4.45	10.61	10.61	4.45
8	9.04	3.14	4.45	9.04	3.14
9	5.90	5.95	2.04	5.90	5.95
10	3.18	9.05	7.49	3.18	9.05
11	5.95	10.58	9.05	5.95	10.57
22	12.00	12.00	10.58	12.00	12.00
13	13.26	13.26	12.00	13.26	13.26
14	14.31	14.31	13.26	14.31	14.31
15	15.55	15.08	14.31	15.55	15.08
16	15.49	14.05	15.08	15.49	14.05
17	14.93	9.83	15.69	14.93	9.83
18	9.83	8.10	9.83	9.83	8.10
19	6.35	6.35	1.81	6.35	6.35
20	1.81	0.83	0.83	1.81	1.81
mean	10.285	9.6075	9.9315	10.2855	9.656

It is important to note that even though the five sampling iterations were randomly and independently performed, the values of the damage feature in many sensors are similar and the mean damage feature values for the whole structure for the five simulations is very close, confirming the ability of the proposed approach to reach a consistent and repeatable solution even when considering random sampling.

Table 3-2 presents the optimal sensor locations for 15, 16, 17, 18, 19 and 20 sensors, as they shall be distributed over the structure. It is interesting to note that the areas of concentration of the sensors do not change dramatically as the number of sensors increase from 15 to 20, as most sensors are located at the areas of high damage probability as indicated by the continuous PDF. Moreover, to demonstrate the higher efficiency of damage detection when distributing the sensors using the optimal allocation approach with a uniform distribution of the sensors over the structure, we compare the POD for the five levels of damage using 15, 17 and 20 sensors. The comparison can be performed for any other number of sensors.

Table 3-2 Optimal locations (m) of 15, 16, 17, 18, 19 and 20 sensors using the proposed probabilistic approach.

	Total number of sensors					
Sensor #	15	16	17	18	19	20
1	7	3	3	3	4	9
2	12	14	7	11	9	10
3	13	15	12	16	12	12
4	14	16	13	18	13	14
5	15	19	14	19	15	16
6	18	34	15	23	16	17
7	19	37	16	30	17	19
8	20	38	18	33	20	30
9	36	40	19	34	22	32
10	38	41	36	37	24	34
11	43	43	37	39	32	35
12	45	44	38	40	33	37
13	46	45	39	42	34	38
14	48	46	40	43	35	39
15	54	47	43	47	36	40
16	---	54	48	48	39	41
17	---	---	51	53	41	45
18	---	---	---	54	43	46
19	---	---	---	---	45	47
20	---	---	---	---	---	48

We calculated the POD for the five levels of damage assuming a probability of damage threshold of $P(\Gamma_\alpha) = 50, 60, 70, 80$ and 90% to correspond to damage levels D_1, D_2, D_3, D_4 and D_5 respectively. The results of the comparison between the optimal and uniform sensor allocation are presented in Figure 3-12 for 15, 17 and 20 sensors respectively. It is obvious that the optimal sensor allocation using the suggested probabilistic approach always resulted in a POD higher than what can be achieved by uniform allocation of the sensors. It is also interesting that this observation was not affected by changing the number of sensors between 15 and 20 sensors. It is therefore evident that a probabilistic allocation of sensors can result in enhancing the efficiency of the SHM system represented here by its POD.

Moreover, to ensure the robustness of the proposed method against noise, we examined the significance of 1, 5 and 10% noise-to-signal ratios for the case of 17 sensors noise-to-signal ratio on POD. The POD for the three levels of noise at the 5 damage levels is shown in Figure 3-13. It can be observed that no significant change in POD took place as the noise to signal ratio changed from 1% to 10%.

(a)

(b)

(c)
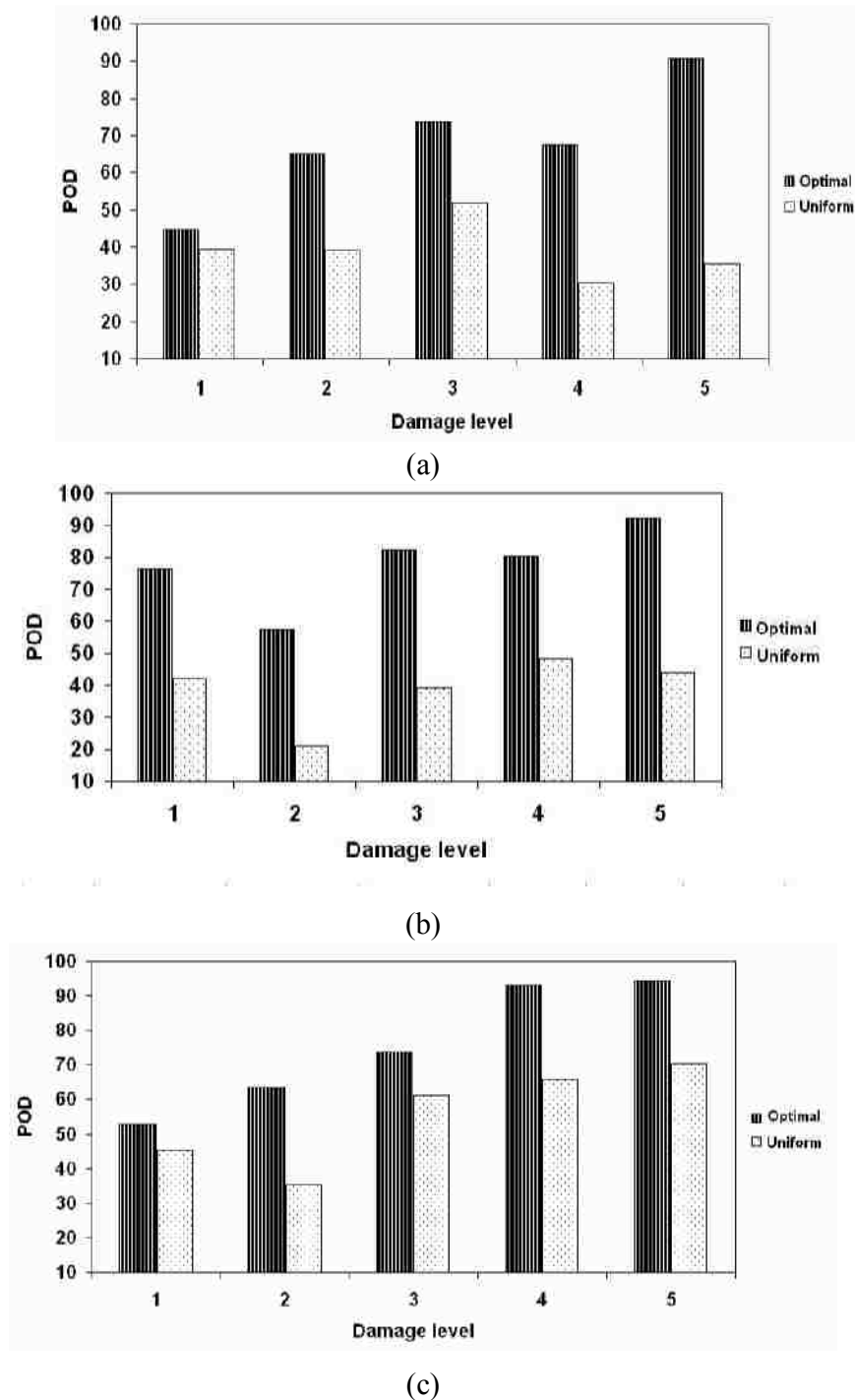
Figure 3-12 Probability of detection (POD) versus damage level when the threshold changes from 50% to 90% for five different levels of damage. Comparison between optimal and uniform sensor allocation. All damage assumed at location L_1 shown on Figure 3-5 Finite element model of bridge showing damage locations. (a) 15 sensors (b) 17 sensors and (c) 20 sensors (Azarbayejani et al. 2008).

59
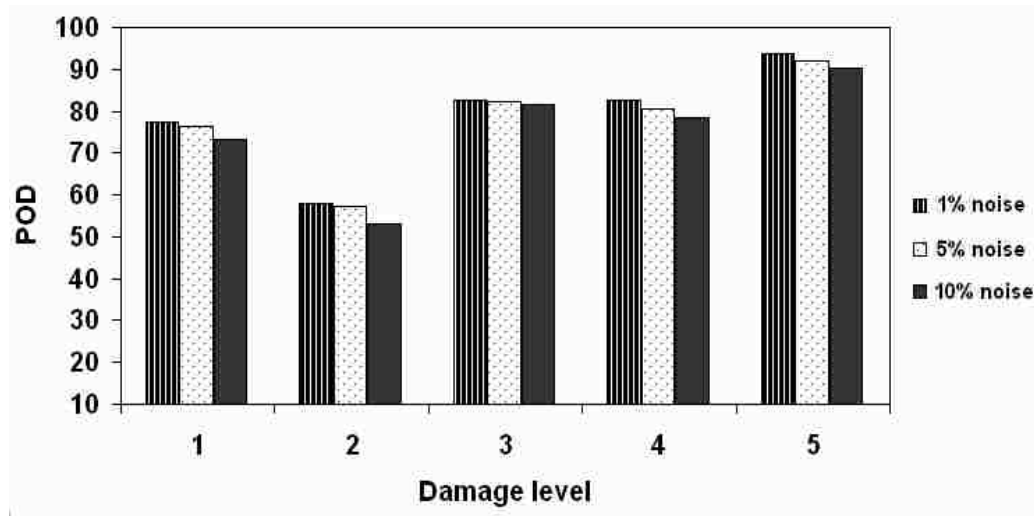
Figure 3-13 Probability of detection (POD) of 17 sensors versus damage level for different noise to signal ratios (Azarbayejani et al. 2008).

Finally, the significance of each of the sensors in the sensor networks was examined by means of "leave one sensor out" analysis. Figure 3-14 illustrate the significance of each sensor for cases of 15, 17 and 20 sensors respectively. For instance, for the case of 17 sensors, it can be concluded from this figure that sensors 4, 12 and 13 are the critical sensors for the damage detection process and it is prudent to consider more than one sensor in these locations. It should be noted that by adding more sensors at critical locations, the POD will increase due to the increase in number of sensors. The analysis also showed for this number of sensors, that sensor number 17 is insensitive to the damage process and will have minimal effect on the sensor network performance if failure occurs. It can also be observed that such sensitivity changes as the number of sensors change. For example, for the case of 15 sensors, sensors 2, 10, 11 and 12 are critical sensors while sensor number 15 does not play a significant role. In addition, for the case of 20 sensors, it is obvious that sensors 3, 4, 15 and 16 are critical sensors and

60

sensor number 8 will have minimal effect on the sensor network performance if failure occurs.

Finally, we point out the fact that experimental verification of the above SHM method is essential to prove its suitability for practical SHM applications. We limit our discussion here to the numerical verification of the proposed method using the finite element method.
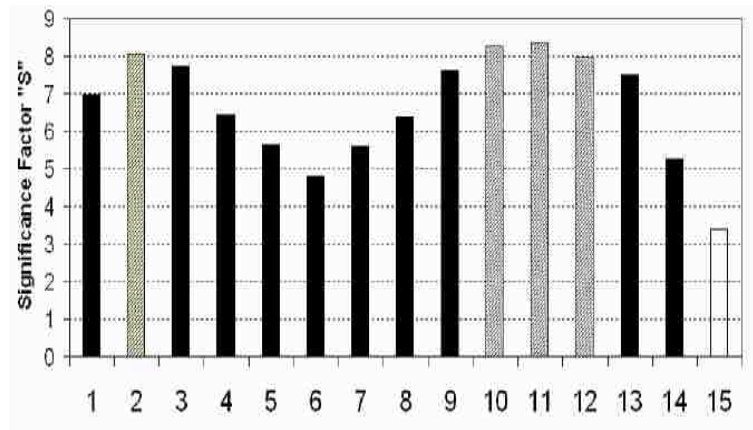
(a)
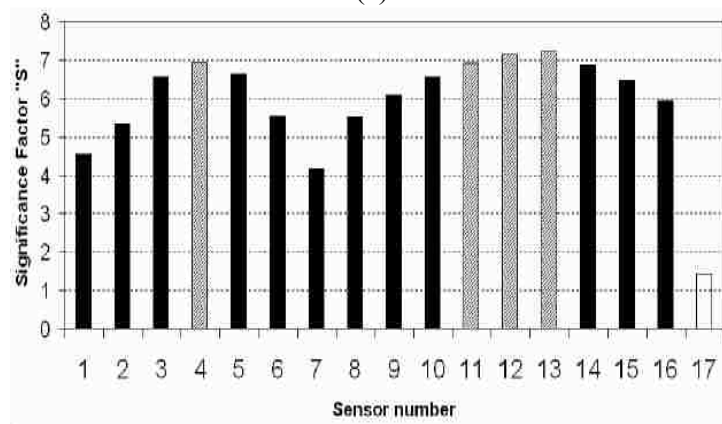
(b)
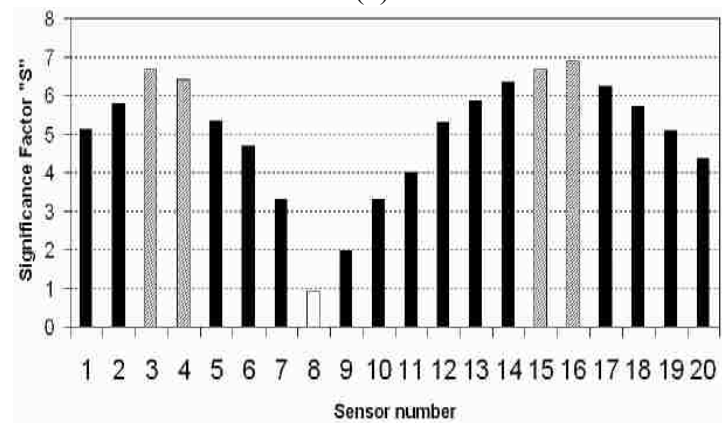
(c)

☐ **Insignificant sensor**

▨ **Critical sensors**

■ **Less critical sensors**

Figure 3-14 Significance factor of each sensor for 15, 17 and 20 sensors distributed on the structure using the proposed probabilistic approach.

62

3.4 Conclusion

A new method for optimal sensor allocation was developed using probabilistic assumptions that utilize *a priori* knowledge of damage locations in the structure. The proposed method utilizes the weights of an ANN trained to detect damage with different severities at damage locations assumed *a priori*. ANN weights were used to generate a probability distribution function that is sampled to determine optimal sensor locations. The proposed method does not neglect the fact that damage at any location of the structure is possible. The efficiency of the proposed method was demonstrated on a simulation case study representing a prestressed concrete bridge modeled using the FE method. It is shown that the optimal sensor locations can be identified. We showed that distributing 15 to 20 sensors using the proposed probabilistic approach resulted always in PODs higher than uniform distribution of these sensors. The identified sensor locations were proved more capable of detecting variable damage levels compared with uniform distribution of sensors on the entire structure. Moreover, the robustness of the sensor network was examined for the optimal sensor network by performing "leave one sensor out" analysis. Robustness of the sensor network can be assured by placing more sensors at critical locations.

CHAPTER 4 ENTROPY-BASED OPTIMAL SENSOR NETWORK IN SHM WITH EXAMPLE APPLICATION TO A CABLE STAYED BRIDGE

4.1 Introduction

Using structural health monitoring (SHM) systems on long span cable-stayed bridges represents a technical challenge where a large number of sensors shall be deployed. To design an efficient, reliable and economical sensor network, the type, number and location of sensors needs to be identified. The type of sensors is directly related to the damage feature that differentiates between healthy and damaged cases. In the past, many researchers used vibration-based damage features to detect damage occurrence in bridges. Most methods suggested in the literature for determining optimal sensor network rely heavily on assumptions directly related to the damage feature used for detecting damage. This limits the usefulness of these methods if such damage feature cannot be used for detecting damage in other structures. An optimal sensor allocation method that is independent of the damage feature is needed by the SHM community.

In this chapter, we introduce an entropy-based method for identifying optimal sensor allocation. A case study for monitoring the Luling Bridge, a cable-stayed bridge over the

64

Mississippi River, demonstrates the ability of the proposed method to successfully identify the optimal number and location of sensors necessary to effectively monitor the bridge. An entropy-based probabilistic method can address the uncertainties existing in sensor allocation without the need to prior assumptions on the damage feature.

4.2 Methods

We suggest an integrated probabilistic and entropy-based technique to identify both the optimal sensor locations and number of sensors in the sensor network. We first explain a probabilistic approach to optimally allocate any number of sensors. We then demonstrate how the optimal number of sensors can be identified through multi-objective optimization. We start by defining a finite set of damage locations and severities such that damage at any location of the structure can be described as ξ_{ij} where $i = 1,2, ..., m$ and $j = 1,2, ..., n$ where m, n represent number of possible damage locations and severities respectively.

Similar to the method explained in Chapter 3, a set of Finite Element (FE) models can thus be created to include all possible combinations of damage locations and severities. The vibration response obtained from each FE model of the structure can be used to calculate the damage feature(s). The selected damage feature can be calculated at each sensor assumed at each FE node location. The damage feature shall be able to differentiate between healthy and damage states of the structure. The damage features computed at each node of the FE models are used to compute the weights of an artificial neural network (ANN). ANN inputs include damage feature values while its outputs are the *priori* known damage locations. ANN is trained therefore to pattern damage features

65

and damage locations as shown in Figure 3-1 in the previous chapter. The weights of the trained ANN are used to demonstrate the relative importance of each sensor in the damage detection process. Normalizing the ANN weights can be used to establish the discrete probability distribution function (PDF), *g(n)* as

$$g(n) = \sum_{k=1}^{N} \frac{\gamma(k)}{\sum_{m=1}^{N} \gamma(m)} \delta(n - kr) \tag{4.1}$$

g(n) is the PDF calculated at *n* locations of the structure, δ is a discrete impulse function and γ*(k)* is the absolute value of the *k*th weight of ANN, *N* is the number of sensors distributed throughout the structure and *r* is the finite element resolution. The continuous PDF can be constructed by interpolation. Since the continuous PDF demonstrates the importance of sensors as a function of structure dimension, by sampling the continuous PDF for any given number of sensors, the optimal locations of sensors can be identified.

4.2.1 Optimal number of sensors

The above approach will allow allocating *N* number of sensors to enhance the damage detection success rate. However, the above approach does not provide a tool for identifying the optimal (minimum) number of sensors. While minimizing the total number of sensors is of less interest in the case of monitoring relatively short bridges (25-100 m long), such number is important for significantly long bridges (e.g. cable-stayed bridges of 200 to1000 m long).

We suggest here that the optimal number of sensors can be identified using multi-objective optimization system. Two objective functions can be realized in formulating the

66

problem. <u>First</u>: the cost of sensors and their deployment and <u>Second</u>: the uncertainty associated with the sensor measurements. The optimal number of sensors shall enable reducing both objective functions simultaneously. While the cost function can be easily formulated, we suggest that the uncertainty can be quantified using principles of information entropy.

Information entropy was suggested as a scalar to quantify uncertainty in probabilistic based information systems (Ross 2004). The principles of information entropy introduced by Shannon (1948) can be used to quantify the uncertainty in damage features computed from a different number of sensor distributions. We suggest using Shannon entropy to quantify uncertainty in sensor measurements for a specific sensor distribution. Considering the fact that minimum uncertainty in damage detection can be associated with the case where sensors are allocated at all nodes, the difference between damage feature values of the case of interest and the case where sensors are allocated at all nodes of the FE model can be used as a measure of uncertainty in the monitoring system. Then the uncertainty objective function based on Shannon entropy can be calculated as

$$E = -(\sum_{i=1}^{N_{max}} \Phi_i - \sum_{j=1}^{N} \Phi_j)^2 \left(\ln(\sum_{i=1}^{N_{max}} \Phi_i - \sum_{j=1}^{N} \Phi_j)^2 \right) \qquad (4.2)$$

In Equation (4.2), N_{max} is the maximum number of sensors where sensors are allocated in all nodes of the FE model and this number is governed by the resolution of the FE model and N is the number of sensors for that specific sensor allocation. Φ_i, Φ_j are damage features computed at nodes i, j respectively. As the number of sensors increase, information entropy will decrease and thus monitoring uncertainty will decrease. On the other hand, the number of sensors is strongly correlated to the cost of the sensor network.

67

However, it is realized that the cost of the sensor network does not increase linearly with the number of sensors because sensor installation and implementation represents part of the sensor network cost. Installation cost does not change significantly as the number of sensors exceeds a specific threshold. The sensor network cost function "C_N" is defined as

$$C_N = \begin{cases} c_1 N & N \le N_1 \\ \\ c_1 N + c_2 (N - N_1) & N > N_1 \end{cases} \qquad (4.3)$$

N is the number of sensors considered for the sensor network, N_1 is the number of sensors beyond which installation cost does not significantly increase. The function constants c_1, c_2, N_1 can be determined from field data. By defining the two objective functions: entropy function "E" and sensor network cost function "C_N", a multi-objective optimization approach can be used to determine the optimal number of sensors.

In multi-objective optimization, the design variable can be determined by establishing the Pareto front (Pareto 1971, Osyczka 1984 and Miettinen 1999). The Pareto front allows realizing the tradeoffs between different objective functions. All the points on the Pareto front are non-dominated set of solutions that are selected based on optimizing different objective functions. To find a single optimal solution from the optimal non-dominated set of solutions, a number of methods were discussed in the literature to perform such optimization by rank ordering the objective functions and performing the optimization in a hierarchical fashion or by defining a global objective function that combines both functions with varying weights (Osyczka 1984). The weighted sum method scalarizes a set of objective functions into a single objective function by pre-

68

multiplying such objective function with a user-supplied weight. We consider here equal weighted objective functions. Weighted sum method is the most widely used classical method for solving multi objective optimization problems. Another classical approach to solve this multi-objective problem is called ε-constraint method. In this approach which is very similar to weighted sum method, we reformulate the problem by just keeping one of the objective functions and restricting the rest objective functions within user-specified values. This approach will alleviate the difficulties that weighted sum method faced in solving problems with nonconvex objective spaces. Since both of the objective functions in this problem are convex functions, there is no advantage between these two methods and the weighted sum method when used to solve this optimization problem. In the above optimization problem, the optimal number of sensors (N) is the design variable. The optimization constraints include the maximum number of sensors (N_{max}) which is related to the number of finite element nodes and is governed by the FE model resolution. Once the optimal number of sensors (N) in the sensor network is determined, the probabilistic approach explained above for allocating these sensors can be implemented.

4.2.2 Redundancy of sensor network

The challenge with optimal sensor networks is the need to ensure network robustness. A robust sensor network shall operate efficiently even after losing one or more sensors. This goal can be achieved by identifying the location of the critical sensors. Redundant sensors shall be used at these critical locations. Here we suggest using '*leave one sensor out analysis*' to examine sensor network sensitivity after Satelli et al. (2000). In this analysis, the critical sensor location is related to the significance factor (ψ_i) defined as

69

$$\psi_i = \frac{\left| \Phi_{opt} - \Phi_i \right|}{\Phi_{opt}} \times 100 \qquad (4.4)$$

Where Φ_{opt} is the mean value of the damage feature computed for the optimal sensor network with the minimum required number of sensors and Φ_i is the mean value of the damage feature computed for optimal sensor network after removing the *i*th sensor from the network. The critical sensors are those with the maximum significance in the network performance compared with its original performance.

4.2.3 Validation of the proposed method

To demonstrate the ability of the proposed method in enhancing damage detection, the probability of detection (POD) is defined as a probability that specific damage can be detected by the sensor network in the structure. We define a threshold value Φ_α for a given damage level (α). The damage feature is assumed to be normally distributed, thus the probability that the damage feature is less than the damage threshold ($\Phi \le \Phi_\alpha$) can be described as

$$P\left(\Phi \le \Phi_\alpha\right) = \int\limits_{0}^{\Phi_\alpha} \frac{1}{\sigma_H \sqrt{2\pi}} e^{\frac{-(\Phi - \Phi_H)^2}{2\sigma_H^2}} \qquad (4.5)$$

Where Φ_H and σ_H are the mean and the standard deviation for the healthy damage feature values and Φ_α is the threshold value that is a function of damage severity (α) level as shown in Figure 4-1 .
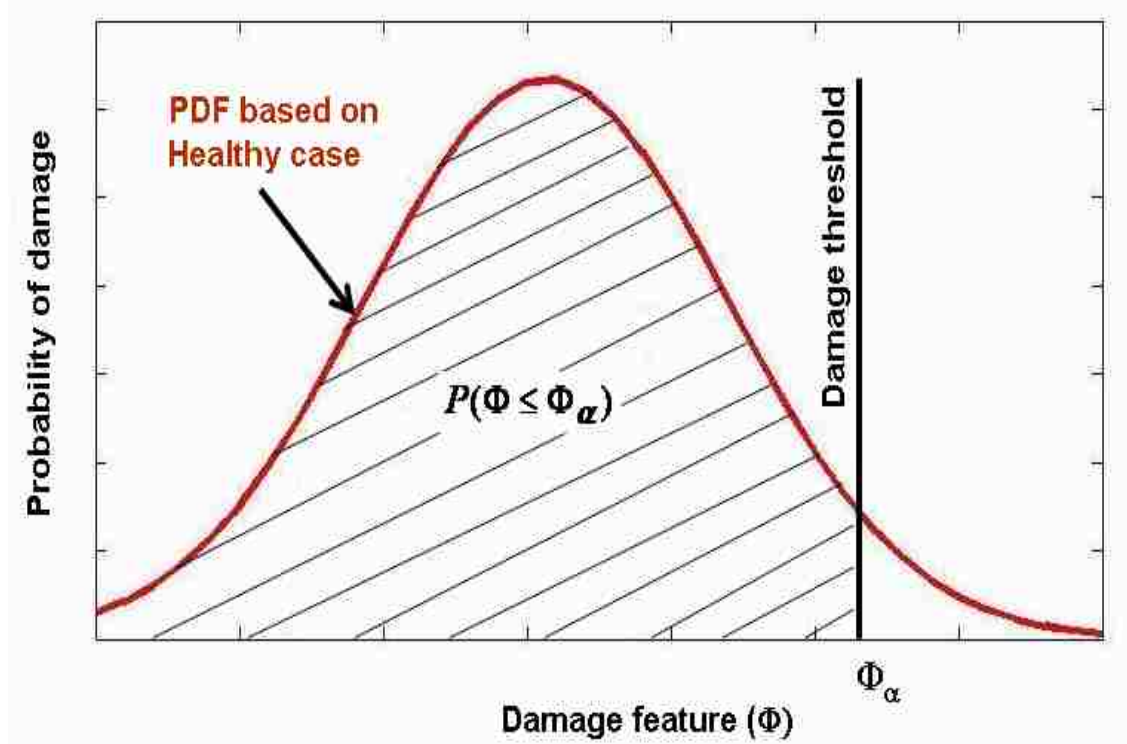
Figure 4-1 Normal distribution of the damage feature showing the damage threshold.

Using the above approach, a damage feature threshold (Φ_α) for a specific level of damage can be computed. To validate the efficiency of the proposed optimal sensor network, the POD is defined as

$$POD = \frac{N(\Phi_{mean} \geq \Phi_\alpha)}{N_{total}} \tag{4.6}$$

Where $N(\Phi_{mean} \geq \Phi_\alpha)$ is the number of simulations where the sensor network was capable of identifying the damage in the structure correctly (i.e. with a mean damage feature higher than the damage threshold). N_{total} is the total number of simulations performed.

71

4.3 Case Study

The proposed method is applied to identify the optimal number of sensors and their locations to monitor the Luling Bridge located over the Mississippi River in St. Charles Parish near New Orleans in Louisiana. The Luling Bridge has been in service since 1984. This bridge was selected to demonstrate the efficiency of such approach for long span cable-stayed bridges that would require large numbers of sensors for structural health monitoring. As-built drawings of the bridge were used to establish the FE model. The cable-stayed spans of the bridge, including three spans 151 m, 372 m and 155 m were modeled for the design of a SHM system. The bridge is 23 m wide. The bridge cross-section consists of two steel box girders that are 2.5 m high, 7 m and 3 m wide at top and bottom flanges respectively. The thickness of the web is 12 mm and the thickness of flanges is 20 mm. A concrete deck (200 mm) is cast on the top of cross section to allow composite action. To hold the main 372 m span, 72 cables, attached to the top of two 122 m high towers, were installed. Each cable is a 7 (6.35 mm) wire strand cable with each wire developing an ultimate strength of 1665 MPa. Figure 4-2 shows Luling Bridge during construction. Figure 4-3 illustrates the structural configuration of Luling Bridge showing longitudinal and cross sections.

Figure 4-2 Luling Bridge during construction.

(a)

(b)
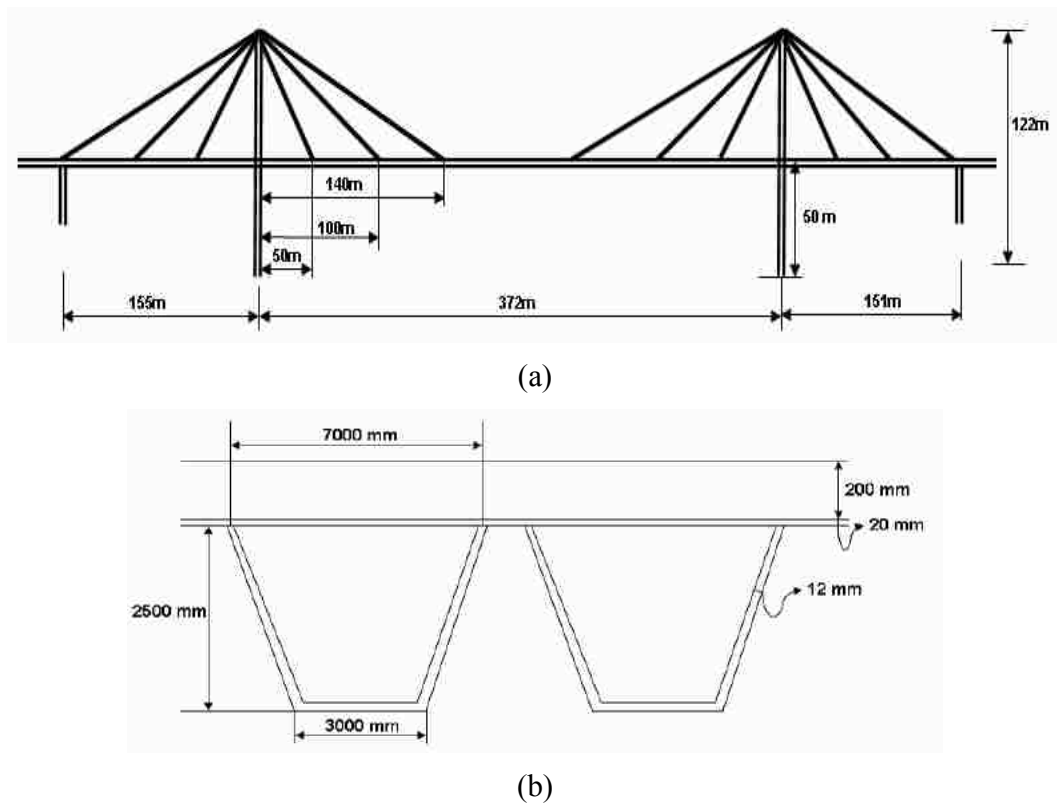
Figure 4-3 Luling Bridge (a) configuration and (b) cross section.

73

A FE model of the cable-stayed spans of the bridge was developed. The FE model includes 226 frame elements, each 3 m long. The frame elements were used to model each girder. Shell elements were used to model the bridge deck. Finally, cable elements were used to model the cables in the bridge. Figure 4-4 shows the 3D FE model of the Luling Bridge.
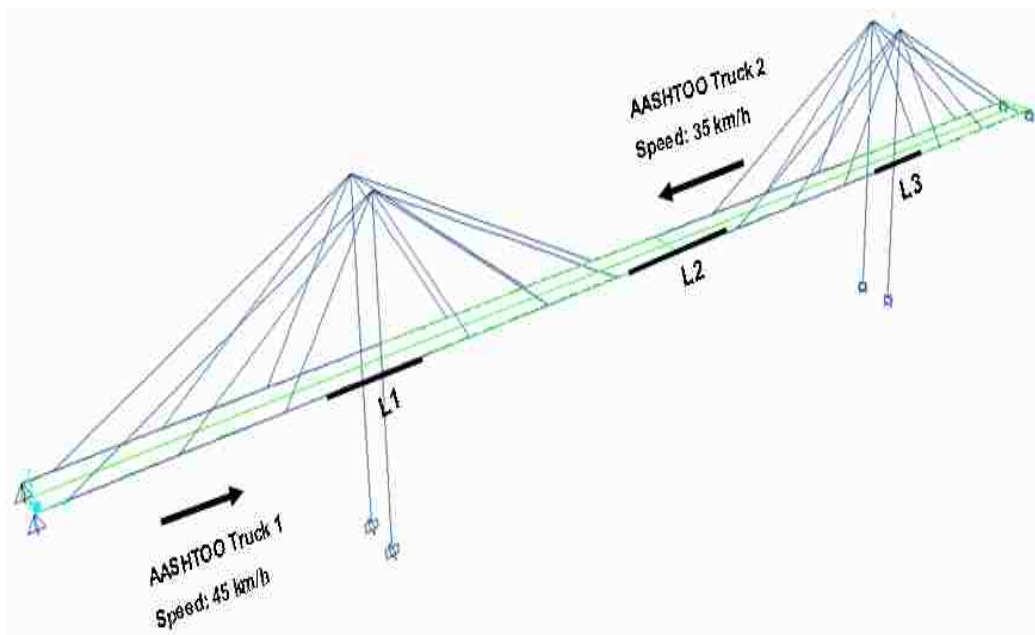
Figure 4-4 FE model of the Luling Bridge with damage locations.

A time history loading function with trapezoidal time-step shape that has 0.15 seconds duration was used to model the traffic loading on the bridge. The trapezoidal loading function simulates two HL-93 trucks according to the American Association of State Highway and Transportation Officials (AASHTO 2006) moving with 35 km/h and 45 km/h in opposite directions on the bridge. The FE model was developed in SAP2000®.

74

The acceleration signals at the structural nodes in z-direction were evaluated using the FE model. The energy of the acceleration signal released at the nodes (assumed to be the sensor location) was calculated. This energy has been shown by Reda Taha et al. (2004) and Kumara et al. (1999) to be related to the structural damage and thus can be used as a damage feature for damage detection. The energy of the acceleration signal can be calculated as

$$\Phi_i = \sum_{t=1}^{T} \varepsilon\left[a_{zi}^{2}(t)\right] + \varepsilon^2\left[a_{zi}(t)\right] \tag{4.7}$$

In Equation (4.7), Φ_i is the energy of the ith accelerometer, $a_{zi}(t)$ is the z-axis direction acceleration measured at accelerometer i, ε is the expected value, t is time instant and T is the time window width. 5% noise was added to the FE simulation data to simulate field data. Three damage locations (L_1, L_2 and L_3) on the first Girder illustrated in Figure 4-4 were considered as possible locations of damage on the bridge based on the maximum stress due to maximum bending moment. Two different levels of damage, D_1 and D_2 representing 40% and 50% loss in stiffness of the girder were considered at each damage location. Due to the size of the bridge considered in the case study, relatively large loss of stiffness of the first girder is required to enable damage detection using the sensor network. To train the ANN, the damage features Φ_i and the three associated locations for damage level D_2 were considered. The training process was repeated 10 times to obtain non-biased ANN weights. Non-normalized weights of ANN are shown in Figure 4-5. The ANN weights were normalized to establish the discrete PDF. The continuous PDF was established by considering interpolation function. Figure 4-6 illustrates the continuous

75

PDF. The POD for the optimally allocated sensors is computed and compared to uniformly distributing these sensors.
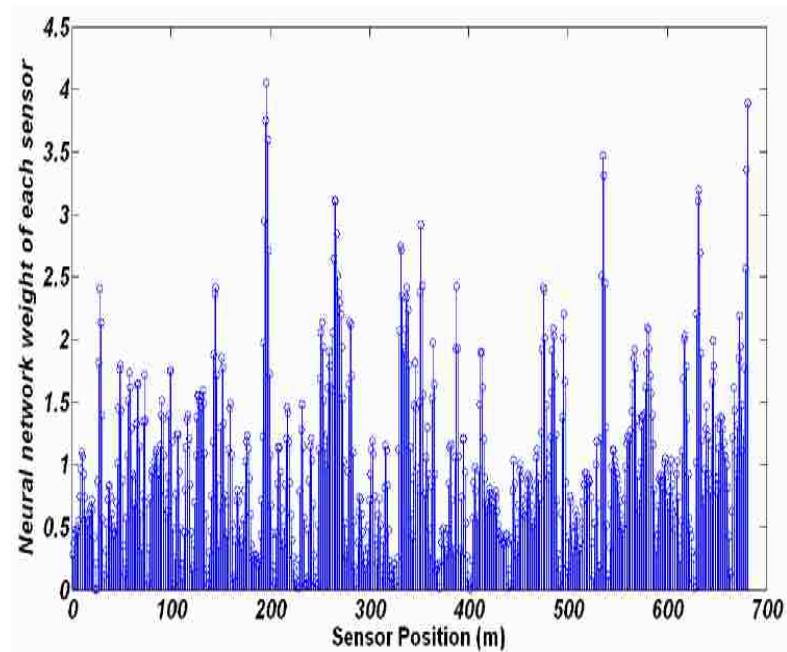
Figure 4-5 Weights of each sensor obtained from ANN.
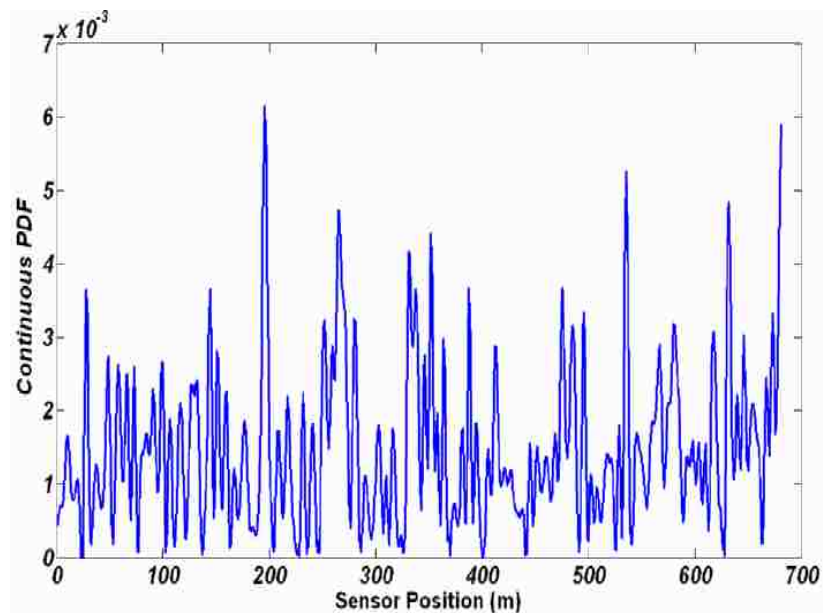
Figure 4-6 Continuous probability distribution function (PDF).

76

4.4 Results and Discussion

By sampling the continuous PDF shown in Figure 4-6 for any given number of sensors, the optimal sensor locations on the first girder of the bridge can be identified. Table 4-1 presents the optimal sensor locations for 100 sensors (number arbitrarily chosen) distributed over the first girder. Distribution of 50, 100, 150 and 200 total sensors were calculated. Only the distribution of 100 sensors is presented here for space limitation.

Table 4-1 Optimal locations of 100 sensors on the first girder of the Luling Bridge identified using the probabilistic method

Sensor Number	Sensor Location (m)									
S1-S10	3	6	9	15	27	30	33	36	45	48
S11-S20	54	60	63	75	78	81	84	87	114	117
S21-S30	123	126	132	135	138	141	144	156	159	162
S31-S40	165	168	174	177	186	195	210	213	216	225
S41-S50	246	255	264	282	285	291	294	303	324	336
S51-S60	345	351	369	375	381	405	408	411	414	420
S61-S70	423	450	453	459	465	468	474	477	492	501
S71-S80	507	510	513	516	519	522	525	528	531	537
S81-S90	540	570	573	576	579	582	585	588	594	597
S91-S100	606	609	618	621	627	630	639	645	654	666

77

Figure 4-7 represents the POD values for detecting severe damage for 50, 100, 150 and 200 sensors compared to uniform distribution of sensors. It is evident that the proposed method always achieved a higher POD than uniform distribution of sensors.
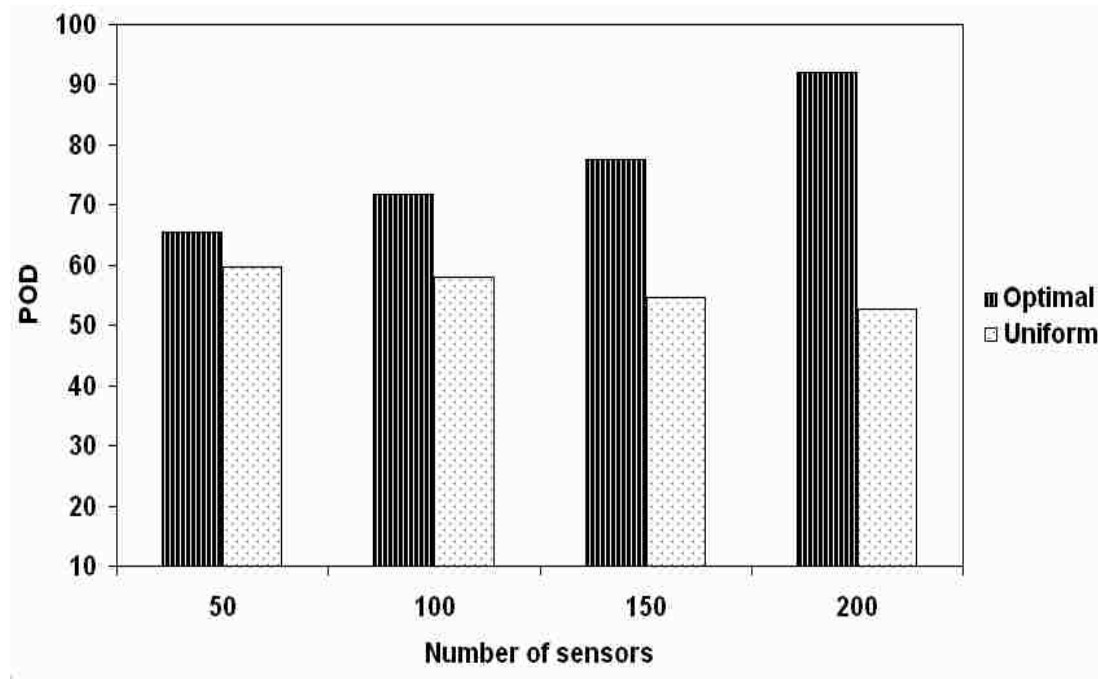
Figure 4-7 Probability of detection (POD) versus number of sensors for optimal versus uniform distribution of sensors (Azarbayejani et al. 2009).

The two objective functions for the information entropy and the sensor network cost were evaluated. Weighted sum method, as described earlier in this chapter, was used to solve this multi-objective optimization problem. Two objective functions were weighted equally to establish the global objective function. Here we used derivative-based optimization methods to find the optimal number of sensors. Levenberg-Marquardt which is one of the modified Newton's methods was used to find the optimal number of sensors by minimizing the global objective function. The Pareto front of the two objective

78

functions is shown in Figure 4-8. An optimal solution that satisfies both functions lies at the zone indicated in Figure 4-8. The optimal solutions in the Pareto front achieve the balance between the two objective functions. It can be concluded from Figure 4-8 that 85 sensors will be able to monitor the bridge efficiently while minimizing the sensor network cost and monitoring uncertainty.
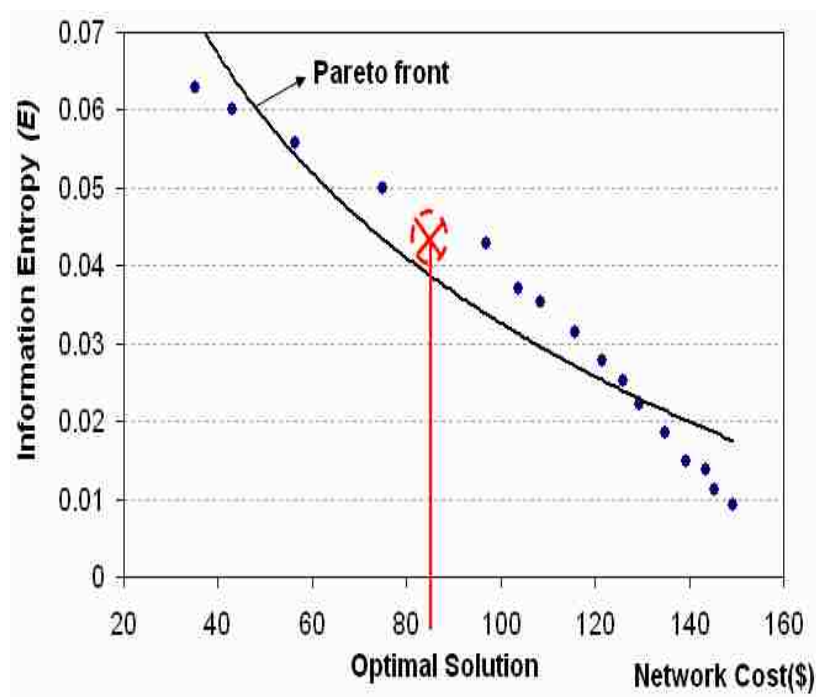
Figure 4-8 Information entropy versus sensor network cost functions showing the Pareto optimal solutions in the marked area (Azarbayejani et al. 2009).

Sampling the continuous PDF with 85 sensors, the optimal locations of 85 sensors are presented in Table 4-2. We repeated the process by slightly changing the damage level from 50% to 40% and by considering a constant noise to the signal ratio. These changes did not affect the results of the optimization process.

79

Table 4-2 Optimal locations of 85 sensors on the first girder of the Luling Bridge identified using the above proposed method

Sensor Number	Sensor Location (m)									
S1-S10	6	12	21	33	36	39	42	84	87	93
S11-S20	96	99	105	108	126	129	132	135	138	153
S21-S30	165	180	183	201	204	219	222	225	231	240
S31-S40	246	270	273	276	291	297	300	318	327	333
S41-S50	336	339	342	348	354	357	363	366	369	378
S51-S60	381	399	417	423	438	447	450	471	474	480
S61-S70	483	489	492	513	516	528	537	543	546	549
S71-S80	552	555	558	564	567	588	591	594	597	624
S81-S85	636	645	654	663	669					

Finally, the critical sensor locations can be identified by calculating the significance factor using Equation (4.4). Figure 4-9 illustrates the significance factor for the 85 optimal sensors. It can be observed that sensors 43-45 and 55-60 seem to be the most critical sensors. It is also evident that sensors 11, 12, 13 and 65 seem to have minimal effect of the sensor network robustness. It is worth noting that redundant sensors shall be used in the locations of significant sensors.

80
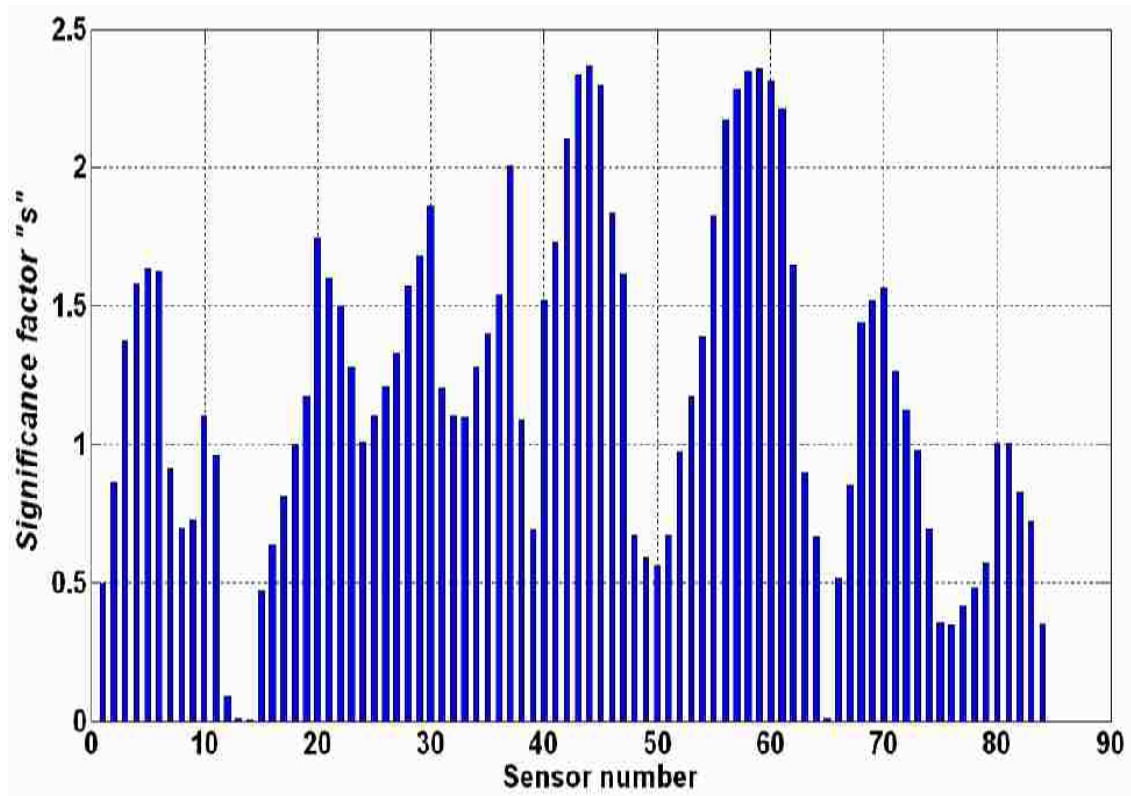
Figure 4-9 Significance factor for each sensor of the sensor network shows critical sensors for sensor network robustness with high significance (Azarbayejani et al. 2009).

4.5 Conclusion

In this chapter, we introduced an entropy-based multi-objective optimization approach to identify the optimal number of sensors for large sensor networks for SHM. The multi-objective optimization approach combines an entropy-based objective function to represent monitoring uncertainty and a sensor network cost function for cost limitations. The optimal number of sensors can be distributed on the structure using a probabilistic approach that is based on identifying location importance using knowledge on common damage locations. The proposed approach utilizes an artificial neural network which is

81

trained based on *a priori* knowledge about damage locations and severities and selected damage features. Unlike other methods described in the literature, the proposed method does not rely on a specific damage feature and is also able to address the redundancy of the sensor networks. The proposed method was applied to find the optimal sensor network for the Luling Bridge, a long cable-stayed bridge over the Mississippi river. The optimal number of sensors and their locations are identified. The significance of sensors was also examined using 'leave one sensor out' analysis.

Identifying optimal number and location of sensors in a sensor network, this chapter completes the previous chapter which only considered optimal location of a given number of sensors. In the next chapter, a complete SHM system is designed and implemented on a field application of an RC bridge located at Tucumcari, New Mexico.

CHAPTER 5 DESIGN AND FIELD APPLICATION OF AN INNOVATIVE SHM SYSTEM FOR MONITORING OF RC BRDIGES ON INTERSTATE 40 AT TUCUMCARI, NEW MEXICO

5.1 Introduction

The purpose of this chapter is to report on the design of an innovative structural health monitoring (SHM) system designed to provide continuous monitoring of the reinforced concrete (RC) bridge, Bridge 7937, in Tucumcari, New Mexico. Bridge 7937 was first strengthened with carbon fiber reinforced polymer (CFRP) laminates at one weak area on the bridge as a showcase strengthening project. The detailed design of CFRP sheets are also mentioned in this chapter using a 2D finite element (FE) model of the girder which CFRP sheets are attached to it. The effectiveness of the CFRP laminates was tested by a field test. The SHM system was designed to monitor the structural performance of the bridge. The proposed monitoring system's calibration and effectiveness in detecting damage is examined on a prototype truss bridge built in the Structural Engineering Laboratory at University of New Mexico (UNM). Moreover, a 3D FE model of the bridge was developed and calibrated using the static field test data. The vibration data measured from the bridge after installing the SHM system was compared with that predicted using the FE model.

83

Using principles of inductive reasoning and fuzzy set theory, fuzzy damaged sets were established. That included the known healthy state of the bridge and the damaged states of the bridge using data extracted from the 3D FE model. Unknown states of the bridge based on different datasets from field measurements could then be classified using principles of fuzzy pattern recognition. The following sections describe all the details of the proposed monitoring system and the calibration process.

5.2 Bridge description and design of CFRP sheets

Bridge 7937 on Interstate 40 (I-40) in the city of Tucumcari, New Mexico was selected for implementation of the monitoring system. As shown in Figure 5-1 and Figure 5-2 , the bridge consists of five reinforced concrete K-Frame girders. The K-Frames form three spans; 42 ft, 104 ft and 42 ft. Each K-frame has a rectangular reinforced concrete cross-section whose depth varies along the length of the bridge. This RC bridge has been conveying a large amount of traffic from New Mexico to Texas and vice versa for more than twenty years. Asphalt overlay is used on the top of Bridge 7937. Moreover, the longitudinal and transverse reinforcements vary along the length of the bridge. Figure 5-3 illustrates the cross section and the longitudinal and transverse reinforcements of this bridge.

Figure 5-1 Bridge 7937 at Tucumcari.

Figure 5-2 K-Frames of Bridge 7937.
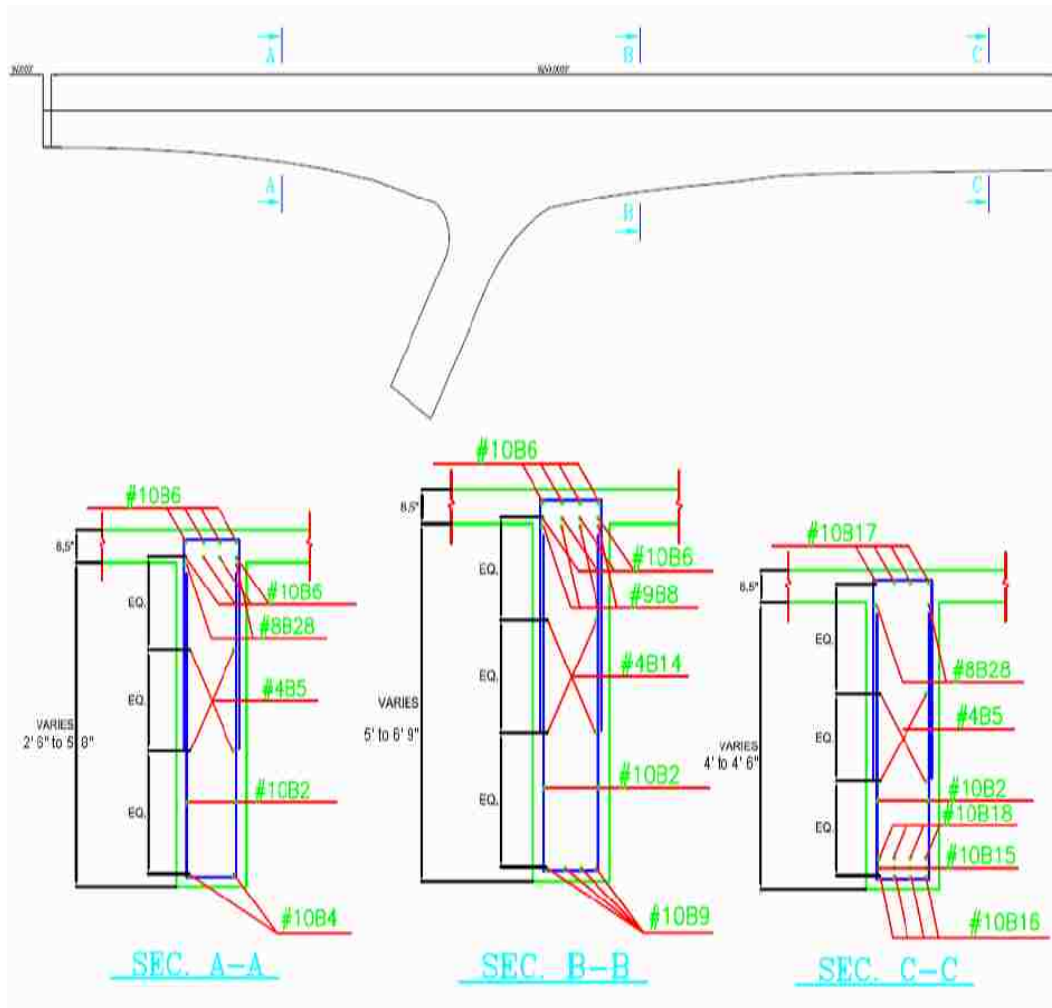
Figure 5-3 Schematic of as built structural drawing of Bridge 7937.

During the last two decades since the bridge was constructed, the size and weight of trucks passing over I-40 have increased dramatically. Based on AASHTO 2006 (AASHTO 2006), it is expected that the moment and shear demand of the current traffic load might exceed bridge capacity. Four different types of New Mexico legal trucks were used in the FE analysis, in addition to a design truck by AASHTO and tandem load. These four trucks included New Mexico Department of Transportation (NMDOT) two-axle legal load truck, NMDOT three-axle legal load truck, NMDOT five-axle legal load

86

truck, and NMDOT permit truck P327-B. Characteristics of each truck including axle loading are presented in Figure 5-4. Moreover, the distance between the two 145,000N axles in the AASHTO design truck was used as a variable from 4.3 m to 9.0 m as specified in AASHTO (2006).
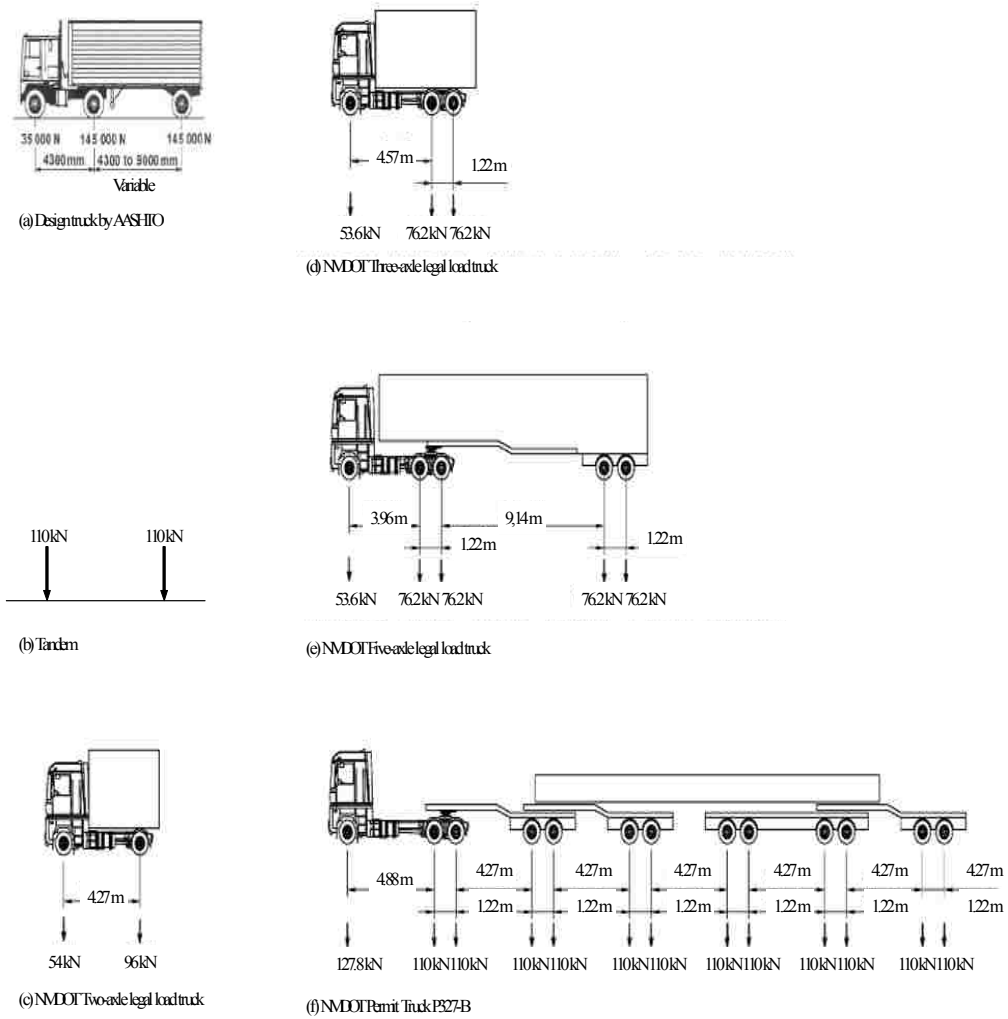
Figure 5-4 Characteristics of the trucks used in FE analysis.

Furthermore, a 9.3 kN/m, uniformly distributed design lane load in the longitudinal direction was also considered as specified by AASHTO (2006). The dynamic load

87

allowance was computed to be (1.33) and was applied to the truck and tandem loads to consider the dynamic effect of traffic load. Finally, dead loads including self weight of the K-frames, concrete deck weight, rail load and asphalt weight were also included in the FE analysis. In computing the total load on each K-frame of the bridge, since a 2D FE model was used, traffic load distribution between the frames needed to be calculated. The load distribution factors of the exterior and interior frames were computed separately. For exterior K-Frames the load distribution factor was considered one based on number of lanes, which were two for this bridge. For interior K-Frames the load distribution factor is different, but because CFRP laminates were designed only for the exterior frame, the interior load distribution factors were not calculated.

5.2.1 Finite Element (FE) analysis

Static structural analysis was performed for the exterior K-frame of Bridge 7937. Considering the diaphragm action of bridges due to transverse beams and deck, each K-frame was analyzed as a separate frame instead of using entire bridge model. Then, the load distribution between each frame was considered by using load distribution factors. In general, bridge structures are analyzed assuming linear elastic behavior unless cracking was evident. No indication of cracks in the K-frames indicated the need for cracked/non-linear analysis. Therefore, according to AASHTO, the elastic material behavior was assumed in the FE analysis and the stiffness of the girder was calculated using uncracked cross-section. Moving load analysis for live load was considered to identify the maximum effect of all moving loads considered in the analysis. Figure 5-5 shows the FE model used in SAP 2000®. 58 nodes and 12 nodes were used to model the girder and inclined columns respectively. Also 57 and 12 frame elements were used to

model the girder and inclined columns respectively. The girders and the columns were assumed to be monolithic and therefore enabling moment transfer. At each node, the FE model has the same depth of real K-frames shown in drawing.
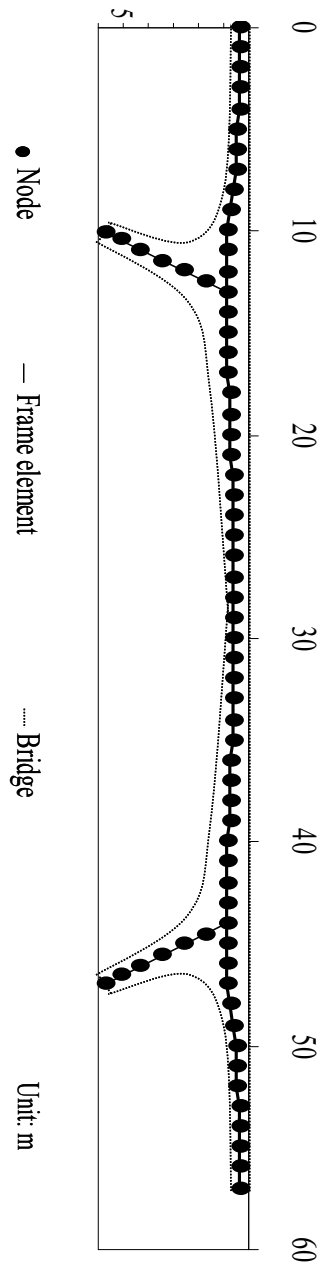
Figure 5-5 FE model showing nodes and frame elements.

89

The final shear and moment effects from all load cases were obtained from SAP 2000®. These values need to be combined to represent the final straining action affecting the bridge structure. Based on AASHTO (2006), several load combinations were considered. This includes *Strength I* and *Strength II* load combinations which can be described as

Strength I

Factored load = 0.9*(Self weight of girder and deck load) + 0.65*(Asphalt and railing) + 1.75*Maximum moving loads and design lane load   (5.1a)

Strength II

Factored load = 0.9*(Self weight of girder and deck load) + 0.65*(Asphalt and railing) + 1.35*Maximum moving loads and design lane load   (5.1b)

Here, "*maximum moving loads and design lane load*" was defined as the maximum moment (or shear) of moving trucks and tandem plus design lane load. According to AASHTO, *Strength I* and *II* combinations include the basic load combination relating to the normal vehicular use of the bridges without wind and load combination relating to the use of the bridge by owner-specified special design vehicles, evaluation permit trucks, or both without wind. Therefore, in *Strength I*, AASHTO design truck and tandem load were considered in calculation of "maximum moving loads and design lane load" while in *Strength II*, in addition to AASHTO design truck and tandem load, NMDOT legal trucks (two-axle legal load truck, NMDOT three-axle legal load truck, NMDOT five-axle legal load truck, NMDOT permit truck P327-B) were considered. Figure 5-6 and Figure 5-7 show the moment and shear distribution of an exterior beam of Bridge 7937 for

several sources of loading: self weight of girders, deck, design truck by AASHTO, tandem, and NMDOT permit truck P327-B.

(a) Moment distribution due to self weight of a girder

523.1 kNm

(b) Moment distribution due to deck

357.2 kNm

(c) Moment distribution due to design truck by AASHTO

773.1 kNm

(d) Moment distribution due to tandem

848.1 kNm

(e) Moment distribution due to NMDOT Permit truck P327-B

1698.4 kNm
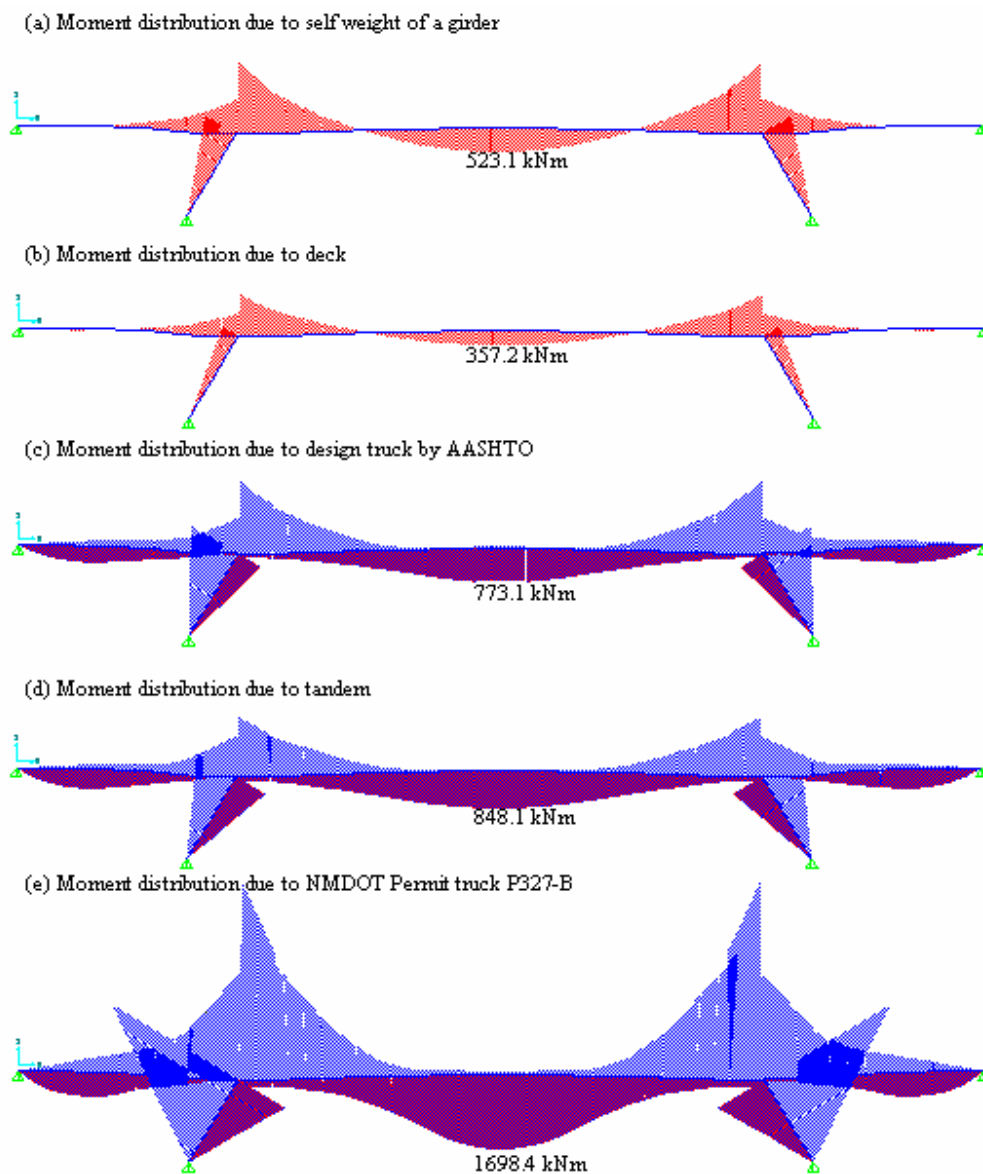
Figure 5-6 Moment distribution of an exterior beam of Bridge 7937.

91

(a) Shear distribution due to self weight of a girder

362.8 kN

(b) Shear distribution due to deck

216.5 kN

(c) Shear distribution due to design truck by AASHTO

417.7 kN

(d) Shear distribution due to tandem

292.2 kN

(e) Shear distribution due to NMDOT Permit truck P327-B

1019.1kN
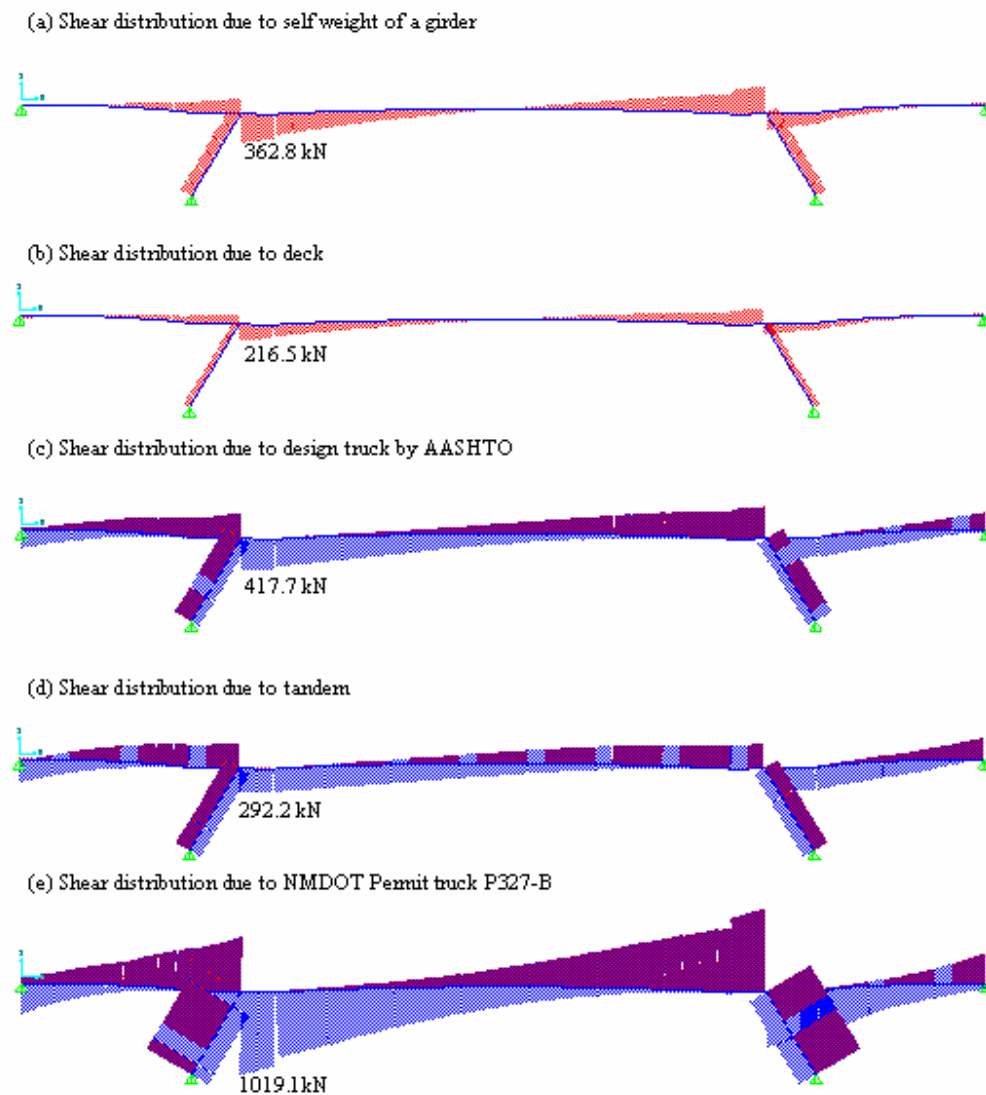
Figure 5-7 Shear distribution of an exterior beam of Bridge 7937.

5.2.2 Design of CFRP sheets

According to the results of FE analyses performed, it was found that the exterior girders of Bridge 7937 showed shortage in negative moment capacity around the K-frame connections. Therefore, it was therefore recommended to strengthen this bridge using

92

Fiber Reinforced Polymer (FRP). More details about calculating the shortage in negative moment capacity can be found in Reda Taha et al. (2007) report. The moment resistance to be provided by FRP is calculated as

$$M_u - \phi M_n \leq \phi M_{frp} \tag{5.2}$$

where: M_u = factored applied moment, M_n = nominal moment-carrying capacity

and ϕ is the moment reduction factor.

In ACI 440 (2002), ϕM_{frp} is evaluated as

$$\phi M_{frp} = \phi \varphi_{frp} A_f E_f \varepsilon_{fe} \cdot jd \tag{5.3}$$

where: φ_{frp} = additional reduction factor (=0.85), A_f = area of FRP reinforcement

ε_{fe} = effective ultimate strain developing at FRP, E_f = Young's modulus of FRP

jd = length of moment arm.

The ACI 440 (2002) design method for FRP strengthened sections is basically similar to ACI 318 design method, which is based on strain-compatibility and equivalent concrete stress block (refer to Figure 5-8). In this design, it is assumed that the existing strain is negligible compared with ultimate design strains. Moreover, considering the fact that no tension cracks were observed in the top of the K-frame in the field inspection before strengthening, the existing service strains can be considered negligible. Therefore, the effective strain of FRP at ultimate state is defined as
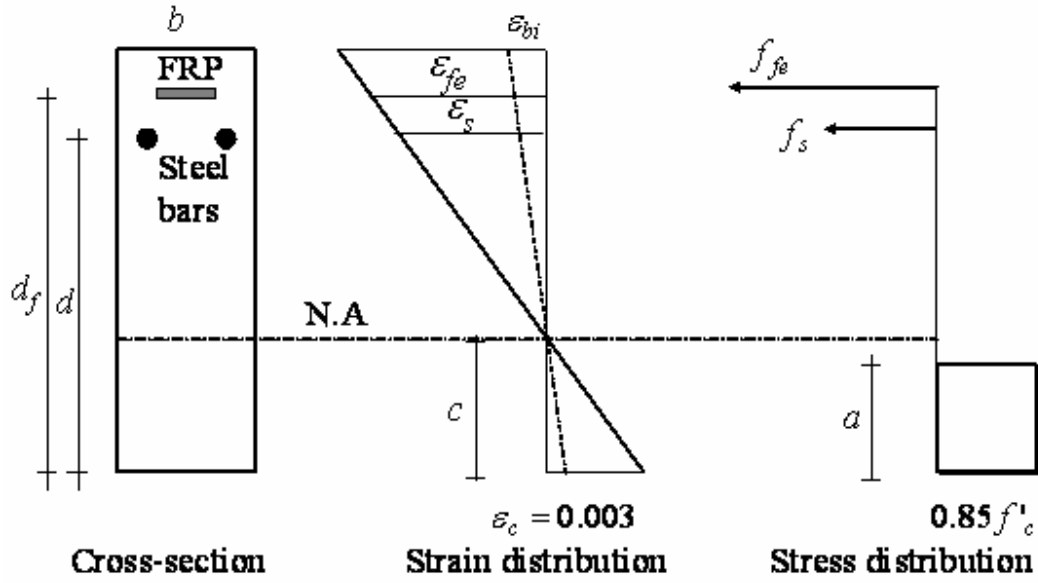
Figure 5-8 Stress and strain distribution of the concrete beam strengthened by FRP.

$$\varepsilon_{fe} = 0.003 \left(\frac{d_f - c}{c} \right) \leq \kappa_m \cdot \varepsilon_{fu} \qquad (5.4)$$

where: d_f = effective depth for FRP reinforcement, c = depth of compression zone

κ_m = bond-dependent coefficient for flexure (=0.9 for CFRP based on ACI 440 (2002))

ε_{fu} = design rupture strain of the FRP reinforcement.

According to the results of FE analysis for the exterior girder of Bridge 7937 the maximum shortage of negative moment capacity ($M_u - \phi M_c$) is 3,788 kN.m at the connection (x = 17 m) as shown in Figure 5-9. Moreover, Appendix A presents the factored moment and shear demand and the corresponding factored cross sectional capacity each 1 m along the bridge length for this bridge.

94
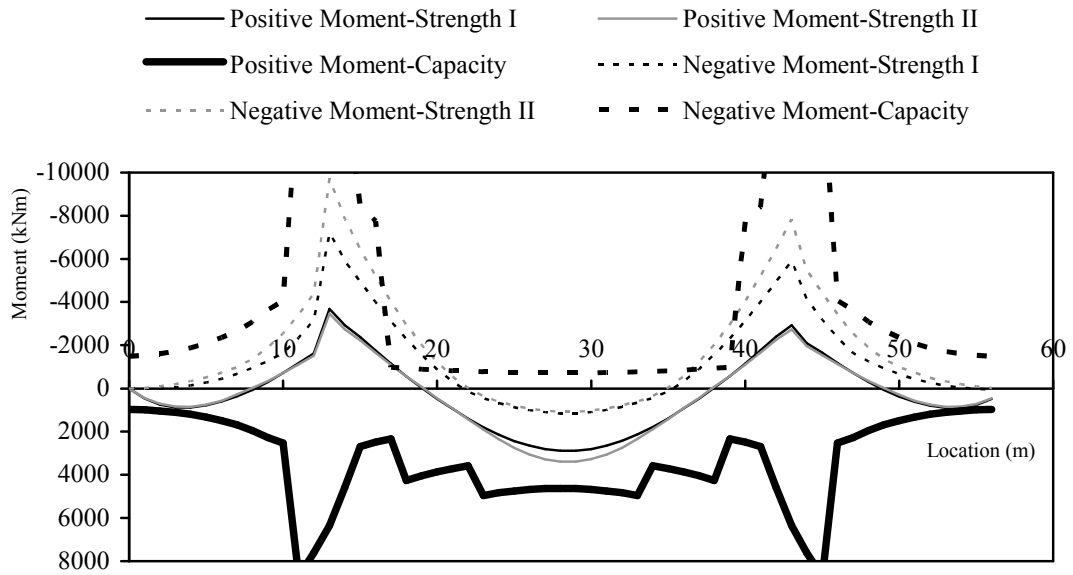
Figure 5-9 Factored moment and capacity of exterior beam of bridge 7937.

From Equations (5.3) and (5.4), the required amount of FRP reinforcement can be evaluated as:

$$A_f = \frac{M_u - \phi M_c}{\kappa_m \cdot \varepsilon_{fu} E_f \phi \varphi_{frp} \cdot jd} = \frac{3788}{0.9 \cdot 0.0134 \cdot 150000 \cdot 0.85 \cdot 0.85 \cdot 0.9 \cdot 1.8} \times 1000 = 1789 \, mm^2 \quad (5.5)$$

Here, we use CFRP for its enhanced strength and durability with a Young's modulus of $E_f = 150,000 \, MPa$ and an ultimate strain capacity of $\varepsilon_{fu} = 0.0134$. Moreover, it is assumed that the moment arm after application of FRP is jd to be $0.85d$. Based on the calculation, CFRP needs to be applied between $x = 16.2$ m (53 inch) and 20.1 m (66 inch) from the west side of the bridge. The required area of CFRP reinforcement shall be used for each K-Frame at both connections. Here, in strengthening Bridge 7937, we will reinforce one K-joint on one K-Frame only for the proof of method efficiency. NMDOT will strengthen the full bridge at a later time when more funding becomes available. The

amount of CFRP reinforcement area required for strengthening one K-frame at the K-connection on Bridge 7937 can be provided by means of 4 strips of CFRP plates, whose cross-section of CFRP strips is 1.52 mm thick (0.06 inch) and 305 mm (1 feet) wide. Since FRP strips are not manufactured in 11 foot lengths to cover the entire application zone, it was decided to overlap the FRP strips using two 1.83 m (6 feet) FRP strips. The CFRP strips are therefore lap spliced to cover the entire strengthening zone. To ensure the performance of spliced FRP strips, the lap splice location was alternated along the strengthening area such that no single section has more than two lap splices. The schematic layout of CFRP strips designed for the exterior girder of Bridge 7937 at Tucumcari is shown in Figure 5-10.
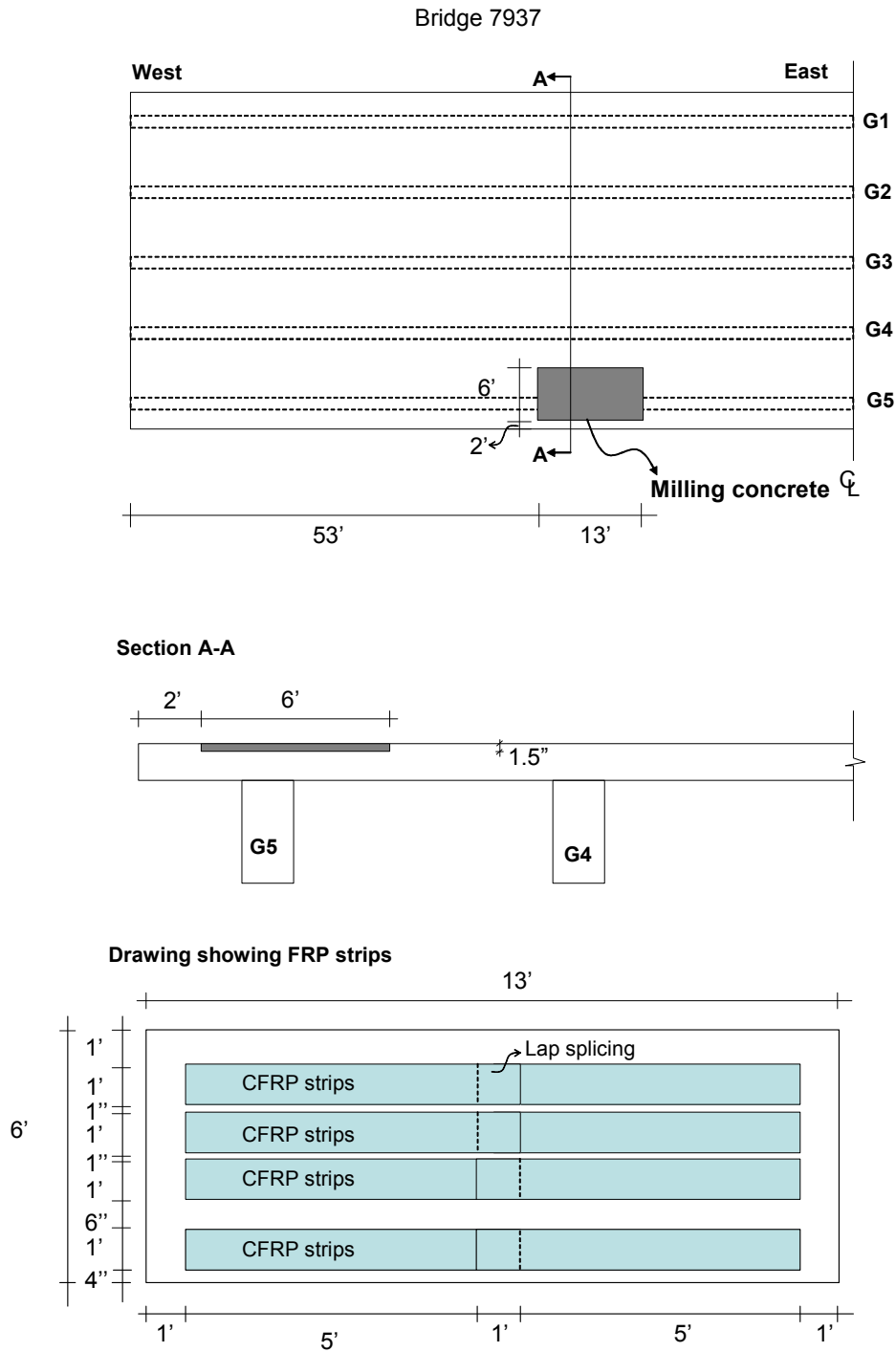
Bridge 7937

Figure 5-10 Schematic figure shows the layout of four CFRP strips for strengthening the exterior girder of Bridge 7937.

97

5.2.3 Installation of CFRP plates on Bridge 7937

The application of FRP strips to an exterior girder of Bridge 7937 as an example case for FRP strengthening application was performed by the UNM team with cooperation of NMDOT in Tucumcari. It is worth noting that in the strengthening work of the bridge using FRP strips, several different types of materials were used: putty, epoxy and FRP. Therefore, the manufacturers' specifications of each material were considered in this installation. Moreover, the different material specifications were checked with the AASHTO and ACI code requirements for FRP materials.

- **Step 1: Concrete surface milling**

As the bridge deck surface of the exterior girder of Bridge 7937 is concrete, it needed to be milled to enable application of the CFRP strips. The milling process is shown in Figure 5-11. The strengthening zone was marked first and then milled by a concrete milling machine attached to a wheel loader. The milled area was cleaned using air blowers and construction vacuum as shown in Figure 5-12. To obtain a surface with equal milling, the milling process was repeated twice.

Figure 5-11 Concrete surface milling showing the process of marking the zone and milling.

Figure 5-12 Concrete surface cleaning.

- **Step 2: Concrete surface preparation**

The second step was to prepare the concrete surface. We started by establishing an even surface with thickness differences less than 4 mm (ACI 440, 2002 and CEB-FIP, 2001). Moreover, surface cracks formed due to the milling process were filled with putty materials and the surface was made even. An even surface is essential to enable good bond between concrete substrate and the FRP strips. To obtain an acceptable level of surface evenness, the concrete surface was first covered with a putty material in accordance with ACI 440 and AASHTO recommendations. The putty was applied to the application locations as shown in Figure 5-13 and then left to dry and bond to the concrete surface. It took one week for the putty to dry before applying the CFRP strips. Putty drying normally takes around two weeks, but it took less time because of the hot temperature on the bridge deck (around 100 $^{\circ}$F). Moreover, at the locations where putty application was found to be too thick, the redundant putty was removed by grinding before FRP application.

99

Figure 5-13 Application of putty material to obtain even concrete surface.

- **Step 3: Implementing FRP strips on Bridge 7937**

After the concrete surface was readied for implementing FRP strips, the epoxy composed of resin and hardener was mixed in order to obtain the required bond strength. The specific mixing ratio (5 to 1) of resin and hardener was used according to the specification of the materials as shown in Figure 5-14. After mixing the resin and hardener to 80% of the allowable working time (pot life), the FRP plates were attached on the deck surface. The pot life for the epoxy used was 20 to 25 minutes which represented enough time to lay down the FRP strips on the locations identified on the bridge deck slab. Moreover, it is important to note that the epoxy hardening time is also a function of the temperature at time of mixing. Manufacture's specifications need to be considered carefully. It is also noted that during the hardening process (chemical

reaction), epoxy becomes extremely hot, requiring special care from those applying it to the concrete surface.

Figure 5-14 Mixing resin and hardener according to specific mixing ratio.

Immediately after applying epoxy to the concrete surface, the CFRP strips were applied considering the locations marked and the lap splice alternating arrangement as shown in Figure 5-15. Because of the short pot life of the epoxy, it is recommended to mix enough resin and hardener to facilitate the application of one line of FRP strips at a time.

Figure 5-15 FRP strips attached to the concrete surface.

101

After applying the FRP strips, as shown in Figure 5-16, additional pressure was applied on FRP sheets for better attachment to the concrete surface. This pressure was also used to protect the location of the applied FRP strips against the significant wind currents at the top of the bridge deck.

Figure 5-16 Applying pressure for better attachment of FRP strips.

- **Step 4: Curing and finishing**

After applying CFRP, the construction site was properly covered by plastic sheets to prevent exposure of the CFRP to rain and water. When the epoxy was fully hardened (two weeks after attaching CFRP sheets to the concrete surface), the construction site was covered by a cold dry asphalt mix. The use of a dry asphalt mix was to prevent FRP direct exposure to moisture, rain or traffic. This will also enable accessibility of the FRP surface during the next phase of the project, which entailed field testing and the installation of monitoring sensors.

5.2.4 Field testing and examining FRP effectiveness

To validate the analytical prediction by the FE model, a field load test was performed before and after the application of CFRP strips. First, the concrete strain of the top of the exterior girder was monitored when subjected to a test truck with pre-determined weight of 50 Kips as shown in Figure 5-17. Moreover, after the application of CFRP strips, the strain on the top of the CFRP strips was monitored using the same test truck and weight. The ability of the CFRP strips to attain strain values close to those observed at the concrete surface prior to strengthening ensured that the CFRP strips were properly attached to the concrete surface based on strain compatibility at the same location. Figure 5-18 shows the FE model of the exterior girder subjected to the truck load and the moment distribution obtained from the FE analysis. It is noted that in this analysis the bridge deck was taken into account in the calculation of effective width of the girder assuming elastic behavior during the loading test. This can be justified by the fact that the load of the test truck was significantly lower than the load carrying capacity of the bridge and thus the bridge behavior can be considered to follow linear elastic behavior. To compensate for the temperature effect, orthogonal strain gauges were placed as dummy gauges. The longitudinal gauges were used to measure the load effect and the dummy strain gauges were used to compensate temperature effects. Figure 5-19 shows the strain gauges attached to the concrete surface as well as to the FRP strips. Figure 5-20 presents a schematic location of strain gauges on FRP strips.

103

Figure 5-17 Mack 10 yard dump truck as test truck with weight of 50 Kips. Truck weight was determined at the day of field test.
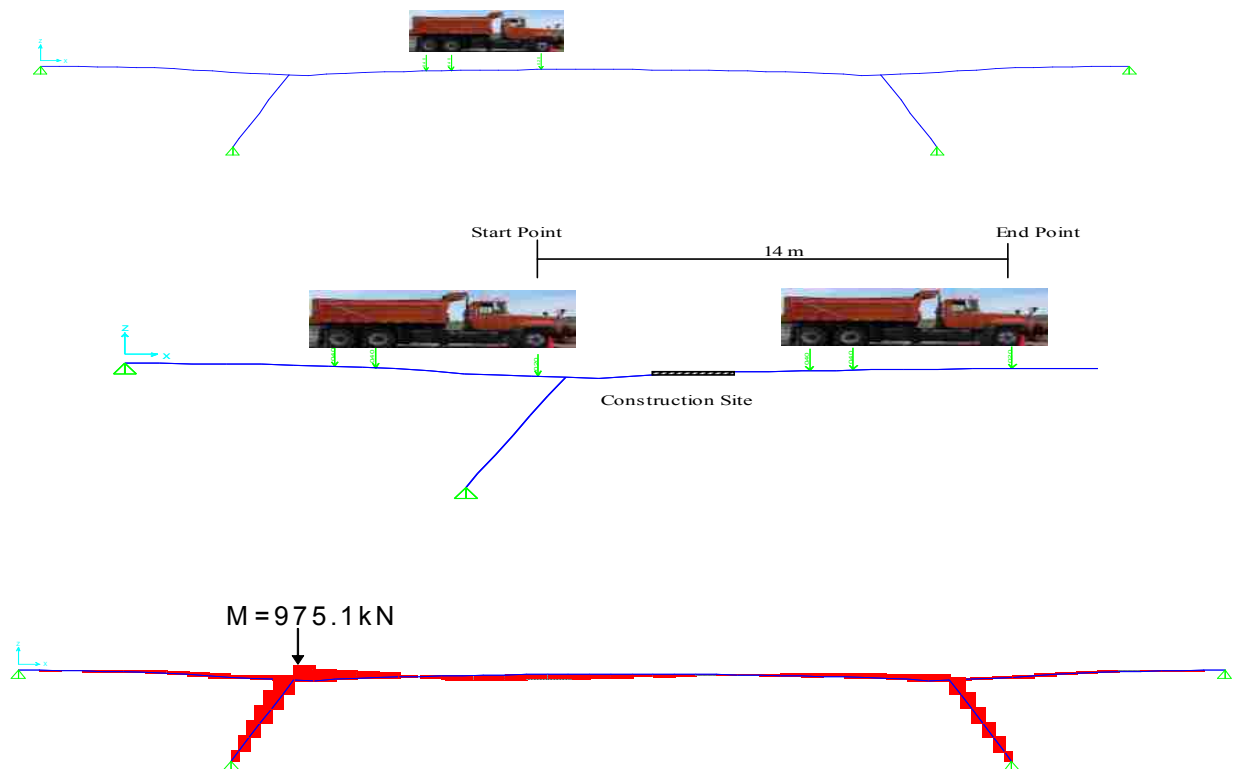
Figure 5-18 FE model based on the truck position and the maximum moment distribution of the exterior girder.

Figure 5-19 Strain gauges attached to the concrete surface and FRP strips.
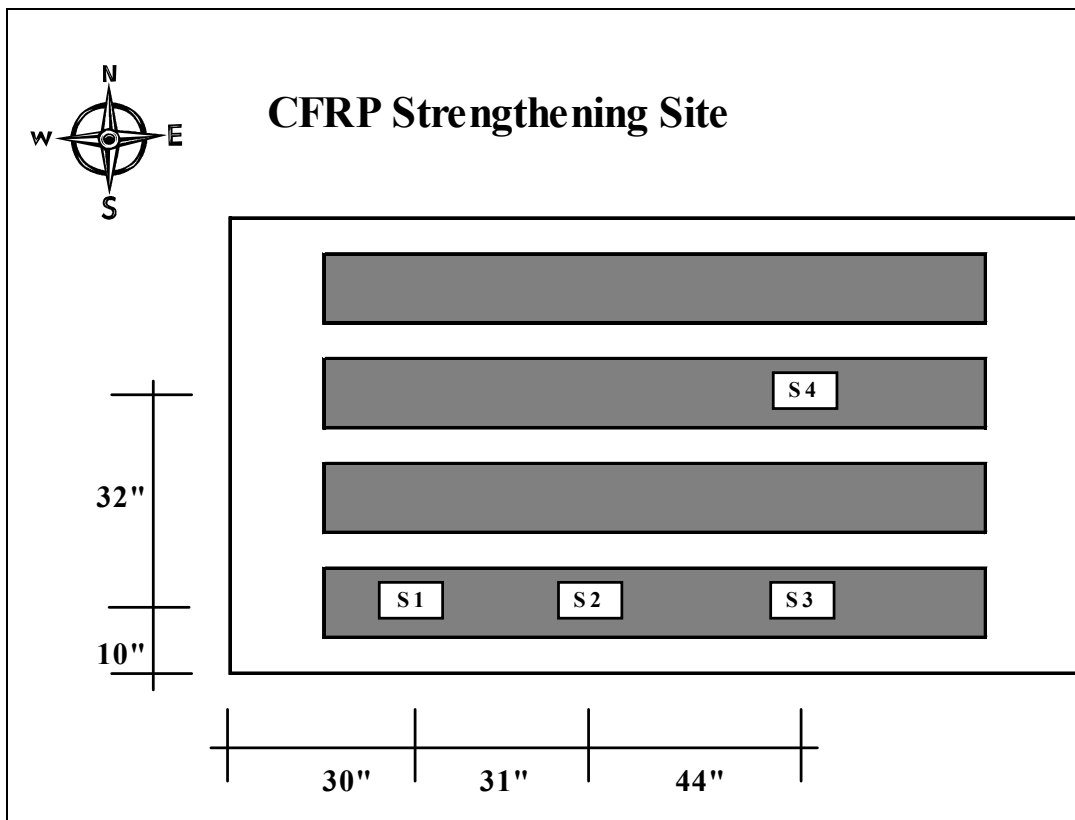
Figure 5-20 Schematic drawing showing the location of strain gauges on FRP strips.

105

Here, we compare the strain measurements observed at spot S1 in Figure 5-20 with the ones predicted by the calibrated FE model. The strain measurements on the concrete surface prior to strengthening are shown in Figure 5-21. It can be observed that under the designated test truck, 21.7 με (με = micro strain) was recorded as the maximum strain on the concrete surface. This number is very close to the maximum predicted strain on concrete surface of 23.2 με predicted by the FE analysis. This confirms that the FE model is calibrated properly based on the strain field measurements of the RC structure.
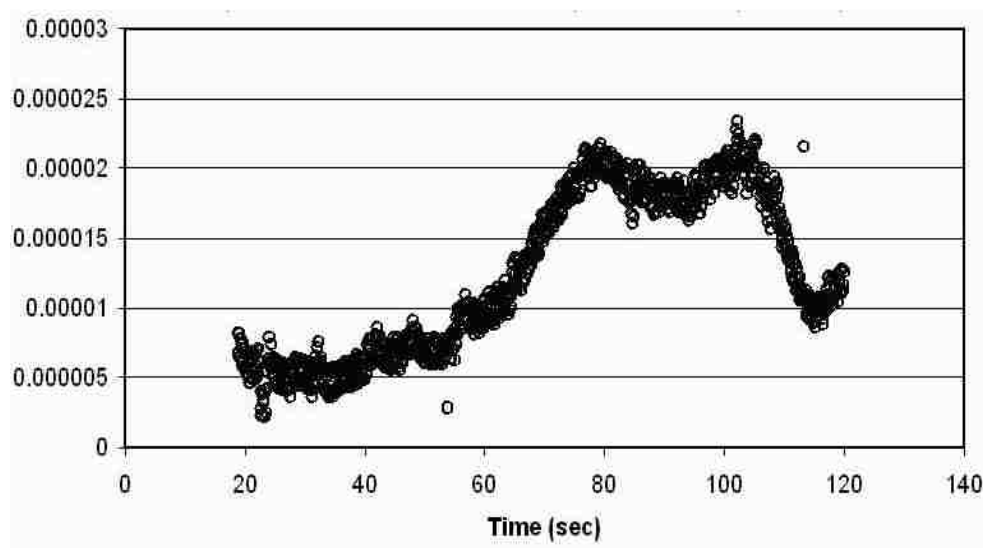
Figure 5-21 Strain measurements at spot S1 on concrete surface using the test truck.

After calibrating the FE model with the strain field measurements data, the effectiveness of FRP sheets in carrying the live load from the bridge is examined by comparing the strain measurements at four different locations shown schematically on Figure 5-20 with those predicted by the calibrated FE model. Figure 5-22, Figure 5-23, Figure 5-24 and Figure 5-25 illustrate the strains calculated from FE model and from the

106

field tests at strain gauges S1, S2, S3 and S4 respectively. From these figures, it can be concluded that the strains calculated from the FE model, which represents the strains at the concrete surface, are similar to the strains collected from field tests as the truck moving. Based on the strain compatibility at the concrete surface and FRP strips, the similarity between these strains proves the efficiency of FRP strips in carrying the live load from the concrete surface. It also confirms complete bond between concrete surface and FRP strips. This confirms that FRP strips enhance the bridge girder capacity.
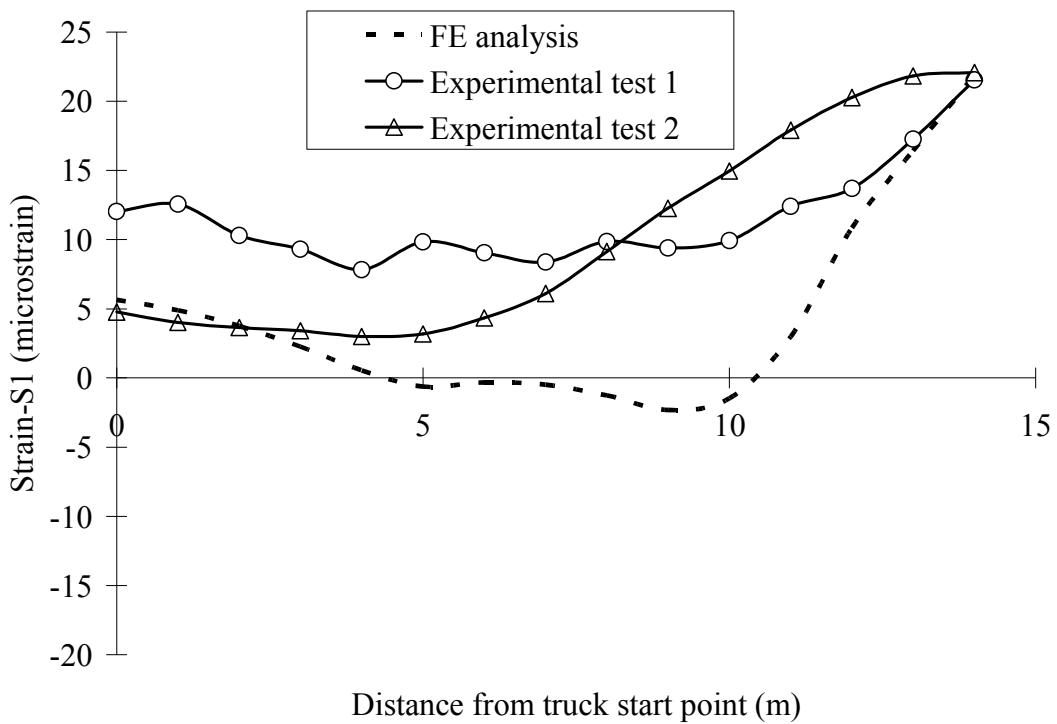
Figure 5-22 Strains calculated from FE model and field test at strain gauge S1 on FRP strips.
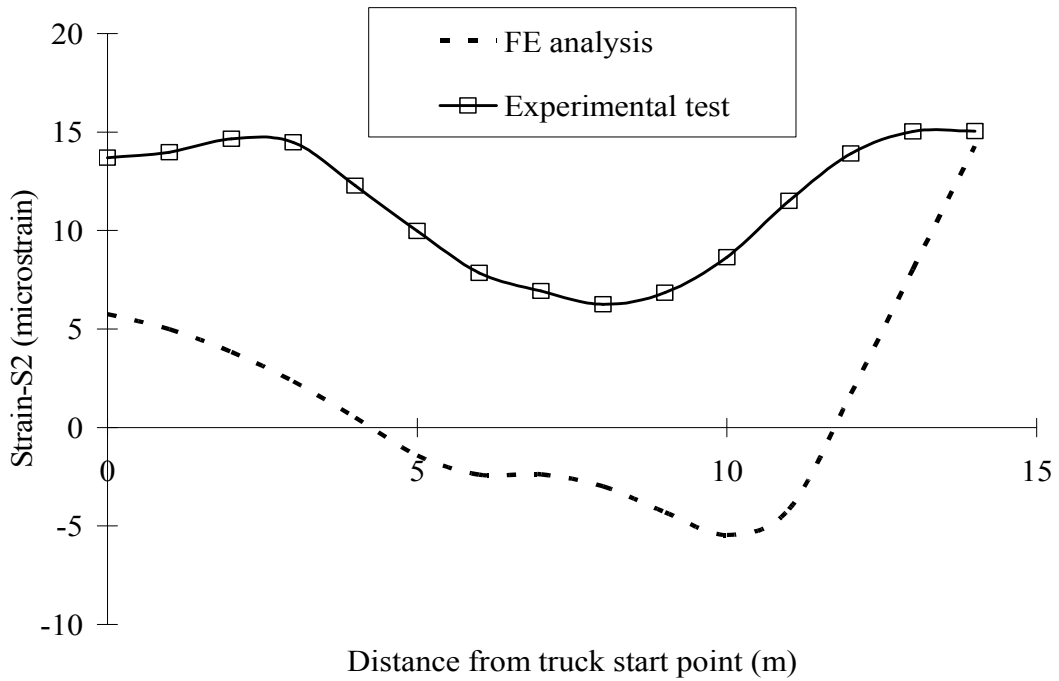
Figure 5-23 Strains calculated from FE model and field test at strain gauge S2 on FRP strips.
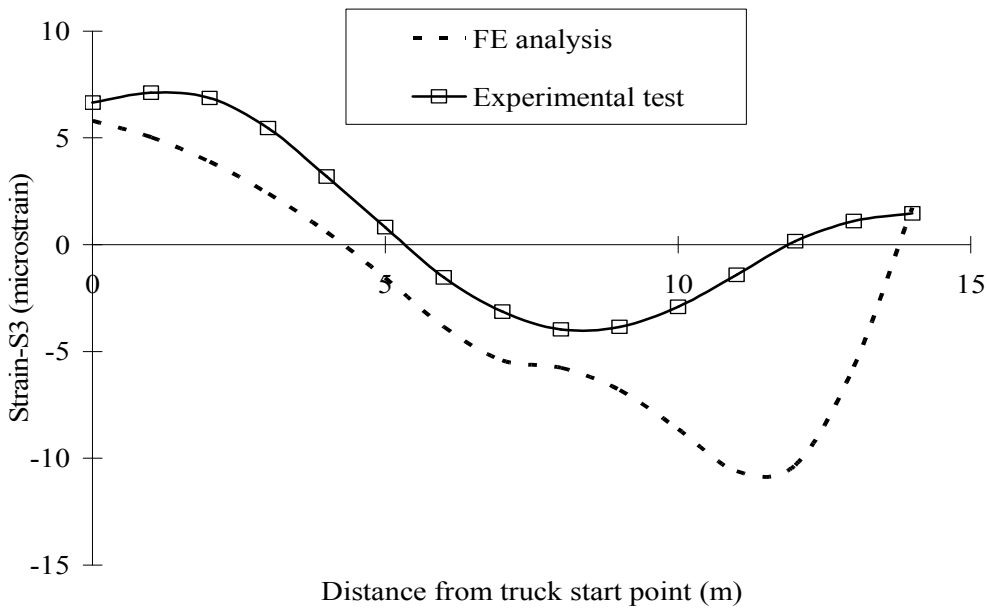
Figure 5-24 Strains calculated from FE model and field test at strain gauge S3 on FRP strips.

108
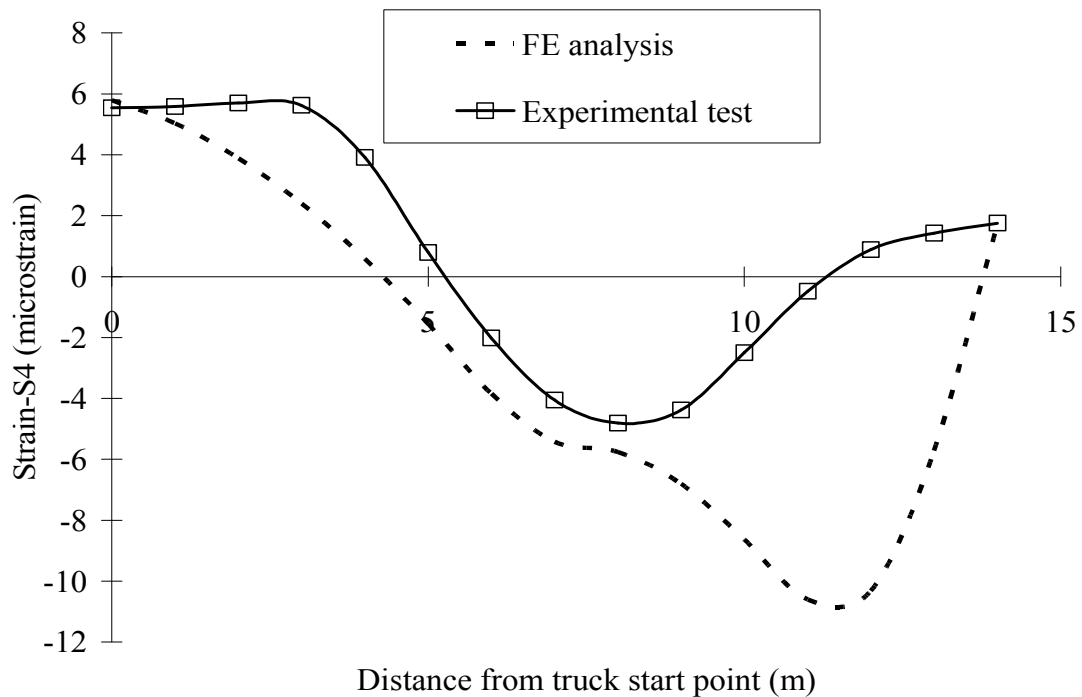
Figure 5-25 Strains calculated from FE model and field test at strain gauge S4 on FRP strips.

5.3 Design of SHM system to monitor Bridge 7937

A structural health monitoring (SHM) system consists of a number of sensors that observe structural response, such as accelerations or strains, to acquire and integrate the observations using a data acquisition system. The data collected from data acquisition can then be processed to extract proper monitoring features and patterns that identify structural performance. These patterns can be used at a later time to detect damage occurrence in structures.

The SHM system to monitor Bridge 7937 includes *accelerometers* and *strain gauges* along with *thermocouples*. Twenty accelerometers were used to extract structural

109

dynamic information at different locations on the bridge. The acceleration data was used to extract damage feature(s) which can differentiate between healthy and damage conditions and enable warnings when the bridge is damaged.

To find acceleration on different locations of the bridge, *model 333B50 accelerometer* from PCB, Inc. was utilized. This model is a piezoelectric accelerometer that has a frequency range of 0.5 to 3 kHz and operates with 1000 mV/g sensitivity, which means an accelerometer produces 1000 milli volt (1 volt) for the acceleration of gravity (g =9.8 m/sec^2 or 32.2 ft/sec^2). Moreover, these accelerometers are stud mounted, which makes them stable on the bridge. Figure 5-26 illustrates a schematic for the accelerometer used in monitoring accelerations of Bridge 7937.
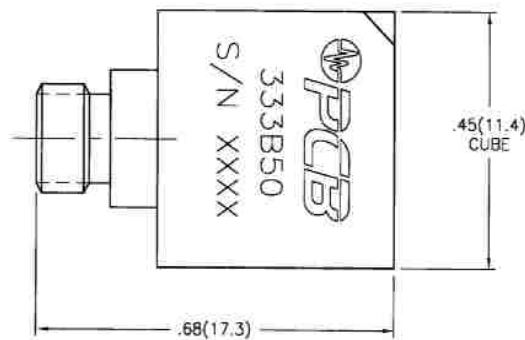
Figure 5-26 Schematic representation of accelerometer used on Bridge 7937.

Accelerometers were mounted at the bottom slab of the bridge, close to each girder. Accelerometers are shown with their placement location in Figure 5-27. As shown in the figure, four accelerometers are installed on each girder of the bridge. Accelerometer placement is determined based on locations of maximum bending moment and those locations more prone to cracking. Exact accelerometer locations are provided in Table

110

5-1.
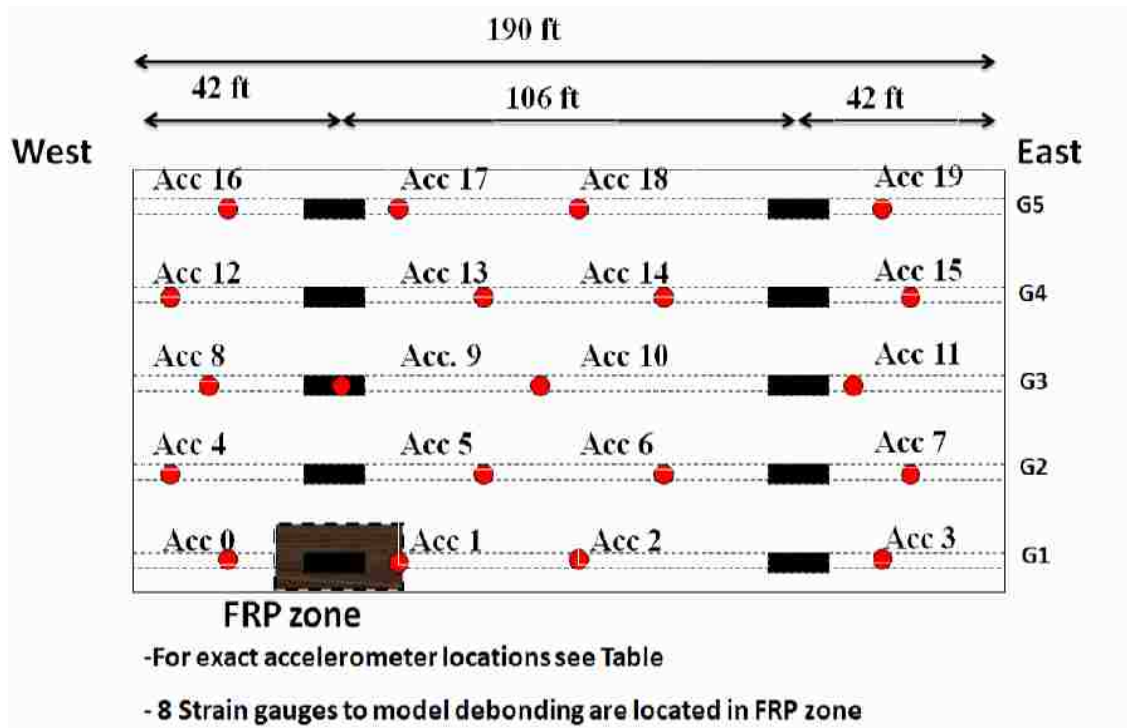
Figure 5-27 Location of sensors used on Bridge 7937.

Table 5-1 Sensor Locations on Bridge 7937

Girder	Sensor	Location	Sensor	Location	Sensor	Location	Sensor	Location
G1	Acc 0	30	Acc 1	48	Acc 2	100	Acc 3	175
G2	Acc 4	20	Acc 5	80	Acc 6	140	Acc 7	180
G3	Acc 8	25	Acc 9	35	Acc 10	95	Acc 11	165
G4	Acc 12	20	Acc 13	80	Acc 14	140	Acc 15	180
G5	Acc 16	30	Acc 17	48	Acc 18	100	Acc 19	175

All locations are measured on each girder from west side.

To monitor the effectiveness of FRP sheets, strain gauges are also distributed over the FRP application zone. By comparing the strain data of FRP sheets to strains on the concrete surface, the maximum strain due to the traffic and environmental loadings on FRP sheets can be monitored. While it is anticipated that traffic loading will produce very little strain in FRP sheets (in the range of 20-30 microstrains), as observed under load test and as shown in previous section, it is believed that the very low measurements will change if FRP debonding takes place on the bridge surface. Therefore, the FRP strains are basically used to detect possible FRP debonding.

Another possible option was to use fiber bragg grating technology with optical fibers to accurately determine the strains in the FRP plates. However, dramatic cost increases prevented us to use this option due to the difficulty to integrate Fiber Optic Sensing (FOS) technology with Field Programmable Gate Array (FPGA) technology. It was therefore determined to use electrical strain gauges to monitor possible FRP debonding.

Moreover, thermocouples are placed on the top and bottom surfaces of the bridge at several locations in order to find the temperature gradient on the bridge and thus monitor strain changes due to temperature change. It is well known that most of the cracks on the bridge deck are induced because of temperature gradient effects and thus correlating changes in behavior to thermal effects is of great interest. Figure 5-28 shows schematic locations of strain gauges and thermocouples on FRP sheets.
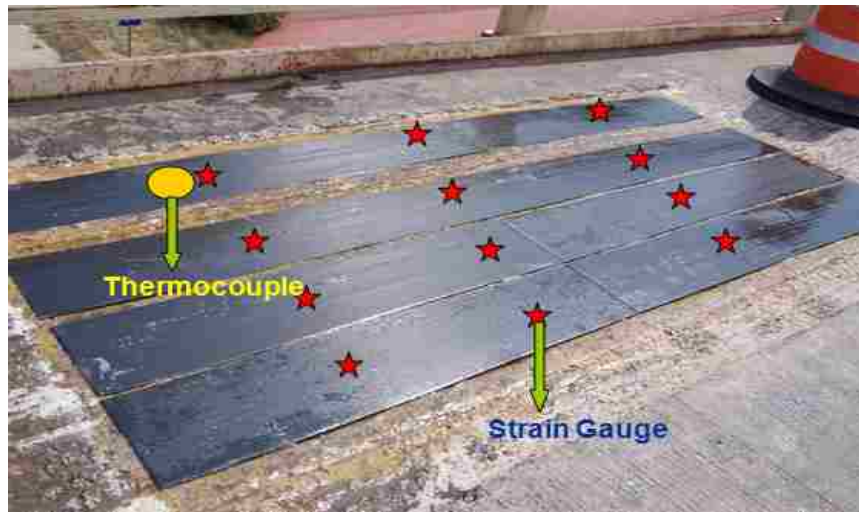
Figure 5-28 Schematic locations of strain gauges and thermocouples on FRP sheets.

All sensors are connected by wires to a smart data acquisition (SDA) system as described in the next section of this chapter. The SDA system has the ability to connect the data to the office using a wireless system. The data can then be downloaded using HTTP or FTP internet protocols. A schematic representation of the SHM system and all of its components used in Bridge 7937 is represented in Figure 5-29.
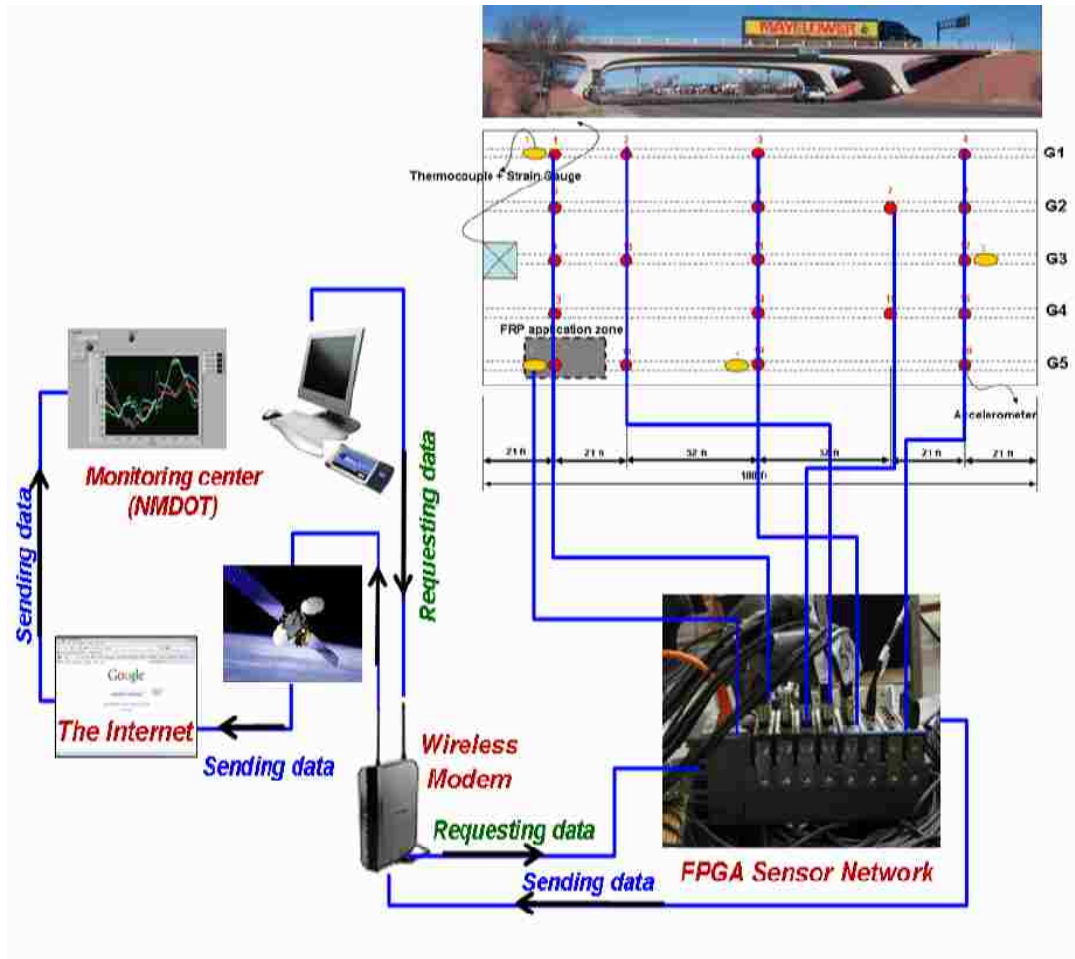
Figure 5-29 Schematic representation of SHM system shows all its components as designed for Bridge 7937.

5.4 Smart Data Acquisition (SDA) System

A new data acquisition system for acquiring data from all the sensors is developed to be used on Bridge 7937. The new data acquisition system utilizes a data acquisition platform that consists of two different parts: 1) a real-time controller that has volatile memory and nonvolatile memory for data storage. The real-time controller also encompasses an Ethernet port with built-in file servers allowing access by HTTP and FTP, and 2) a multi-slot reconfigurable chassis that contains FPGAs and a Peripheral

114

Component Interface (PCI) bus interface that connects between the FPGA and the real-time controller. This built-in data transfer protocol is used to communicate data to the controller where post processing, data logging and communication to a host computer can take place. The FPGA chip connects directly to the analogue input modules using FPGA functions. Different types of sensors can be connected to different types of analogue modules. We denote the system here as Smart Data Acquisition (SDA) system for its ability to incorporate programmable logic on the hardware. Figure 5-30 shows this SDA system, including the controller and eight slot chassis where different modules connect to the chassis. The SDA system has a commercial brand name (Compact Rio$^{®}$) produced by National Instruments (NI), Inc.
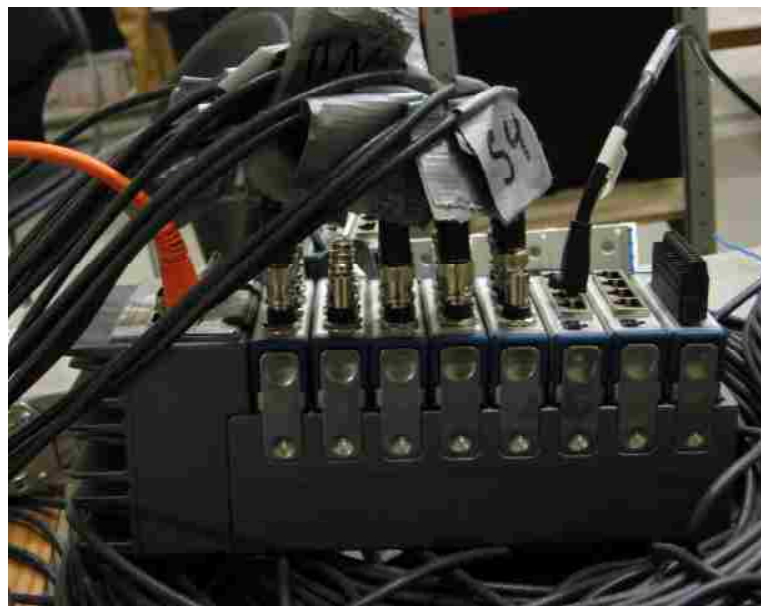
Figure 5-30 SDA system showing the analogue modules integrated on the SDA system by National Instrument.

115

The SDA system replaces the conventional data loggers and computer modules that have been long used for SHM systems. This is achieved by integrating both data acquisition and computational logic gates on the same hardware. The SDA system also has the ability to connect to the worldwide web using wireless modems. Field implementation of the SDA system will enable establishing smart wireless SHM where damage feature extraction protocols can be processed at the bridge site. Therefore, the SDA system enables a unique opportunity for establishing SHM where data transfer can be limited to take place only when needed. Limitation of data transfer not only helps reduce the cost of the SHM system, but it also prevents data overflow reported by many researchers where the SHM system becomes a burden rather than an aide for engineers (Shrive et al. 2003). Moreover, the use of FPGA technology and real-time controllers enables synchronizing signals received from different sensors in real-time as well as the ability for remote hardware reconfigurability. This overcomes a fundamental challenge met by many conventional data loggers.

Developing data acquisition applications to operate on the SDA requires building a system that consists of three different modules, each operating at a different level. Figure 5-31 shows schematic representation of three modules and how they connect with each other. Figure 5-32 illustrates the hierarchy of these modules on a project and how they connect to a host computer through worldwide Internet.

116
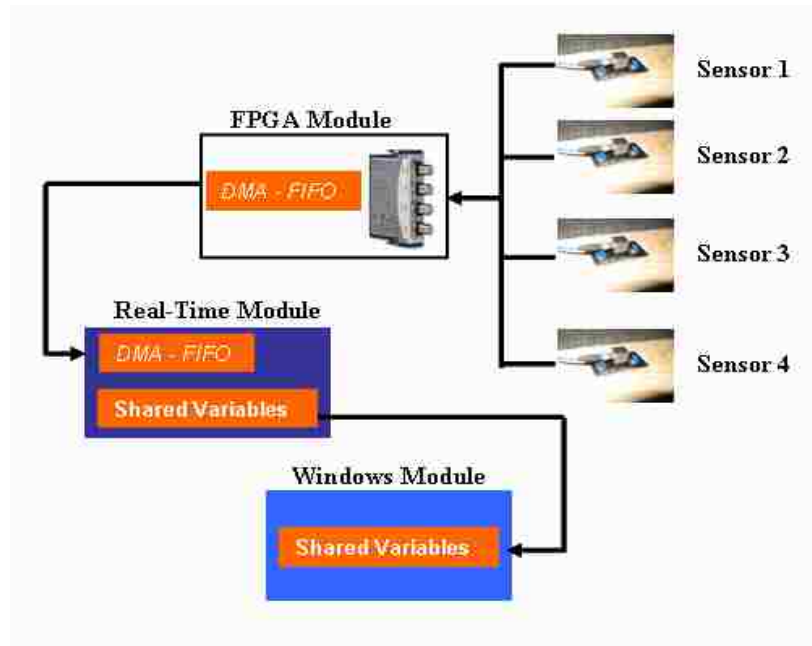
Figure 5-31 SDA system components and how they connect with each other.
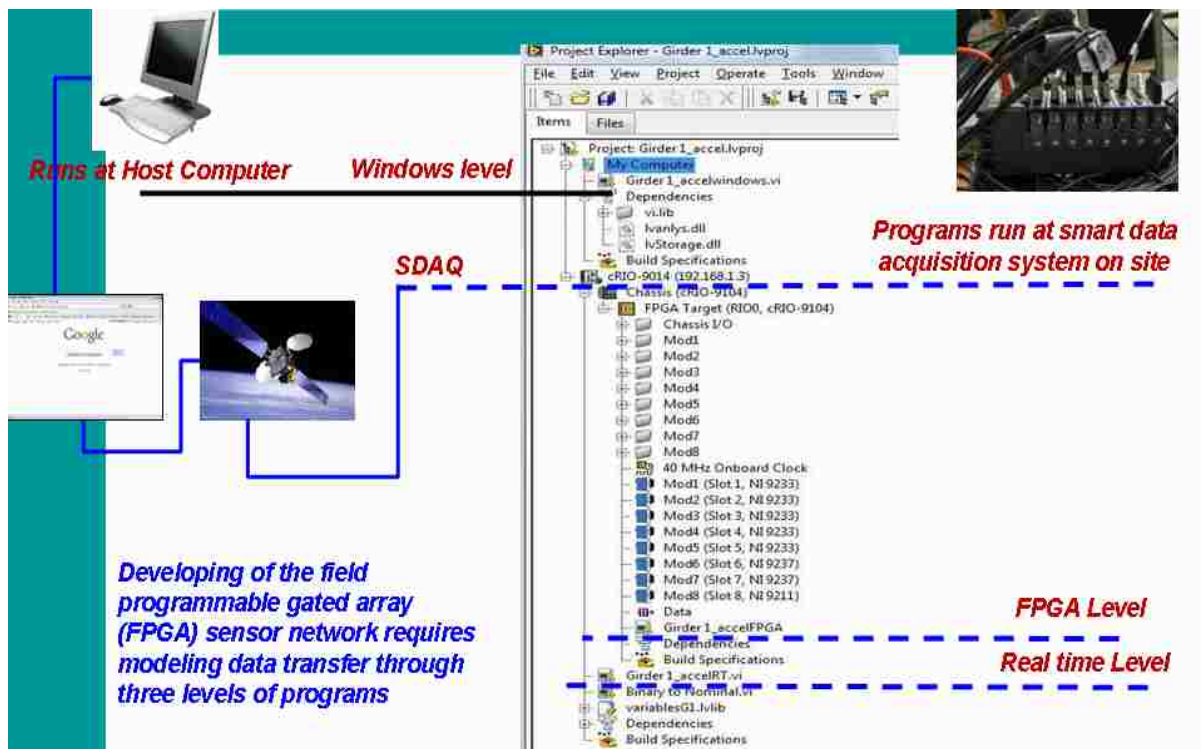
Figure 5-32 Hierarchy of different components of a SDA system.

117

The modules shown in Figure 5-31 and Figure 5-32 include:

1. *FPGA module* This module is a low level program coded on FPGA. FPGA is a semiconductor device that can be reconfigured. An FPGA consists of logic blocks, I/O blocks and interconnection wires and switches (Brown and Vranesic 2009). Interconnection wires are organized in horizontal and vertical routing channels running between the logic blocks. The routing channels contain wires and switches that allow for a variety of combinations of logic circuits. In most cases logic blocks are look-up tables (LUTs) which contain storage cells that are used to implement small logic function. Hardware description language (HDL) is used to describe the desired hardware specification that will be later synthesized. There are many HDL languages some are proprietary while others are not. The two main HDL languages that are officially endorsed by IEEE are Very High Speed Integrated Circuit Hardware Description Language (VHDL) (IEEE Std. 1076, IEEE Std. 1374) and Verilog HDL (Hemmert and Underwood 2005). As density and speed of new FPGAs are improved they are now able to support double-precision floating point arithmetic making them more capable when implementing sophisticated algorithms. There are several available floating point kernels that performed fairly well on FPGAs (Hemmert and Underwood 2005 and Underwood and Hemmert 2004). Such advances increase the promise and the effectiveness of highly configurable hardware and increase the applications that they can be used for.

2. *Real-time module* This module is a program coded on the controller of SDA. The controller receives the data from the FPGA module and keeps it in the nonvolatile memory of the SDA system. Using FPGA read/write control function through the PCI bus, real time module gets connected with the FPGA module. To transfer data from

118

FPGA module directly to the SDA real time controller, Direct Memory Access First In First Out (DMA FIFO) buffers are used where the first data item written to memory is the first item read and removed from memory. Each FIFO consists of two parts: the write part used by the FPGA module to record the sensors data on FIFO and the read part used by the real-time module to read data from FIFO. The FPGA module operates using a nanosecond clock while the real time module operates on microsecond clock. Therefore, the writing process on FIFO runs faster than the reading process. That can result in data loss. To avoid losing data and make complete synchronization between FPGA and real-time modules, interrupt functions are implemented to send a trigger from the FPGA module to the real time host. An interrupt notifies the real-time module about the time when data is ready or when the task finishes and makes it possible for the real-time module to read all the data recorded by the FPGA module.

3. *Windows™ host module* This module runs on the host computer. This is Windows™ based software, coded in any language, where simple graphical user interface and user friendly options can be developed. The Windows™ module communicates with the SDA system through wireless link and the data is transmitted via the worldwide web. Shared variables are used to communicate between real-time and Windows™ modules.

To make a complete embedded (self-contained) SHM system that communicates the data wirelessly, the FPGA module communicates the data to the real-time module via the DMA FIFO. The data is then saved on the SDA nonvolatile memory in the real-time module. In the next step, the data is transferred through a FTP to the host computer where the Windows™ module operates at the host computer. Figure 5-33 illustrates a block diagram describing the program implemented at the FPGA module for the Bridge 7937

119

monitoring. Part I of the FPGA module enables to recognize all the analogue modules on FPGA level and how to identify data rates for different modules. Parts II and III show how the configuration of strain modules is identified and how to define the interrupt function to synchronize the FPGA, and the real-time modules as explained above. Part IV in the block diagram also shows how the binary data is written on the DMA FIFO.

It is important to note that the above details are a fundamental part of the SHM code necessary for data acquisition of sensors' data. These codes need to be established and tested to meet specific needs for each monitoring project.
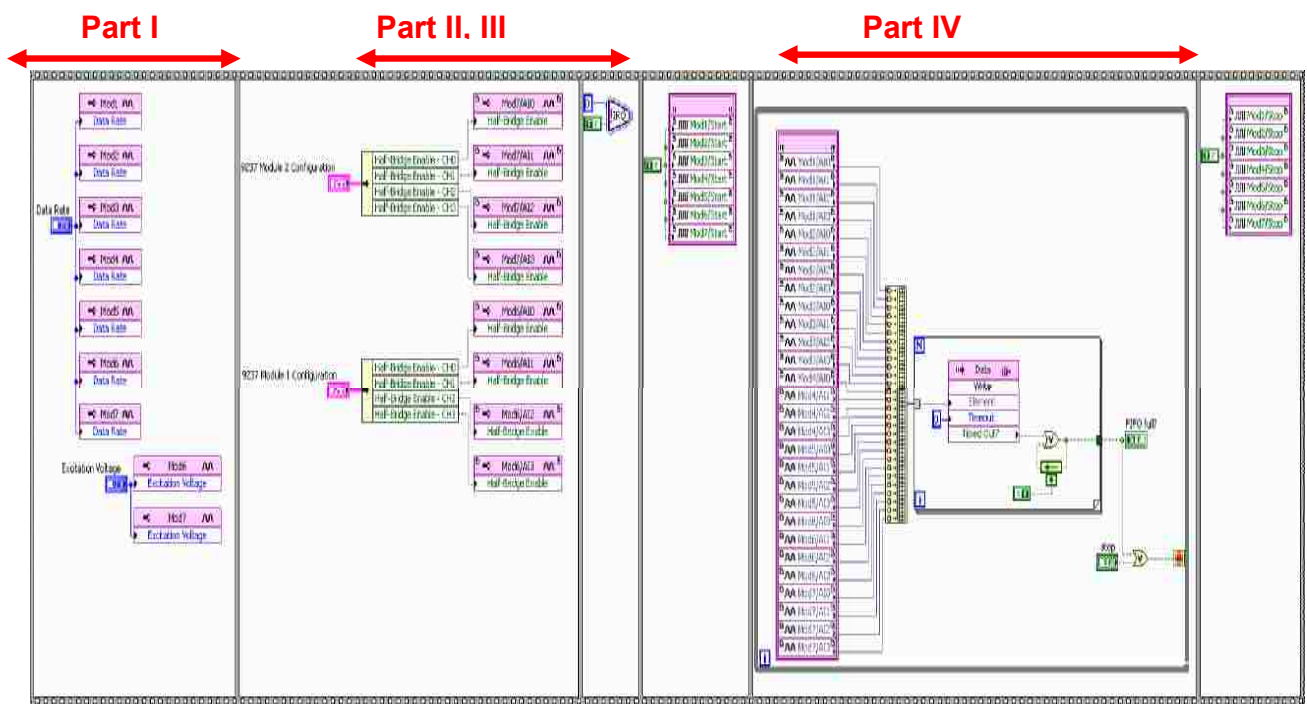
Figure 5-33 Block diagram of the FPGA module showing data acquisition from different analogue modules (Part I), interruption functions for synchronizing FPGA and Real-Time modules (Parts II and III) and the read and write process to DMA FIFO (Part IV).

5.5 Model bridge for testing and calibrating the SHM system

To test and calibrate the designed SHM system and the SDA system, a model steel bridge was constructed and tested in the Structural Laboratory at UNM. This model bridge used for calibrating the SHM system is shown in Figure 5-34. The model bridge is 3.1 m long and 1.1 m wide; it consists of two structural steel trusses. The bridge is divided into three longitudinal traffic lanes spaced at 250 mm each. Underneath the bridge, lateral transverse elements have been used to connect the bottom chord of two trusses. The trucks and their weights to simulate the random traffic on the model bridge are shown in Figure 5-35.

Figure 5-34 Model bridge constructed at UNM structural laboratory.

Figure 5-35 Model trucks with their weights.

The cross-section of connecting members is a 25 mm hollow steel rectangular tube with 1.5 mm thickness. Three 18 mm thick pieces of Plexiglass were used as the bridge deck. Three model trucks made of plastic with rubber wheels were used to model the traffic loading on the bridge. The model trucks have three different weights and weight distributions to realistically simulate traffic as shown in Figure 5-35. Weights of the trucks were controlled using lead beads of known weights. Additional weights are added to each vehicle by adding bags of lead shot of predetermined weight. Moreover, a CFRP sheet was attached to the bridge deck. Strain gauges were attached to the CFRP sheet to simulate CFRP strengthening that has been used to strengthen the original bridge. The CFRP strip installed on the model bridge with its strain gauge is shown in Figure 5-36.
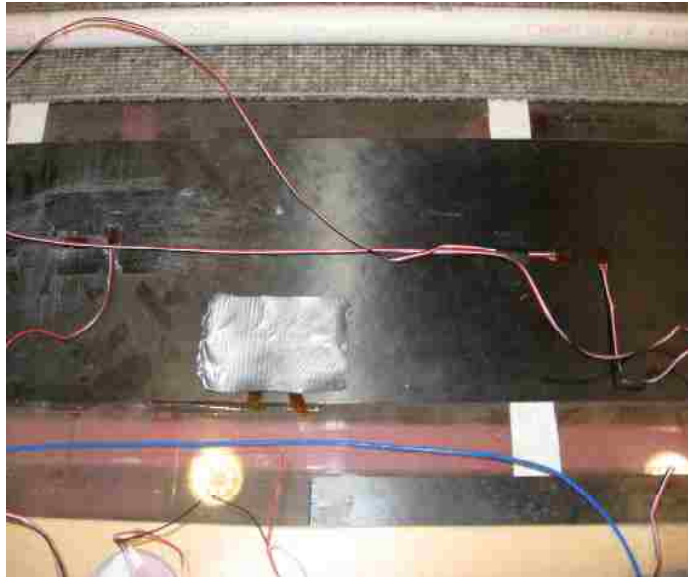
Figure 5-36 CFRP strip installed on the model bridge deck with strain gauges installed on the CFRP.

To avoid direct contact between the model truck and the Plexiglass deck, a 5 mm thick piece of carpet was attached on top of the Plexiglass deck. The carpet enables damping of the high frequency spikes produced by direct interaction of truck tires and Plexiglass material. This mimics the interaction between the asphalt layer of real bridges and tires. Using polyvinyl chloride (PVC) tubes, three equally spaced lanes were created on the deck of the model bridge. Moreover, two pieces of wood bolted into the Plexiglass bridge deck were used to attach the accelerometers to top of the bridge. Twenty accelerometers were installed on the prototype bridge. These are the same twenty accelerometers to be installed on Bridge 7937 in Tucumcari. A stainless plate was designed to enable easy installation and replacement of the accelerometers. The same plate will be used to mount the accelerometers on Bridge 7937. The design of the steel plate ensures that there is no

vibration at the plate location and excellent fixation to the structure. The accelerometer connection with the steel plate is shown in Figure 5-37.
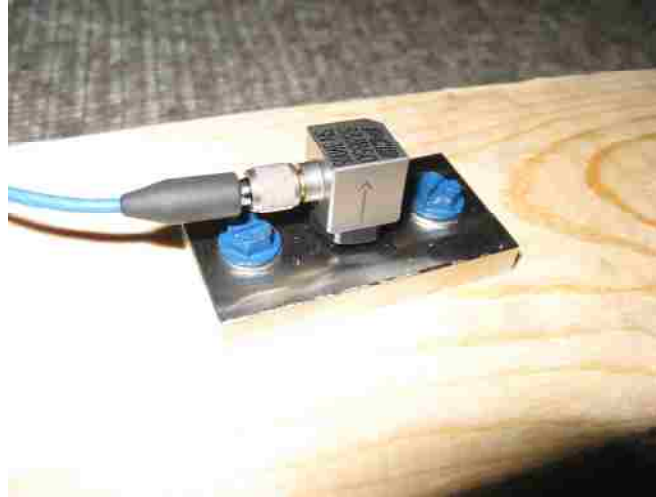
Figure 5-37 Stainless steel plate to mount accelerometer on the model and real bridge.

The acceleration data was acquired from the model bridge under simulated traffic using the SDA system. Figure 5-38 shows a snap shot of the real-time program displaying the acceleration data in real time while monitoring. A display program was developed to present all the monitored accelerations. Figure 5-39 presents snap shots of the acceleration data measured at four locations on the model bridge while being monitored.
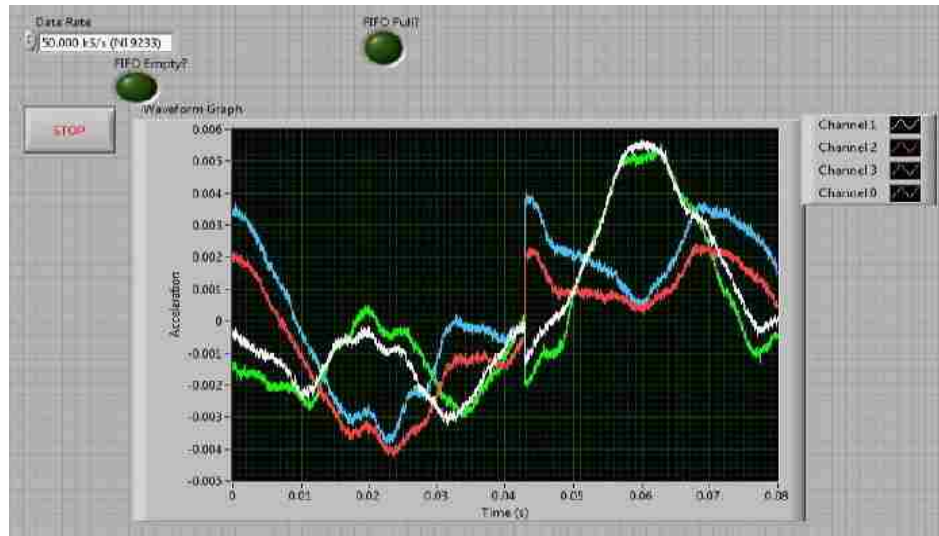
Figure 5-38 Real-time acceleration signals obtained from the SDA system.
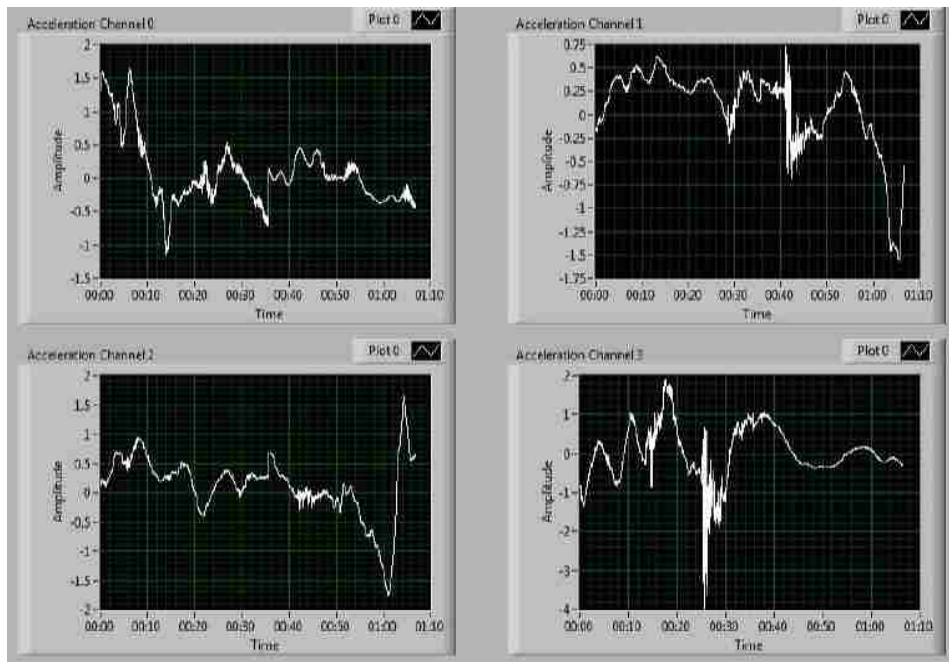
Figure 5-39 Acceleration signals from four different locations on the model bridge.

125

5.5.1 Damage Detection on the Model Bridge

The structural vibration of the model bridge was monitored by recording the accelerations from the twenty accelerometers and strain gauges installed on the bridge. To detect damage occurrence on the bridge, a damage feature will be extracted from the observed acceleration data. This damage feature can then be patterned and damage can be directly related to departure from this pattern. Here, the *Wavelet* method is used for digital signal processing of the acceleration signals. While Fourier transform provides information on the signal in frequency domain, wavelet has the ability to provide information in both time and frequency domains. Using Wavelet Multi Resolution Analysis (WMRA), the original signal can be decomposed to its original components.

Using wavelets, the acceleration signal is decomposed into approximation and detail signals with low and high frequency components respectively. The wavelet decomposition provides means to break down the signals into groups of signals at different frequency levels. The decomposed signal of $x'(n)$ at level p can be computed as

$$x'(n) = \sum_{k=-\infty}^{\infty} a_{p,k}.\phi_{p,k}(n) + \sum_{j=1}^{p} \sum_{k=-\infty}^{\infty} d_{j,k}.\varphi_{j,k}(n) \tag{5.6}$$

where $x'(n)$ is the decomposed signal. Moreover, $\phi_{p,k}(n)$ and $\varphi_{j,k}(n)$ are the scaling and wavelet basic functions respectively. The decomposition of the acceleration signal into a group of approximation and details signals is shown schematically in Figure 5-40. In this SHM system for Bridge 7937, the scaling and wavelet functions are selected for the *Daubechies db4* mother wavelet. The approximation coefficients $a_{p,k}$ and the detail coefficients $d_{p,k}$ are calculated as

126

$$a_{p,k} = 2^{(-p/2)} \sum_n x(n)\phi(2^{-p}n - k) \qquad (5.7)$$

$$d_{p,k} = \sum_n x(n)\varphi_{p,k}(n) \qquad (5.8)$$
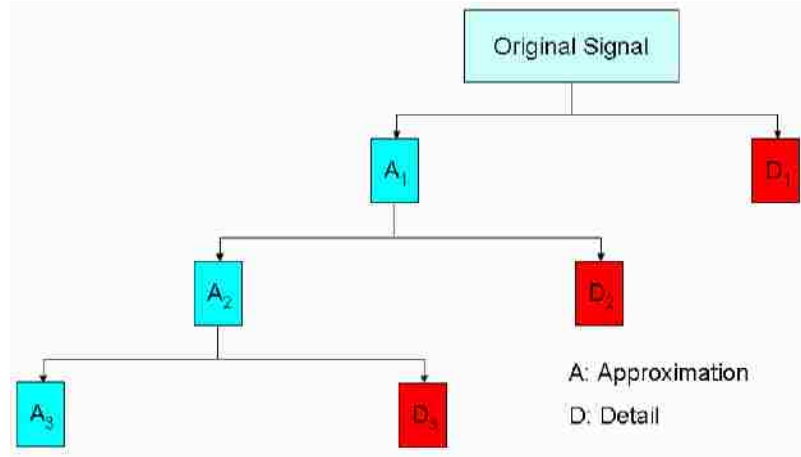
Figure 5-40 Schematic representation of WMRA decomposition of the acceleration signal.

After decomposing the signal, the third approximation signal (denoted A_3 in Figure 5-40) is used to extract the damage feature. The third approximation signal is computed for each accelerometer signal and then the approximation signal is down sized to 500 Hz. The model bridge was tested by performing traffic load simulation while acquiring data from the bridge using the SDA system to calibrate the SHM system before installation on Bridge 7937 in Tucumcari. Acceleration data was collected for 6 seconds by moving model trucks on the bridge so 3000 data points were extracted for each experiment. Figure 5-41 illustrates an example of original acceleration signal obtained from one of the accelerometers along with its third approximation signal denoted A_3.

127
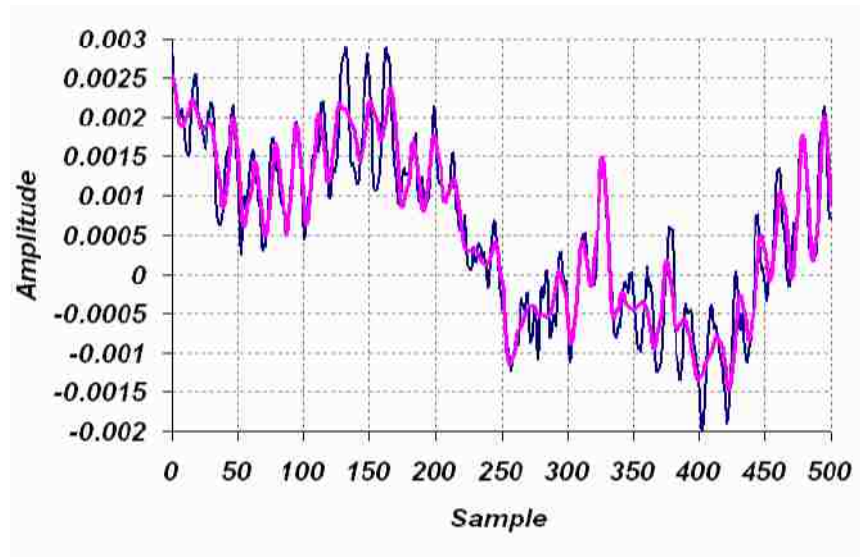
Figure 5-41 Original acceleration signal (Blue) along with its approximation 3 signal (Red) showing the ability of wavelet decomposition to smoothen the observed signal.

Figure 5-41 shows that WMRA is capable of removing the noise and all high frequency components from the signal and then down sample the sampling rate without changing the original signal. The third resized approximation A_{3R} of the acceleration signal is then used to compute the damage feature as shown in Equation (5.9).

$$\lambda = \sum_{k} (a_{3,k})^2 \tag{5.9}$$

The damage feature (metric) λ represents the energy of the third approximation signal computed over a time window. Experimental and analytical investigations (Reda Taha et al. 2004, Horton et al. 2005, McCuskey et al. 2006 and Azarbayejani et al. 2008) have proven the ability of the proposed damage metric λ to detect and quantify damage occurrence on bridge structures.

128

To examine the efficiency of the proposed monitoring system, the energy of the third resized approximation signal A_{3R} derived from the acceleration signal at two arbitrary accelerometers at different sides of the bridge was computed for healthy and damage cases. The healthy case is assumed to be the case where all members are attached to each other with completely fixed bolts installed at a specific torque. Damage in the bridge was simulated by removing two diagonal members, one from the first bay of one side and the other from the third bay of the other side. Model trucks were loaded and allowed to move over the bridge simulating traffic in random loading sequence for both the healthy and damage cases. Acceleration signals were recorded for 5 seconds. The signal was divided into thirty time windows, each 166 millisecond wide. The damage metric λ representing the energy of the third resized approximation signal A_{3R} within each time window was computed following Equation (5.9).

A total number of twenty tests for both cases of healthy and damage were performed and thirty values for the damage feature were computed for each test. To be able to compare the healthy and damage performances, the mean value and the standard deviation of the 300 damage feature values collected from two sensors at ten different tests were computed. Assuming that the damage feature (energy of the third resized approximation signal) follows normal probability distribution, the probability of damage feature was computed. Figure 5-42 illustrates the probability of damage feature for healthy and damage scenarios computed at two accelerometers.

129

(a)   (b)
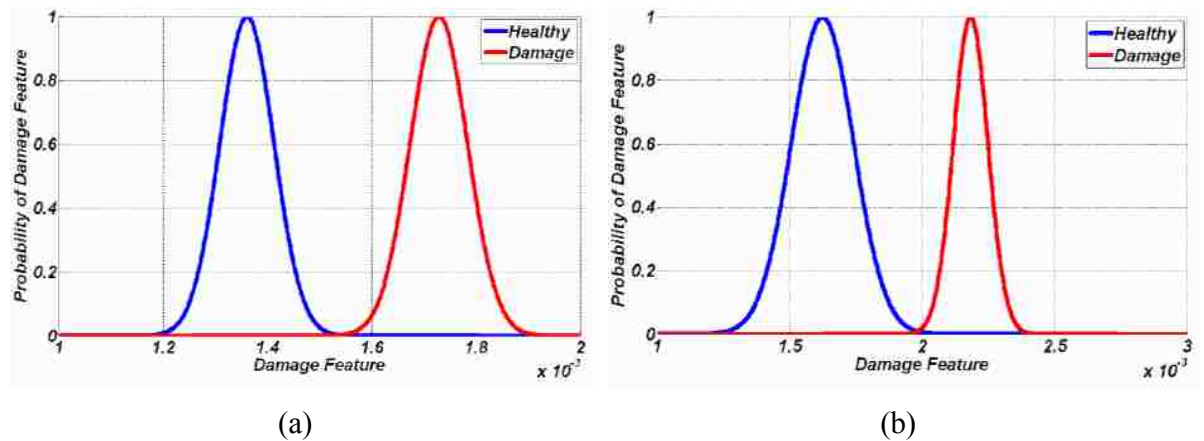
Figure 5-42 Probability of damage feature used to realize cases of healthy and damage performances at two different sensors installed on the prototype bridge.

It can be observed in this figure that the proposed monitoring system using wavelet domain can easily differentiate between cases of healthy and damage on the prototype bridge. Damage pattern recognition methods (Reda Taha and Lucero 2005) can then be used to classify the level of damage in the bridge. The damage feature extraction and pattern recognition algorithms can be used at the host computer level to enable smart SHM. After testing all sensors, the proposed SDA and all sensors were decided to be working as designed. Experiments were also performed for data communication over the worldwide web for all sensor data. Snapshots of the SHM web-based software developed for data control and data transfer of the model bridge is shown in Figure 5-43. Moreover, a webpage for enabling data observation and data transfer via file transfer protocols (FTP) was developed. A snapshot of this webpage is shown in Figure 5-44. The web page and the FTP system were tested and proved capable of communicating the data observed from the model bridge.

130

(a)   (b)
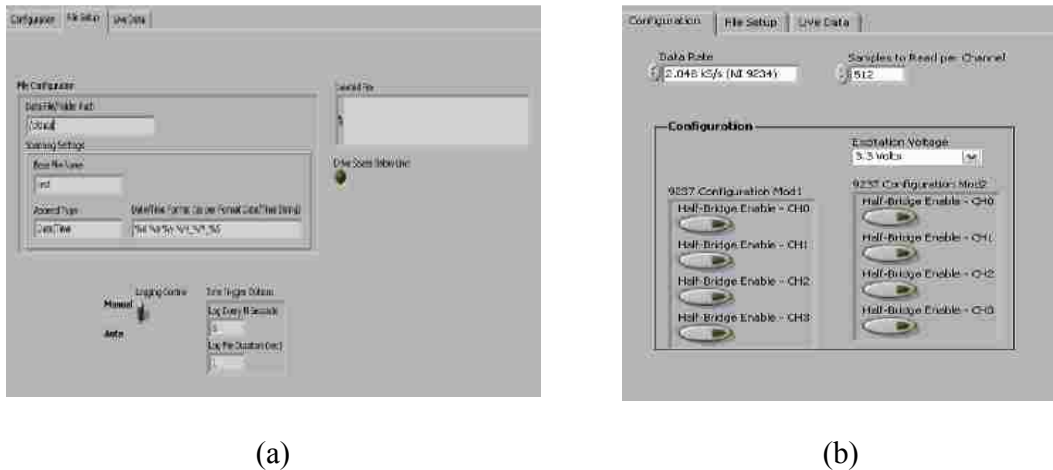
Figure 5-43 Web tools developed for (a) Data transfer from the model bridge and (b) Data rate and sensor selection control on the SDA.
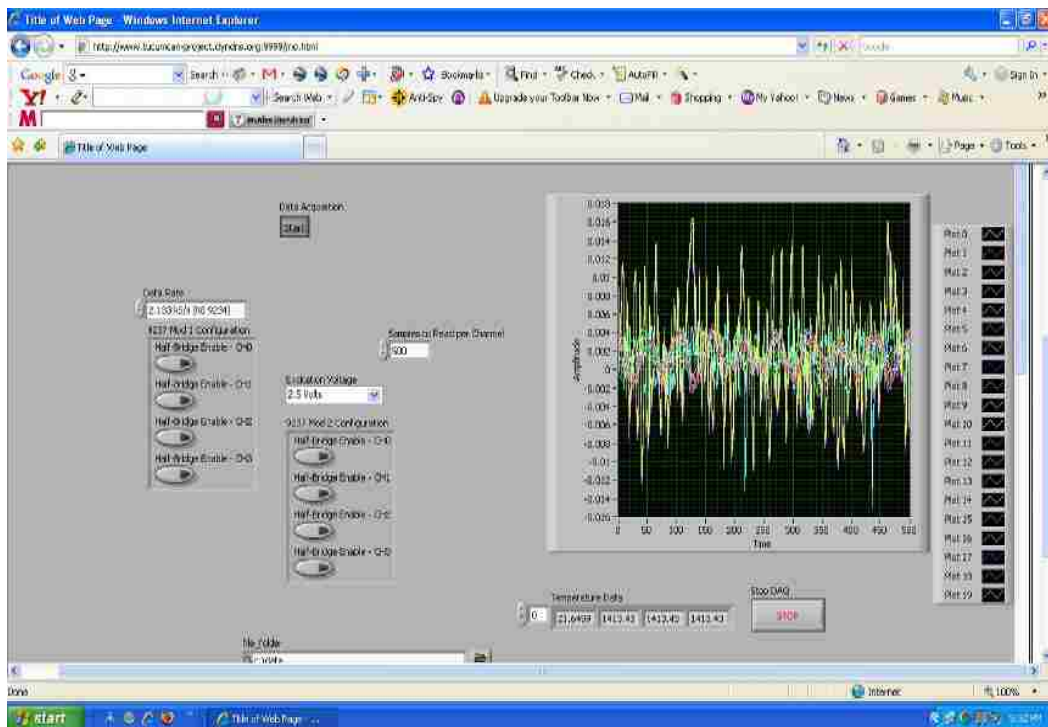
Figure 5-44 Snapshot of the webpage developed for efficient data transfer for the model bridge using the worldwide web.

131

5.5 Design of photovoltaic power system for smart SHM

Installation of an SHM system at a remote location such as Bridge 7937 in Tucumcari necessitated the development of an innovative method to power the system. After careful investigation, it was found that there was no electrical power availability at the bridge site. Therefore, we decided that a photovoltaic (PV) system would need to be designed in order to provide the power energy required to enable efficient SHM. The graphical position of the city of Tucumcari, New Mexico was defined at Latitude: 35° 10' 18" N and Longitude: 103° 43' 27" W. The PV system design consists of estimating the energy load required followed by an estimate of autonomy system requirements for backup. The location of PV system is shown in Figure 5-45. Finally, a layout analysis of the proposed PV system and the structural system to support the solar panels are presented in Appendix B.
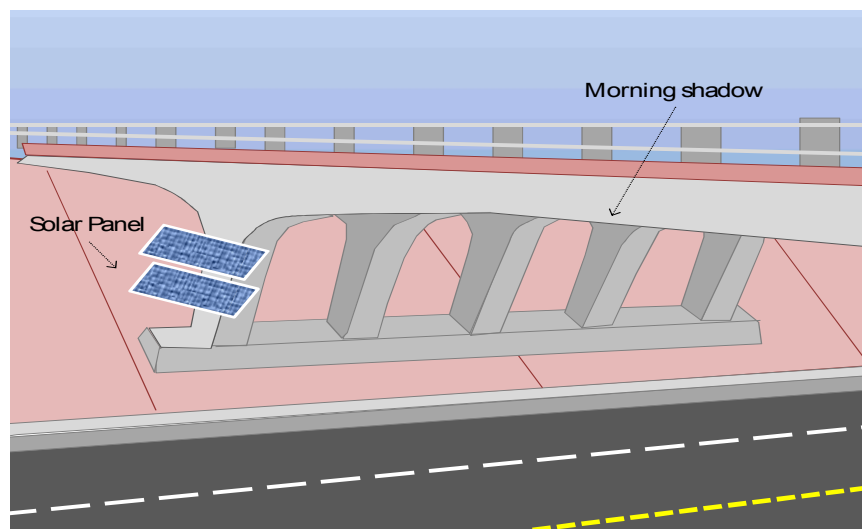
Figure 5-45 Location of the PV system designed for Tucumcari Bridge

5.6 Installation of SHM system on Bridge 7937

After testing and calibrating all the components of SHM system on a model truss bridge in UNM laboratory and ensuring system ability to detect damage, the SHM system was brought to the bridge location in Tucumcari and was installed on Bridge 7937. Installation of the SHM system was performed by UNM SHM research group and 3B Builders who are a certified electrical contractors operating in New Mexico.

The first step was to install a steel box for housing all the data acquisition, wireless modem and other electronic devices such as power inverter and solar panel batteries. The steel box is outdoor rated enclosure (Nema 4) that has two holes on top to connect all the wires into the system. Figure 5-46 and Figure 5-47 show the installation process as well as a photograph of the inside of the steel box before installation of the SHM components. As shown in Figure 5-46 the steel box was installed on the third K-Frame underneath the bridge.

Figure 5-46 Installing of the steel box to house all electrical components at the bottom of Bridge 7937.

Figure 5-47 Steel box used for housing the data acquisition system and all SHM components.

After installation of the steel box on the bridge, hangers were drilled into the bridge and attached using tapcon screws to make a path for accelerometer cables into the steel box as shown in Figure 5-48.

(a)	(b)

Figure 5-48 Installation of hangers underneath the girders of the bridge using tapcon bolts.

By putting enough hangers on each girder of the bridge and connecting wires through the hangers, accelerometers were installed using stainless steel plates that were specially designed and tested before installation in the UNM Structures Laboratory as described earlier. The stainless steel plates were anchored to the bottom of the bridge deck in very close proximity to the girders, and then the accelerometers were attached to the steel plates. After the accelerometers were attached to the stainless plates, a silicon insulator was installed over the sensor and the stainless steel plate to produce a silicon dome over the accelerometer to environmentally protect the sensor against dust and all other harsh environmental effects. Figure 5-49 illustrates the original stainless steel plates and the accelerometers before installation on the bridge and the protected accelerometers with silicon dome after being installed on the bridge with the stainless steel plate. Figure 5-50 shows a view of the bridge where after all the accelerometers were installed and wired to the steel box. In this figure, the wireless antenna can be observed.
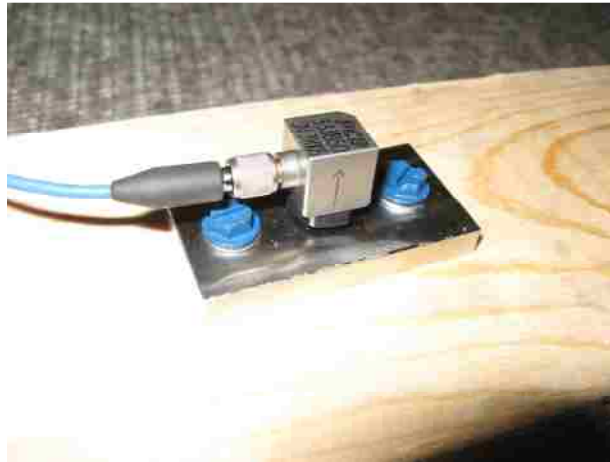
(a)

(b)

Figure 5-49 (a) Accelerometer attached to stainless steel plate before installation.

(b) An accelerometer attached to the bridge slab using a stainless steel plate.

(a)

(b)

Figure 5-50 (a) View of the bridge after installation of all accelerometers. (b) All accelerometers wiring going to the Box. Figure also shows the wireless antenna.

Two conduits with two small electrical boxes were made, one to pass the cables from the solar panel to the steel box housing all the data acquisition system to power the SDA,

137

www.manaraa.com

and the other to pass the cables from strain gauges attached on the FRP zone on top of the bridge to the data acquisition (DAQ) box at the bottom. Figure 5-51 shows these conduits and the electrical box made to house the electrical cables from the solar panels.

Figure 5-51 Electrical boxes and conduits to pass power to the SDA using the solar panels.

After installing all the accelerometers and attaching them to the SDA system, the strain gauges were installed on the FRP sheets to monitor debonding of FRP sheets from the concrete surface. All strain gauges were covered and the wires from them were attached to the cables which transmit the signals from the strain gauges through the aforementioned conduit, to the SDA system located in the steel box. Environmentally protected strain gauges produced by Vishay, Inc. were used. The strain gauges were installed following standard installation techniques considering all cleaning and bonding requirements. Special epoxies were used to attach the strain gauges to the FRP sheets. Dead weights were put on top of the installed strain gauges to produce the required

pressure to ensure the gauges were bonded. The strain gauges were left for 24 hours before connecting to the SDA. Figure 5-52 shows the weights applied on top of each strain gauge to make sure they are attached completely to the FRP sheets. Figure 5-53 shows one strain gauges after being covered by the rubber protection. Figure 5-54 shows all strain gauges attached to the FRP sheets. Figure 5-55 shows concrete casting above the strain gauges and the area strengthened with FRP after being batched with concrete and the sensor connections to the monitoring box.

Figure 5-52 Weights applied on top of each installed strain gauge.

Figure 5-53 Covered strain gauges attached to the FRP sheets.

Figure 5-54 All the strain gauges after being installed on the FRP sheets and connected to the wires transmitting the strain signals to the DAQ device.

(a)	(b)

Figure 5-55 (a) Concrete casting over area of bridge deck strengthened with FRP and (b) Top of bridge deck after concrete casting showing the connection of the sensors to the monitoring box under the bridge.

Moreover, four thermocouples were installed on the top surface and the underside of the bridge to measure the bridge temperature at both these points. Figure 5-56 shows one of the thermocouple sensors attached to the web of the bridge girder.

Figure 5-56 One thermocouple sensor attached to the web of the bridge girder.

Upon completion of the installation of all sensors on the bridge surface, they were connected through their cables to the SDA system housed in the steel box and located underneath the bridge. The SDA was connected wirelessly to the Worldwide Web. Figure 5-57 shows the inside of the steel box with the SDA system and the wireless modem attached. The figure also shows the rechargeable battery for the solar cell, the digital timer and the power inverter that is required to switch the DC power obtained from solar panels through rechargeable batteries to the AC power that can be used by the SDA. The digital timer is programmed to schedule operation time. While the system can acquire data all the time, data transmission using wireless protocol has to be limited for wireless cost and for power limitations associated with using solar panels. The system is designed to operate for 8 hours daily.

141

Figure 5-57 Data acquisition system, rechargeable batteries, power inverter, digital timer switch and the wireless modem located at the steel box.

The solar power was also successfully installed and is timed to work 8 hours every day. Special time for data download during low wireless activity is also scheduled. Figure 5-58 and Figure 5-59 show the solar power panels installed to provide clean renewable energy to the monitoring system and their connection to the monitoring system. In these figures the structural design is also shown. Steel chords used for hanging the solar panels to the bridge have been designed to prevent overturning of solar panels against the wind turbulence.

142

Figure 5-58 Solar power system installed on Bridge 7937 to provide clean renewable energy for the SHM system.

Figure 5-59 Solar power system installed on Bridge 7937 to provide clean renewable energy for the SHM system.

5.7 User interface to monitor Bridge 7937 in Tucumcari, New Mexico

With the SDA system and wireless modem, the user can monitor the bridge wirelessly through the World Wide Web. The SDA system is programmed in such a way that gives the user an easy graphical interface to monitor the bridge and obtain data from all the sensors installed on the bridge. Moreover, the graphical interface gives the user the ability to control the SDA remotely by choosing the data and timeframe to be saved on the SDA device. The user can also observe live data from each sensor at any time remotely. Figure 5-60 shows the graphical interface that needs to be set up by the end user to remotely observe the bridge data.
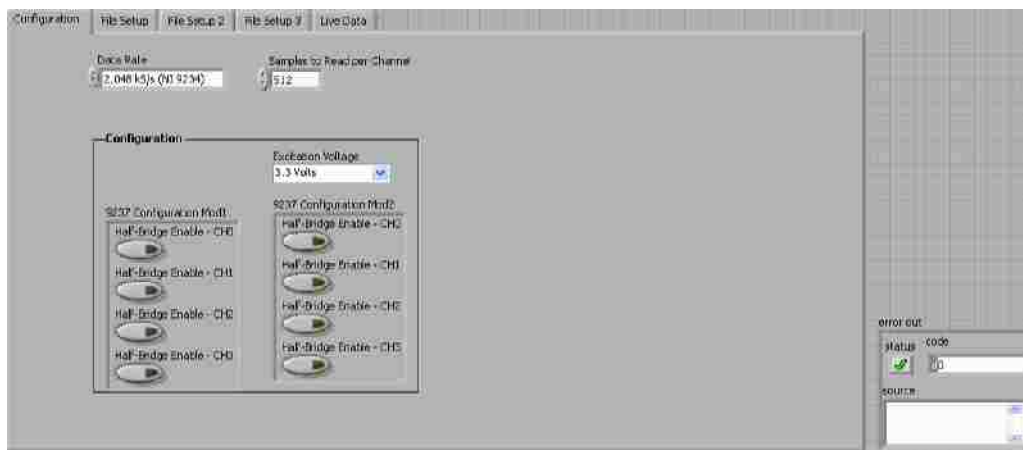
Figure 5-60 Graphical user interface shows the "Configuration" of modules.

On the left side of Figure 5-60, under the tab called "Configuration", the end user can change the rate of acquiring data from accelerometer and strain gauge modules from 2000 samples/sec to 50,000 samples/sec. Moreover, the end user has the ability to change the "Excitation Voltage" needed for strain gauge modules and the "Configuration" of strain gauges in Wheatstone bridge from "Half-Bridge" to "Full Bridge". Two strain

144

gauges are used on each spot of the FRP zone that compensates for temperature effect, producing what is known as Half-Bridge strain gauges.

Figure 5-61 shows the next tab of the above figure. This new view is called "File Setup" and shows how the files are time stamped based on the exact date, hour, minute and second they are acquired along with the base name of the file. File Setup can also give the user the ability to save the file automatically on the SDA for desired time duration and desired gaps between the files or save manually using a control switch.
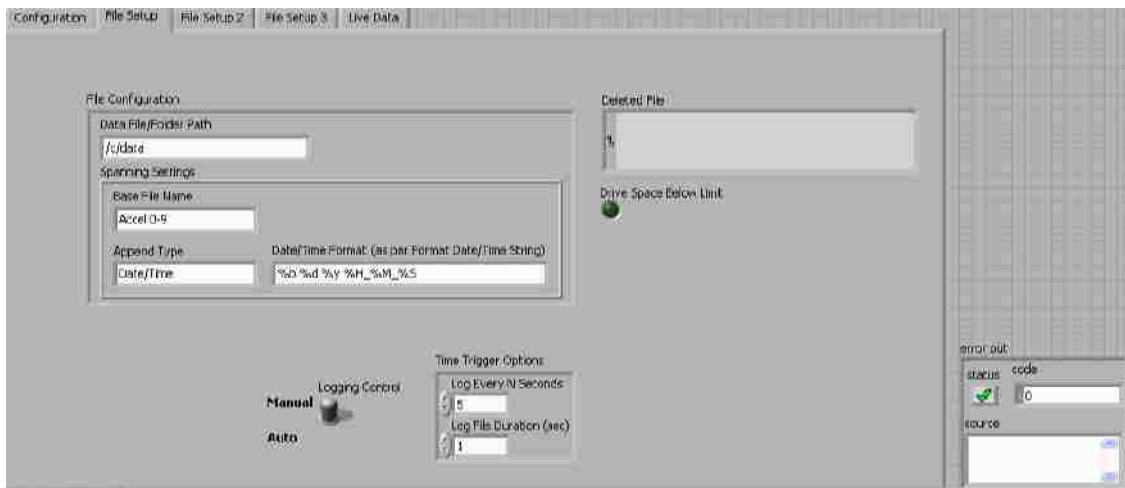
Figure 5-61 Graphical user interface shows "File Setup".

As shown in Figure 5-61, the base file name is Accel 0-9 which saves data from the first ten accelerometers. Saving data in three different categories (Accel 0-9, Accel 10-19, Strain) limits the size of each file to allow transfer of the file using FTP protocol wirelessly. It has been observed that one second duration of the saved file along with logging every five seconds are suitable numbers to acquire data from random traffic passing over the bridge. When the user puts the logging control on manual, no data is

145

saved on the SDA device until the logging switch which is located on the "Live Data" tab, as shown in Figure 5-62, is turned on. When the logging switch turns on, the user can save data on the SDA device for as long as the switch is on. Manually saving data is not recommended since different sizes of data will be saved on the SDA system that might be so large that sending it wirelessly won't be feasible. "File Setup 2" and "File Setup 3" tabs shown in Figure 5-62 are exactly the same as "File Setup" except they are designed for accelerometers 10-19 and strain gauges respectively. The user can observe live data from each sensor. Temperature data from all thermocouples can also be observed in Celsius Degree in the "Live Data" tab.
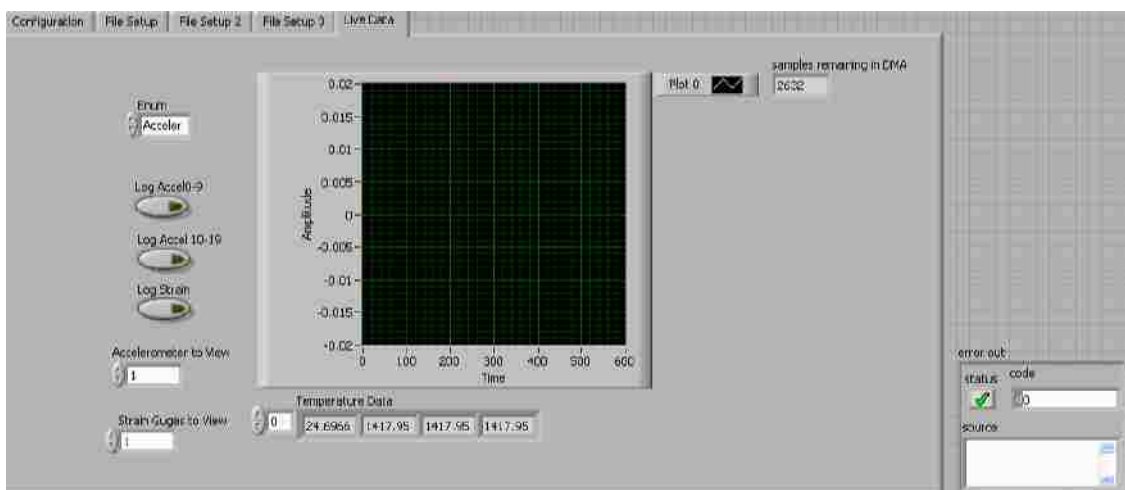
Figure 5-62 Graphical user interface shows "Live Data".

To use the graphical interface discussed above, the user needs to login to the web address given below in Internet Explore (IE).

http:// tucumcari-project.dyndns.org:9999/

146

The website is specifically made for the Tucumcari Bridge using dynamic DNS (dyndns.org) website. After using the web address given above, the user needs to put the following address in IE.

http:// tucumcari-project.dyndns.org:9999/SHM.html

Please note that the web address is case sensitive. A snapshot of this web address viewing live data from Bridge 7937 is shown in Figure 5-63.

If data recording is planned, it is important to realize that the data will be stamped based on the sensors (accelerometers and strain gauges) at the exact time it was acquired. The user then needs to use FTP protocol to transfer the data to a personal computer (PC). The webpage the user needs in order to get the data is

ftp://tucumcari-project.dyndns.org/

The user should allocate a data folder and copy the data and paste it into the folder on the PC. Figure 5-64 shows what will appear to the user after accessing the above address in IE.
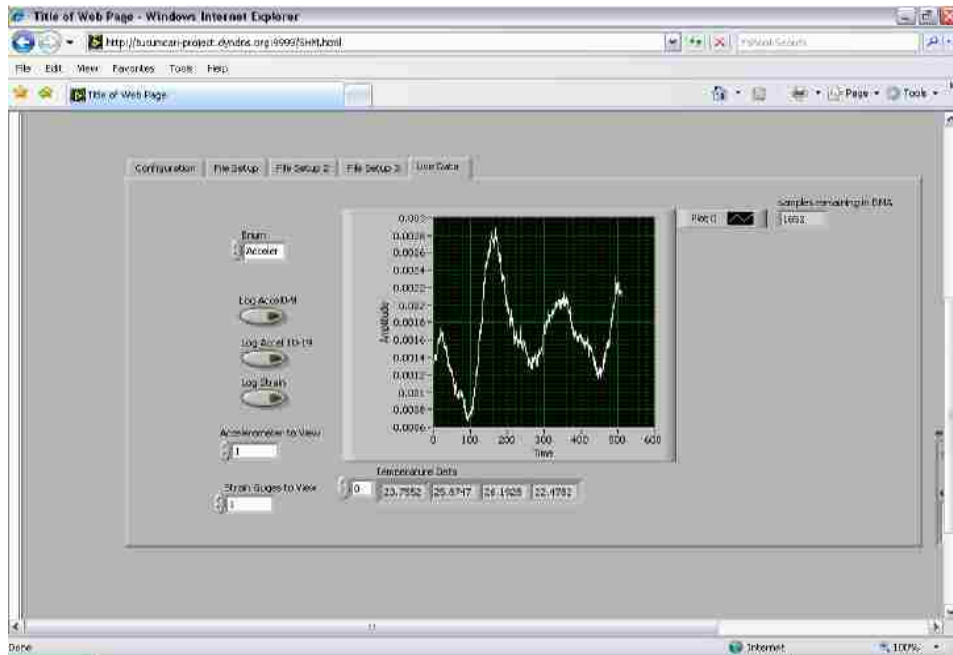
(a)
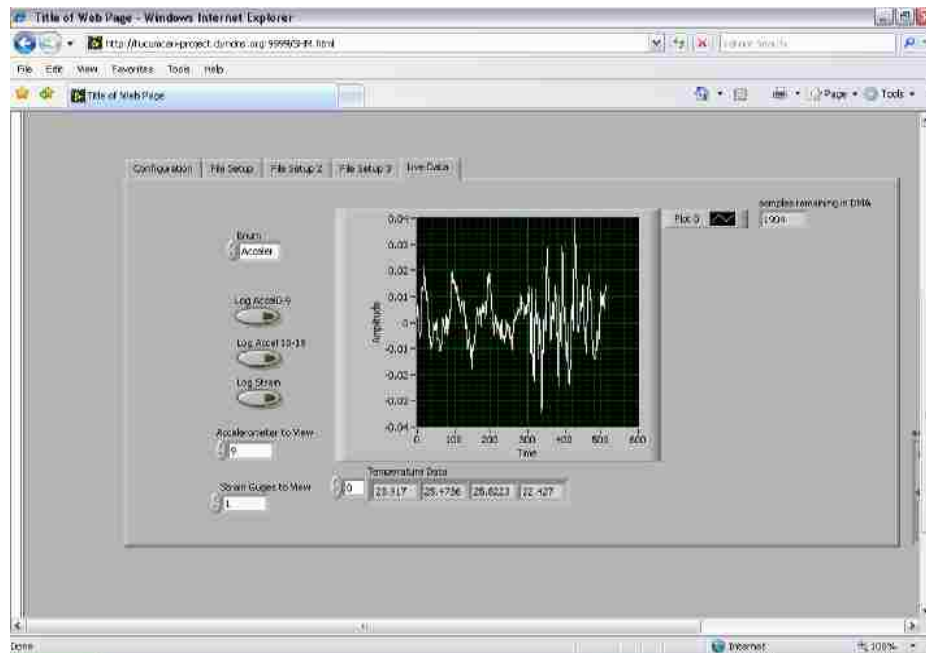
(b)

Figure 5-63 Live data from the web address to view Bridge 7937 recorded on June 26, 2009 (a) Acc 1 & (b) Acc 9 .

148
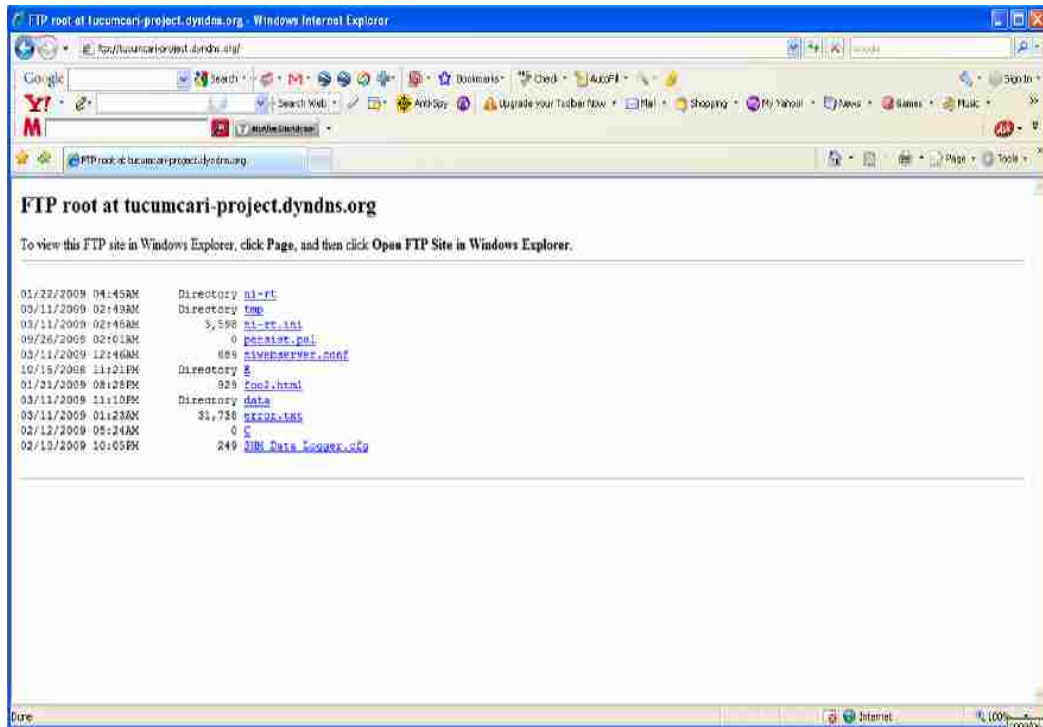
Figure 5-64 FTP graphical interface for transferring the data from SDA.

It is important to note that all the data saving and data-user interface protocols designed specifically by the author for the above monitoring project.

5.8 Data analysis for damage detection of Bridge 7937

The files that are saved on the SDA device and transferred through FTP protocol have TDMS file format which is a format readable by special software for data acquisition. Special software is developed for reading and analyzing this data. The software called SMART-SHM is composed of two executable files that are designed to run on typical PC. The first file is called SMART-SHM-START.EXE which allows the user to view the data files downloaded from the bridge as "raw data" and to save them for further analysis.

149

The second file called SMART-SHM-DAMAGE.EXE, is designed for damage detection. On the first software SMART-SHM-START, the user has the ability to view all the sensors on the bridge and to display the synchronized data from the bridge for up to 4 sensors at the same time. Figure 5-65 provides a snap shot of SMART-SHM-START software. The temperature data is shown at the bottom of the Software in degree Celsius. SMART-SHM-START also allows the user to perform basic analysis of the data. Four types of analysis are available. In addition to time domain data discussed above, fast Fourier transform and Wavelet transform can be performed and displayed. The software also allows the user to view a down-sampled wavelet transform of any desired sensor as shown in Figure 5-65. In Figure 5-65, it is shown that while the data was acquired from the bridge using 2 kHz sampling rate, the Wavelet transform smoothes the signals and the high frequency components of signals are eliminated from the original signal. The down-sampled Wavelet transform will have a sampling frequency of 400 Hz.

.

150
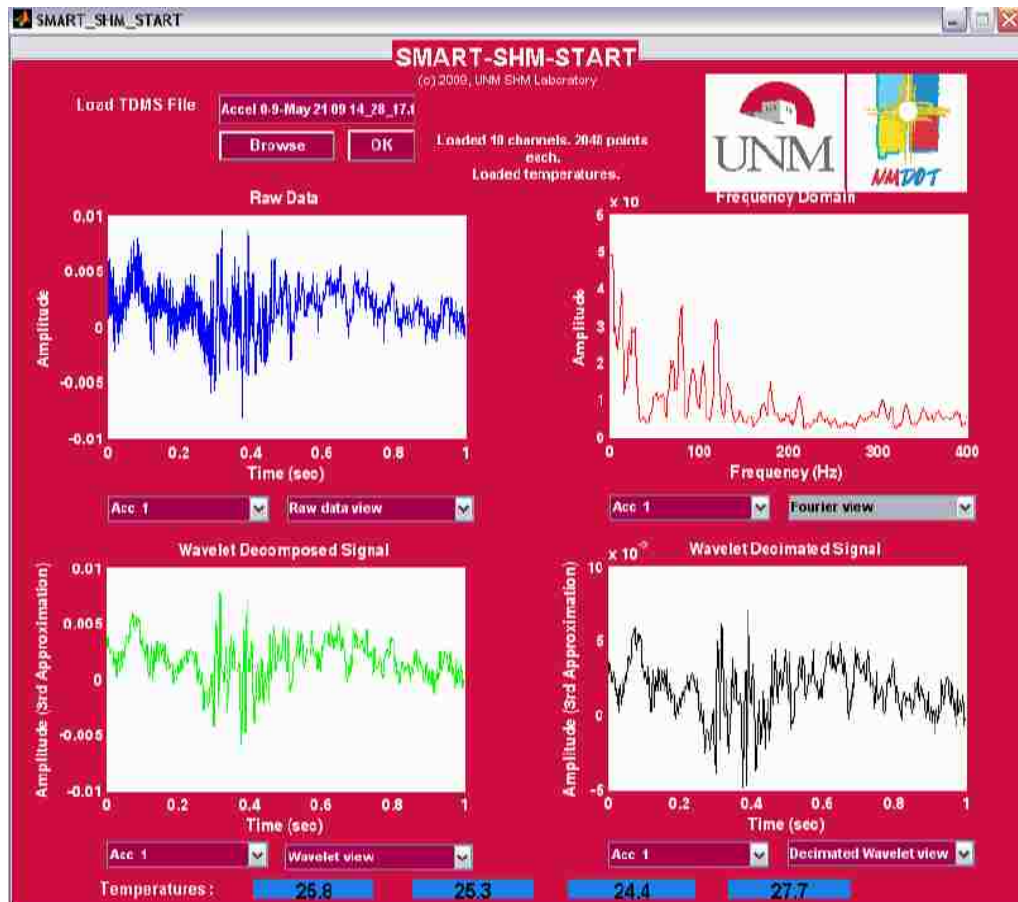
Figure 5-65 SMART-SHM-START software shows raw data, Fourier transform, Wavelet transform and decimated Wavelet signals collected from Sensor 2 (Acc.1) installed on the bridge. The bottom row shows the temperature at four locations on the bridge.

To detect damage on the bridge, another executable software was coded and produced. The second software, called "SHM-SMART-DAMAGE", was designed to perform damage feature extraction using wavelets and fast Fourier transform and to display the history of the bridge damage feature. SHM-SMART-DAMAGE starts by loading the training files, to train the software based on available data gathered during a period of time when the bridge has been monitored. Since the data gathered wirelessly and

randomly from the bridge is a large dataset, it is needed for the training process. The training dataset is used to establish the boundaries of the damage feature (being Wavelet or Fourier). The boundaries were established at 99.7% probability. After the training data is loaded, a new dataset can be loaded. Here, two different methods are used for detecting damage on the bridge:

First, Fast Fourier Transform (FFT), which transforms the raw data from the bridge in the time domain to the frequency domain, is used. When damage occurs to the bridge, the main frequency components of the bridge might change and therefore the maximum frequency of acceleration signals will change. Since the bridge has very large stiffness and mass, the little damage would not be able to change the major frequency components of the bridge. The maximum signal frequency was limited to 45 Hz since the signals with higher frequencies usually represent noise. In the training part of this method, the maximum frequency of signals at each sensor is computed for each training dataset and the mean value of all datasets is used for the training process. The upper and lower limits for the healthy state of the bridge are calculated based on 99.7% probabilities not to exceed the mean (i.e. $\pm3\sigma$). This is represented graphically in the software. For any new dataset, the software will display its location on the chart with respect to the mean boundaries. It should be noted that lack of enough training of the datasets may result in false alarms.

Second, the energy of signals calculated in the wavelet domain is used as a damage feature to differentiate between healthy and damage states of the bridge. The acceleration signal is decomposed into approximation and detail signals with low and high frequency

152

components respectively using Wavelet transform as presented before in Equations 5-6 to 5-9.

Using the energy of the wavelet decomposed signals; the training datasets were computed. The mean value and 99.7% boundaries were established. For any new dataset obtained from the bridge, if the energy of signals calculated in the wavelet domain at the location of each sensor passes the established boundaries, the bridge might be experiencing damage near the location of that sensor. It should be noted again that to not get false alarms about damage on the bridge, the training process should be done for a large number of datasets gathered from the bridge at different times. It is also worth mentioning that the damage features, discussed above, are calculated at the location of each sensor and in this case each sensor has independent damage value from the other sensors. Figure 5-66 represents a snapshot of the SMART-SHM-Damage software showing the mean and boundaries of the Fourier transform damage feature at sensor 3 (Acc 2). It can be observed in the snapshot that 10 datasets were used to establish the damage boundaries.

It is again important to emphasize that all these algorithms and software have been developed by the candidate as part of the SHM research field implementation.

153
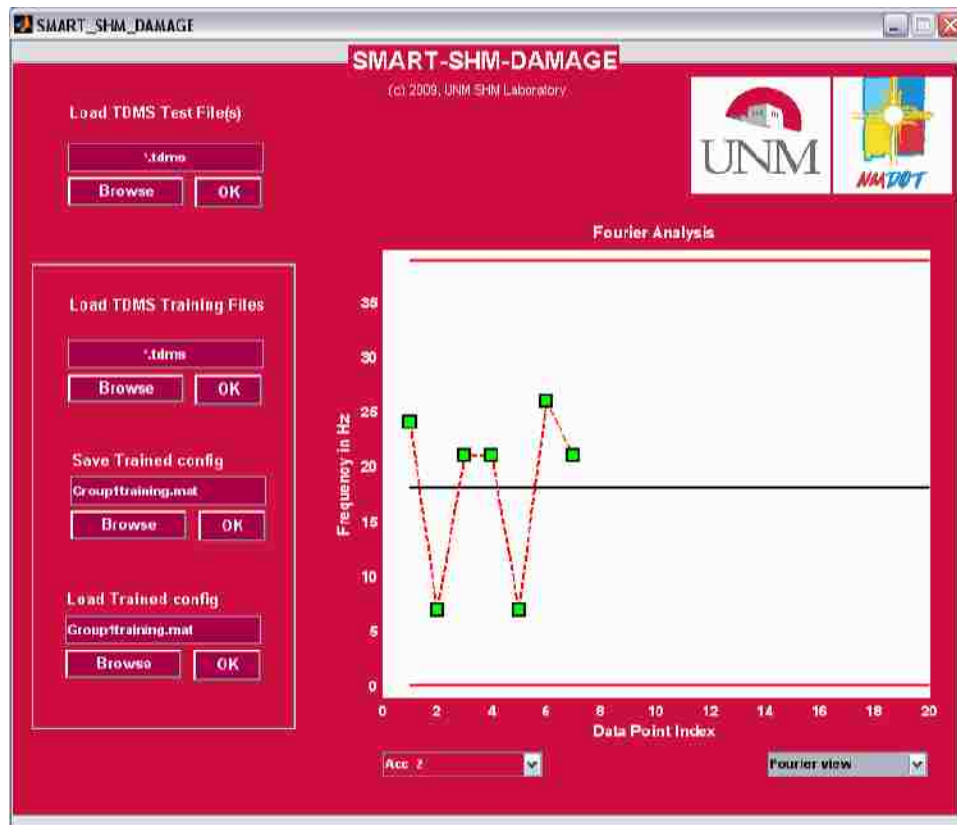
Figure 5-66 Snapshot of SMART-SHM-Damage shows the history of the frequency damage feature at Sensor 3 as extracted from Bridge 7937.

As it is obvious from Figure 5-66, the frequency mean value of all training datasets is around 20 Hz while the lower and upper limits will be between 0 and 40 Hz. Moreover, it is apparent that all the frequencies are within the established range that confirms the healthy state of the bridge. Figure 5-67 represents a snapshot of the SMART-SHM-Damage software showing the mean and boundaries of the wavelet transform damage feature at Sensor 8.
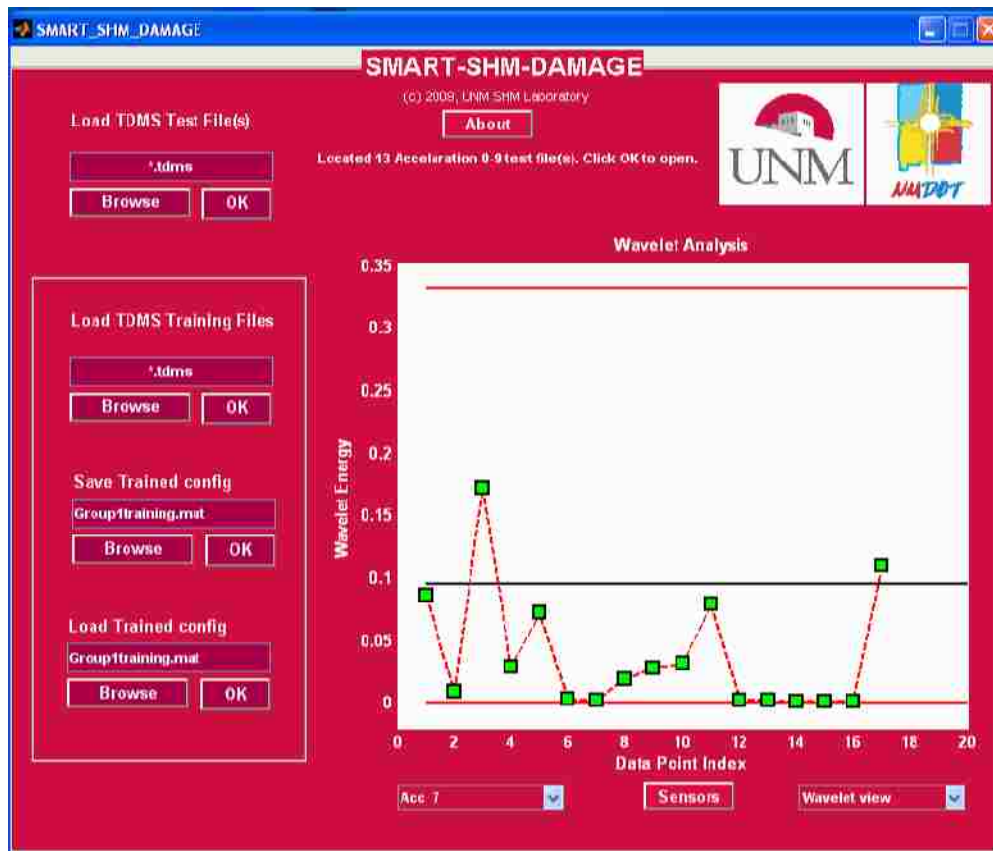
Figure 5-67 Snapshot of SMART-SHM-Damage shows the history of the wavelet damage feature at Sensor 8 as extracted from Bridge 7937.

As shown in Figure 5-67, the mean value of energy of signals calculated in the Wavelet domain at Sensor 8 is around 0.01 while the lower and upper limits calculated from the mean value plus or minus three times of the standard deviation calculated at the location of sensor 8 are 0 and 0.33 respectively. It can also be concluded that for 17 different datasets obtained at different times, no damage has occurred near Sensor 8 since all the results are located within the established healthy limits.

It should also be mentioned that the SMART-SHM-DAMAGE software made for this project has the ability to show up to 20 different datasets obtained from the bridge at

different times in order to give the user a sense of the history of the bridge. Finally, the user is capable of saving the configuration of all the files obtained from the bridge to compare to new datasets at a later date. Moreover, the user can also save the configuration of the files used for training of the program and use different datasets as training files.

5.9 Damage detection of the bridge

The fact that the bridge is healthy hinders realistic damage detection in the bridge. Therefore, virtual damage needs to be made and checked the ability of the proposed method to detect damage in the bridge upon occurrence. Therefore, a 3D FE model of the bridge, using SAP 2000®, is made to simulate the structural behavior of the bridge under traffic loading. This model simulated the variable cross section of girders and their attachments to the concrete slab accurately. The model was first calibrated based on the field test done by a truck with known weight as mentioned earlier in this chapter. The calibration process was based on modifying the bridge cross sectional stiffness such that the strains calculated from the first girder of the 3D FE model to meet the strains measured by strain gauges at the same locations on the bridge with the known test truck (speed and the weight of the truck were known in the field test). Figure 5-68 and Figure 5-69 show the calibration process based on the location of strain gauges shown in Figure 5-20.
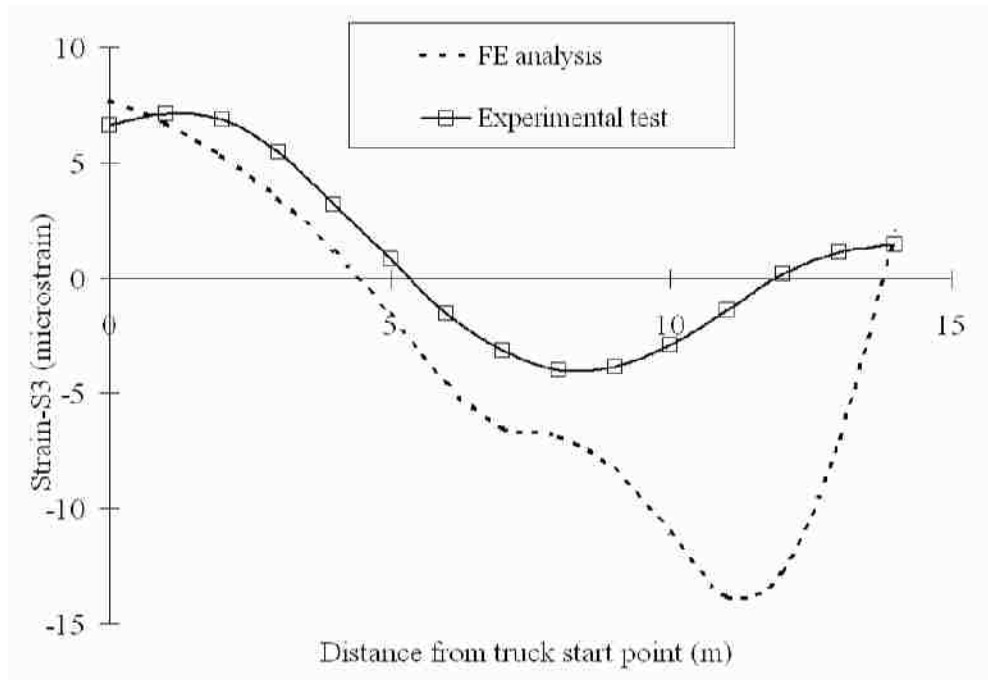
Figure 5-68 Strains calculated from FE model and field test at Strain Gauge 3 as shown in Figure 5-20 to calibrate the FE model.
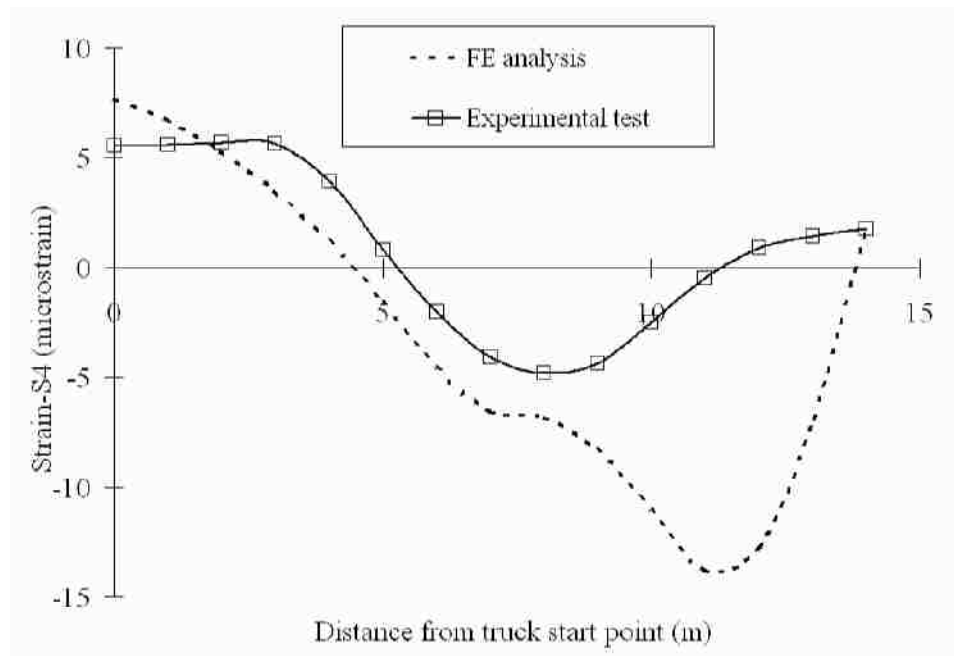
Figure 5-69 Strains calculated from FE model and field test at Strain Gauge 4 as shown in Figure 5-20 to calibrate the FE model.

157

The FE model consists of five K-frame girders with variable cross section based on as built drawings of the Tucumcari Bridge. Fifty-seven frame elements are used to model each girder of the bridge with 1m projectile length on longitudinal axis of the bridge along with shell elements to model the concrete bridge deck slab as shown in Figure 5-70. Different cars and trucks with the speed limit of 75 mph as posted on the bridge are used to simulate the traffic on the bridge. Because of the random traffic passing across the bridge, each monitored file relates to one of these unknown traffic loading scenarios. A time history analysis has been done for several random traffic loadings to identify the acceleration at each node of the calibrated FE model.
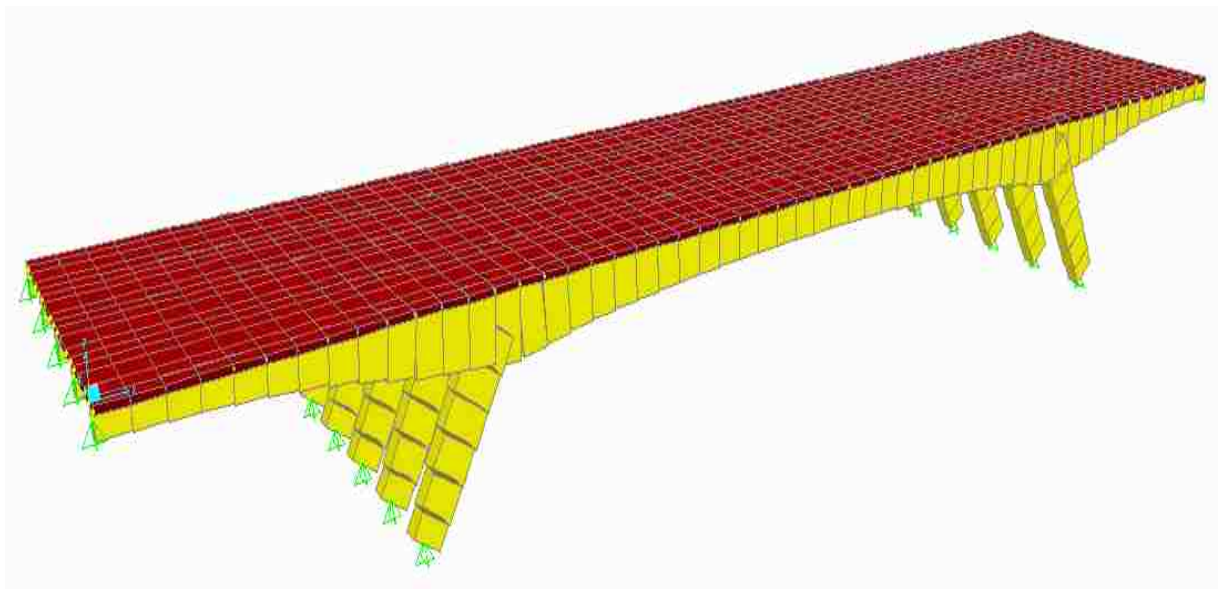
Figure 5-70 3D FE model of Tucumcari Bridge.

By calibrating the FE model with the data obtained from static field test, the FE model can be used to correlate the acceleration data from the accelerometers on the bridge with the accelerations computed from FE model at the same location of accelerometers. Since

158

each dataset measured from the bridge is from an unknown traffic loading, we changed the magnitude and the axles of trucks and cars used to simulate traffic loadings on the FE model to match the field test. The main hurdle to match acceleration datasets other than the unknown type of loading is the challenge to model damping characteristics of the real bridge. This issue can make irregularities in an exact match of signals in the time the signal is damped or reaches its peak. In this FE model, the damping ratio changed from different range of 1% to 50% to correlate acceleration signals. Figure 5-71 illustrates an acceleration signal computed from the FE model at the location of Acc 9 as shown in Figure 5-27 and Table 5-1. This acceleration signal computed from the calibrated FE model of a two axle truck weighing 32 kN passing through the bridge with 75 mph speed. Moreover, Figure 5-72 and Figure 5-73 represent the signals measured from different accelerometers on the bridge and the ones computed from the calibrated FE model at the same locations. As shown in these figures, the calibrated FE model is able to compute acceleration signals similar to that observed from the bridge using distributed accelerometers.
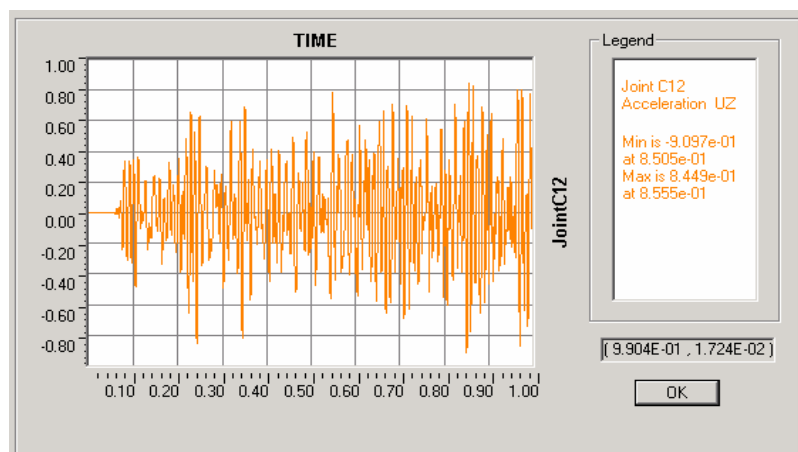
Figure 5-71 Snapshot of an acceleration signal computed from the FE model at the location of Acc 9.
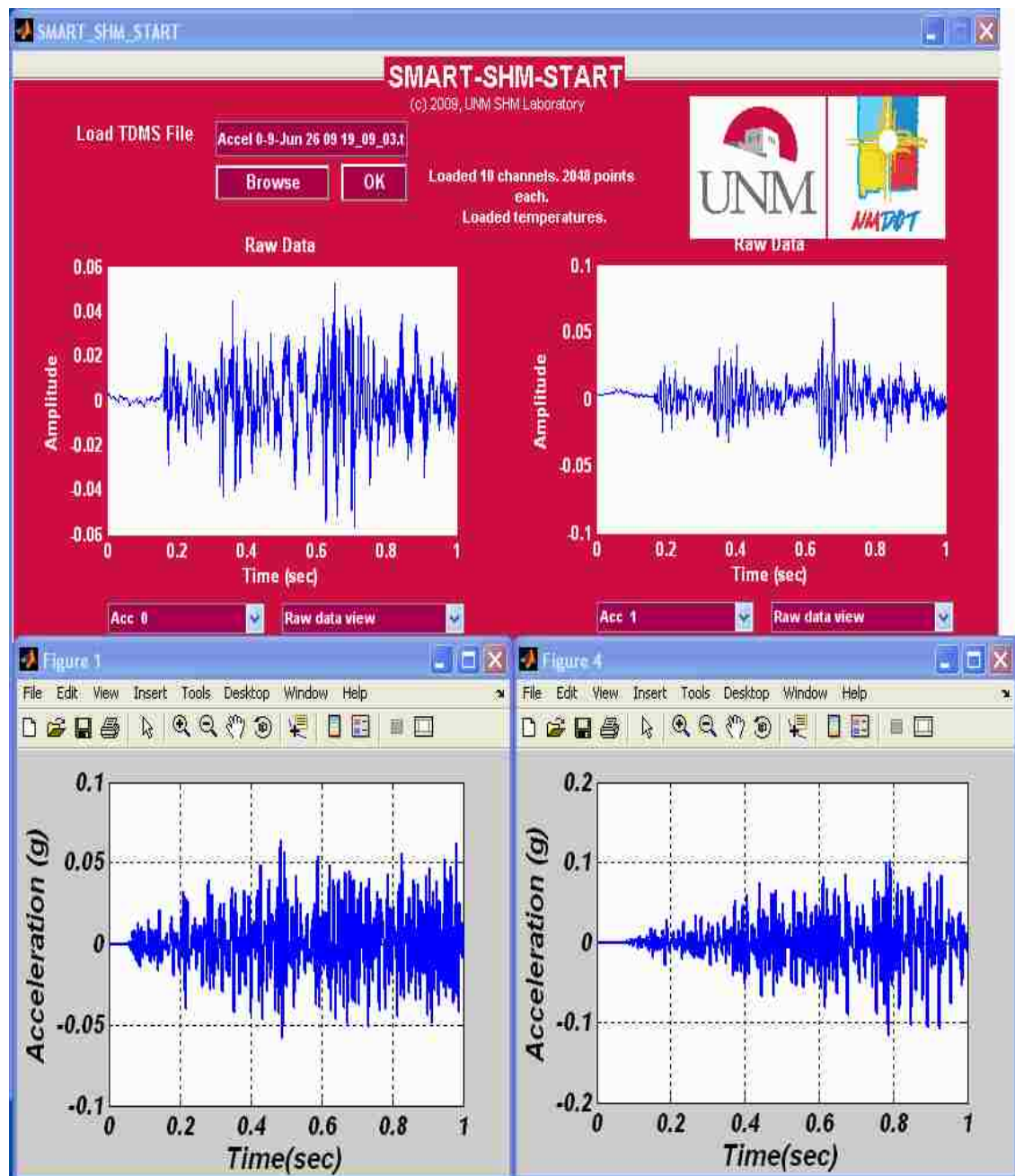
Figure 5-72 Acceleration signals measured from Acc 0 and Acc 1 on the bridge at 19:09:03 June 26, 2009 from the Tucumcari bridge compared with the signals computed from the calibrated FE model at the same location of accelerometers.

160
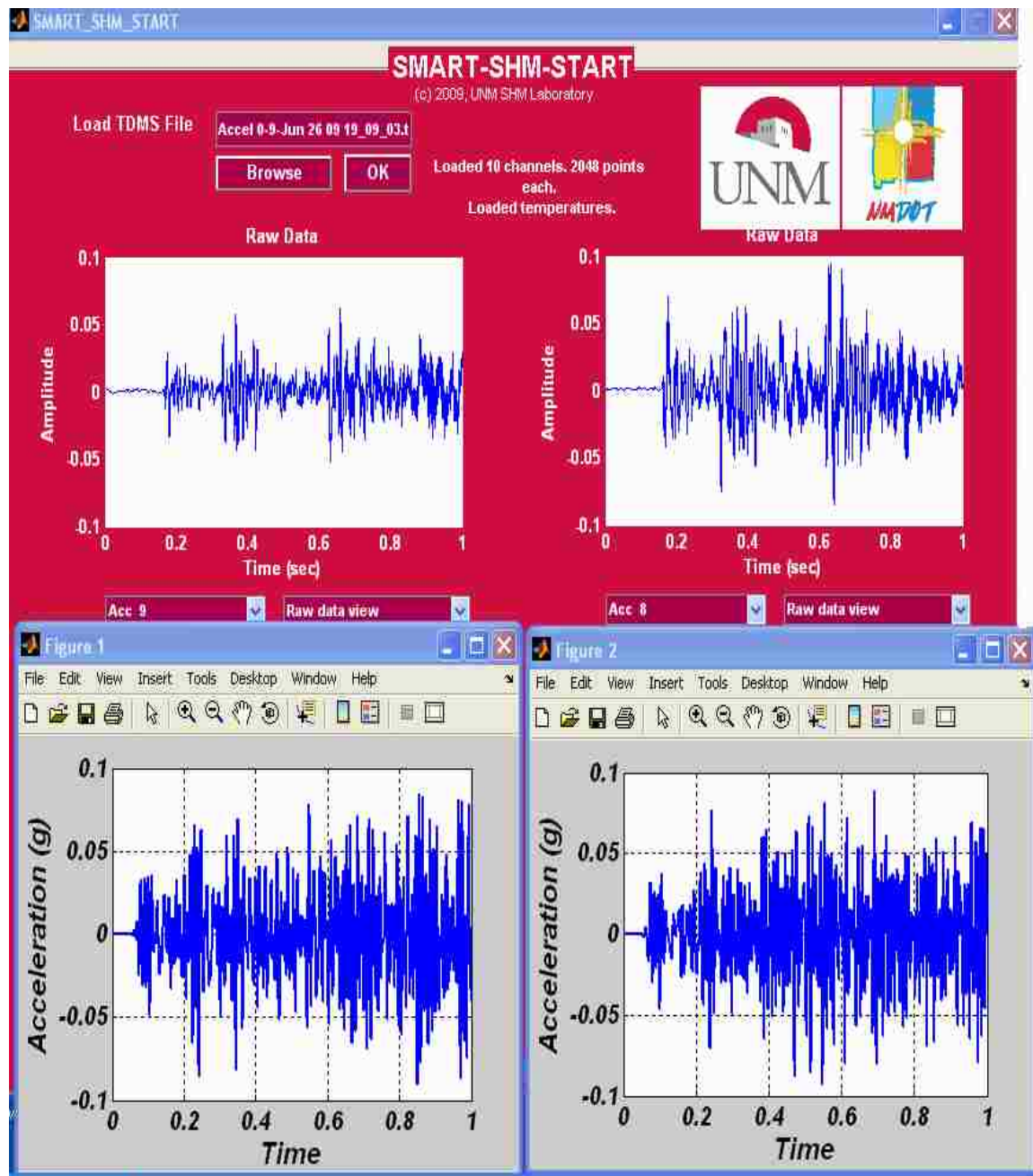
Figure 5-73 Acceleration signals measured from Acc 8 and Acc 9 on the bridge at 19:09:03 June 26, 2009 from the Tucumcari bridge compared with the signals computed from the calibrated FE model at the same location of accelerometers.

161

As shown in Figure 5-72 and Figure 5-73, high correlation between the acceleration signals measured from accelerometers on the real bridge and that simulated by the calibrated FE model can be observed. This means that the FE model can be used to examine the ability to detect damage in the bridge using acceleration signals.

5.10 An inductive fuzzy damage classification method applied to the Tucumcari Bridge

In this section, different states of the Tucumcari Bridge are identified. Most SHM research defined damage states using statistical methods such as Bayesian updating for damage accumulation (Shiao 2005), support vector classifiers (Jonker et al. 1999) and non-linear system identification (Adams and Farrar 2002, Yu 2005) that considers uncertainty due to randomness in measurements (Ross 2004). In these methods, other types of uncertainty such as fuzziness and ambiguity due to the lack of information (e.g. lack of crisp boundaries defining damage states) are neglected because these methods rely on probability theory (Klir and Yuan 1995). Integrated approaches to address aleatoric and epistemic uncertainties in structural safety and reliability have been of interest recently to the research community (Hung et al. 2003, Elms 2004).

In this section, damage features are represented using fuzzy set theory. Different damage states in structures are described by a group of fuzzy sets that are established by principles of inductive reasoning. The vagueness and uncertainties associated with damage definition and the significant overlap between different damage states in structures makes damage-state description amenable to fuzzy definitions and fuzzy pattern recognition. Inductive reasoning or inductive inference is the process of extracting

162

general rules from limited and specific sets of information (Feeney and Heit 2007). Inductive reasoning is considered a cognitive activity that integrates probabilistic and non-probabilistic uncertainty for approximate reasoning of observations (Feeney and Heit 2007). The damage definition process is always based on limited and uncertain information. Damage detection and damage pattern recognition is therefore a fertile field for utilizing principles of inductive reasoning (Tenenbaum et al. 2006).

Our method aims at classifying damage states in the structure by establishing fuzzy sets. Since different damage states in the structure have significant overlap and vague boundaries, fuzzy sets are used to describe these damage states. Using fuzzy set theory, the two kinds of uncertainties (i.e. aleatoric and epistemic) associated with defining damage states in structures is considered.

5.10.1 Establishing Inductive Fuzzy Damage Sets

The use of inductive reasoning for classification is based on the fact that the process of induction is associated with minimum uncertainty. Claude Shannon (1948) introduced entropy as a measure of disorder in classifying data in 1948 to describe uncertainty or to quantify the information content in a dataset. The uncertainty associated with the value of a discrete random variable (ζ) can be measured by the entropy (S) as

$$S(\zeta) = -\sum_{\zeta \in Z} p(\zeta) \log p(\zeta) \tag{5.10}$$

where $p(\zeta)$ is the probability of the occurrence of ζ. In order to minimize uncertainty, the entropy $S(\zeta)$ should be minimized. The value of (ζ) corresponding to the minimum entropy $S(\zeta)$ is an induced threshold value that will partition the domain into two classes

(Kim and Russell 1991, Ross 2004). This entropy can be used as a reasoning basis to obtain generalized classes for a specific set of limited observations. Fuzzy categories are formulated based on the premise of an argument regardless of the fact that such categories are not certain (Applebaum 2003).

In order to establish fuzzy sets to describe damage states of the structure, the threshold values defining the boundaries of these fuzzy sets need to be identified. First, two fuzzy sets can be established as a two class partitioning problem, then other fuzzy sets describing other damage states of the structure can be established by generating subclasses for each individual class. Based on inductive reasoning principles the first threshold partitions a domain into two classes. This point (x^0) that minimizes entropy in the interval $[x_1, x_2]$ can be used to partition this domain. The entropy of point (x^0) on the damage feature domain (x) can divide the interval $[x_1, x_2]$ into two intervals $[x_1, x^0]$ and $[x^0, x_2]$. The entropy S can be calculated as

$$S(x) = \sum_i p^i(x) S_i(x) \tag{5.11}$$

$$S_i(x) = -\sum_j p_j^i(x) \ln p_j^i(x) \tag{5.12}$$

where $p_j^i(x)$ is a conditional probability that the class j sample is in the region $[x_i, x_i+x]$ and $[x_i+x, x_{i+1}]$ and $p^i(x)$ are probabilities that all samples are in the region $[x_i, x_i+x]$ and $[x_i+x, x_{i+1}]$. The values $p_j^i(x)$ and $p^i(x)$ are calculated as

$$p_j^i(x) = \frac{n_j^i(x) + 1}{n^i(x) + 1} \tag{5.13}$$

164

$$p^i(x) = \frac{n^i(x)}{n}, \quad \sum p^i(x) = 1 \qquad (5.14)$$

where $n_j^i(x)$ is the number of class j samples located in ith interval $[x_i, x_i+x]$, $n^i(x)$ is the total number of samples located in ith interval and n is the total number of samples in the interval $[x_i, x_{i+1}]$.

By choosing the type of membership function (MF) (triangular, bell shape and etc), fuzzy sets are established in the damage feature domain. To consider the fuzziness in the damage detection process, some degree of overlapping between two adjacent fuzzy sets needs to be achieved. To establish secondary fuzzy sets accounting for other damage states of the structure, the secondary threshold values are obtained based on the primary threshold value. In other words, the damage feature with the highest membership value in an intermediate fuzzy set corresponds to the minimum membership value in the two neighbouring fuzzy sets. That enables a significant overlap between the damage fuzzy sets which directly correlates to the level of fuzziness (uncertainty) in the damage states (Klir and Yuan 1995). The software code to find these points is presented in Appendix C.

For Tucumcari Bridge, one primary threshold value and two secondary threshold values were identified to establish three fuzzy sets describing three damage states in the bridge: healthy, medium damage and severe damage. It is important to note the importance of correlating that fuzzy level of damage to mechanical damage in the structure. A few methods have been recently proposed for establishing such correlation (Zhang et al. 2008, Sheyka et al. 2008).

5.10.2 Fuzzy Pattern Recognition

The process of classifying an unknown fuzzy vector/set based on known fuzzy sets is called fuzzy pattern recognition. As the fuzzy damage sets are established as explained above, using fuzzy pattern recognition, datasets of damage feature can be classified to one of the damage classes already defined by fuzzy sets on the damage feature domain. Such classification can be developed using the degree of similarity approach (Ross 2004). The degree of damage similarity (*DM*) between two fuzzy damage vectors $\underset{\sim}{D^i}$ and $\underset{\sim}{D^j}$ is defined as

$$DM = (\underset{\sim}{D^i} \circ \underset{\sim}{D^j}) \wedge (\overline{\underset{\sim}{D^i} \oplus \underset{\sim}{D^j}}) \tag{5.15}$$

where $(\underset{\sim}{D^i} \circ \underset{\sim}{D^j})$ is the inner product of the two fuzzy vectors $\underset{\sim}{D^i}$, $\underset{\sim}{D^j}$ and $(\overline{\underset{\sim}{D^i} \oplus \underset{\sim}{D^j}})$ is the complement of the outer product of the two vectors. When the value of *DM* approaches 1, the two fuzzy vectors are similar and when *DM* approaches 0, the two fuzzy vectors are dissimilar.

5.10.3 Identify different states of Tucumcari Bridge

To identify different states of Tucumcari Bridge using the proposed SHM system as installing in the field and the calibrated FE model, the energy of the third approximation of the acceleration signal in wavelet domain, as described in Equation (5.9), is computed at the location of each sensor to be used as damage feature. Assuming the current state of the bridge as healthy, all of the acceleration data obtained from the bridge using installed sensors can be used to calculate the energy of the third approximation of signal as a damage feature for healthy state. Since high correlation was observed between signals

166

obtained from the calibrated FE model and the signals from accelerometers on the bridge, the FE model can be used to generate acceleration signals for different damaged states of the bridge. The damage is defined on the FE model as reduction in stiffness of the frame elements in the locations that are more prone to be cracked. For this reason three elements located on the joint of K-frame on Girder 3 of the FE model are selected as damaged elements. These elements are located at location of maximum negative moment. The designated damaged location is shown in Figure 5-74.
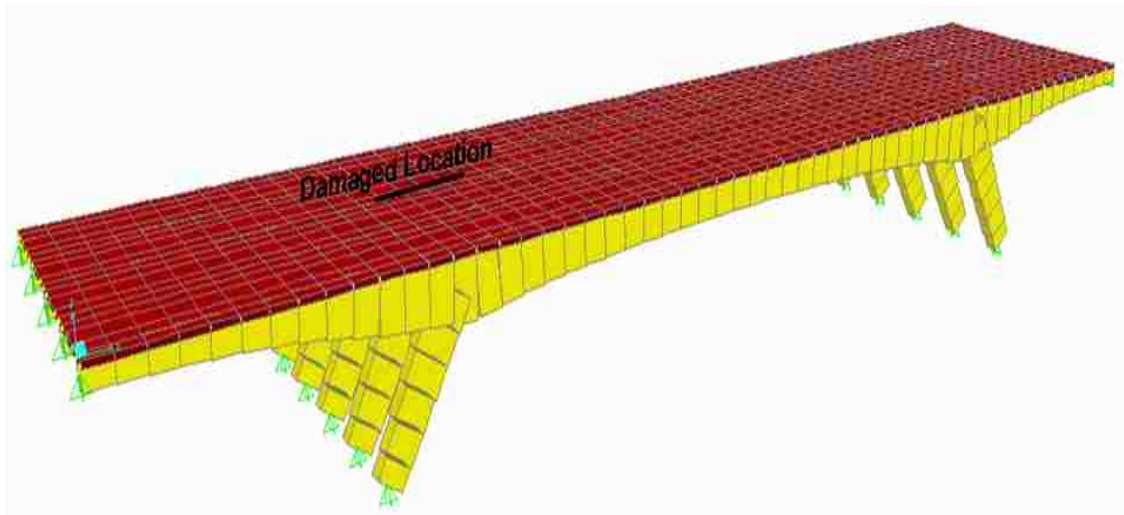
Figure 5-74 Location of damaged elements on the FE model.

By reducing the stiffness of the three damaged elements from 10% to 50% of the original stiffness used in the calibrated FE model, the energy of the acceleration signal in the wavelet domain is calculated at the location of Acc 8. Acc 8 is the closest accelerometer to the damage location. This energy denoted as λ_8 is shown in Table 5-2.

167

Table 5-2 Energy of acceleration signal calculated in wavelet domain for healthy and damaged cases.

Events	λ_8 Healthy	λ_8 Damaged
1	0.019813	0.216293
2	0.026606	0.194609
3	0.602788	0.195518
4	0.041646	0.19808
5	0.074756	0.199828
6	0.059328	0.221345
7	0.024501	0.276584
8	0.031539	
9	0.043087	
10	0.04846	

Using principles of inductive reasoning, the energy of signals shown in Table 5-2 were used to establish two fuzzy sets indicating healthy and damaged states of the Tucumcari Bridge. A bell function is used to describe each membership functions of fuzzy sets. A generalized bell function is specified by three parameters *a*, *b* and *c* as:

$$f(x) = \frac{1}{1 + \left| \dfrac{x - c}{a} \right|^{2b}} \tag{5.16}$$

where the parameters *a*, *c* are used to vary the center and width of MF and parameter *b* is used to control the slopes. Information entropy (*S*) is evaluated and the minimum entropy is assured to occur at the intersection point of the two fuzzy sets using Equations (5.10) to (5.14). The intersection point, which makes the information entropy function minimum, is used to classify the damage metrics into two classes and will have 0.5 membership value at each class. Figure 5-75 illustrates the two initial fuzzy sets for healthy $\underset{\sim}{H}$ and damaged $\underset{\sim}{D}$ states using bell function as described in Equation (5.16) to establish membership functions and the datasets from Table 5-2. The segmentation process is repeated to find secondary threshold values that make three fuzzy damage states in the structure: healthy ($\underset{\sim}{H}$), medium damage ($\underset{\sim}{MD}$) and severe damage ($\underset{\sim}{SD}$) as shown in Figure 5-76.
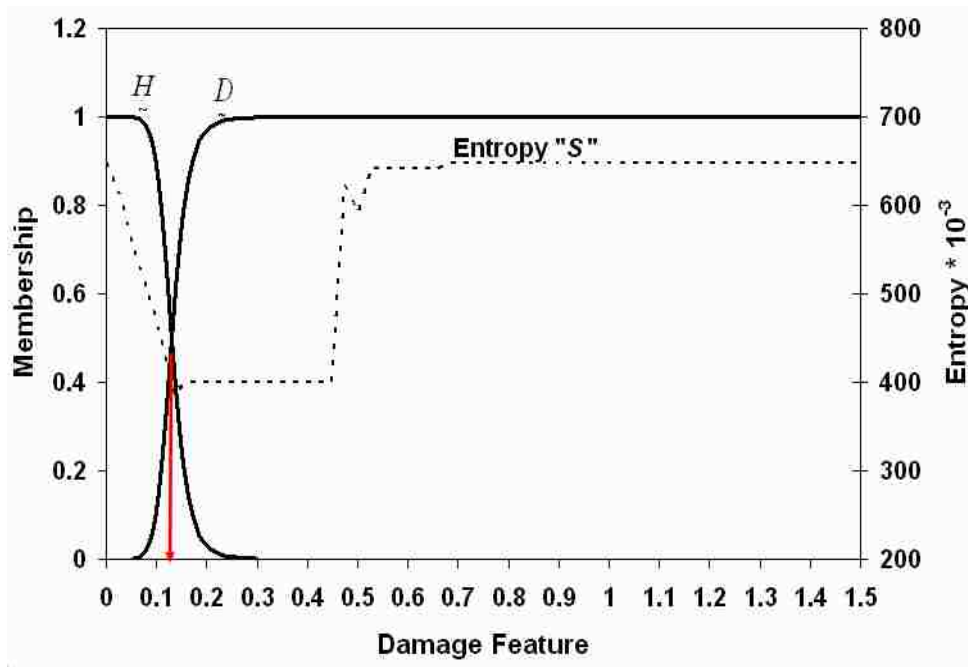
Figure 5-75 Fuzzy sets representing healthy and damaged states of Tucumcari Bridge. The dashed line represents the entropy function (*S*).

169
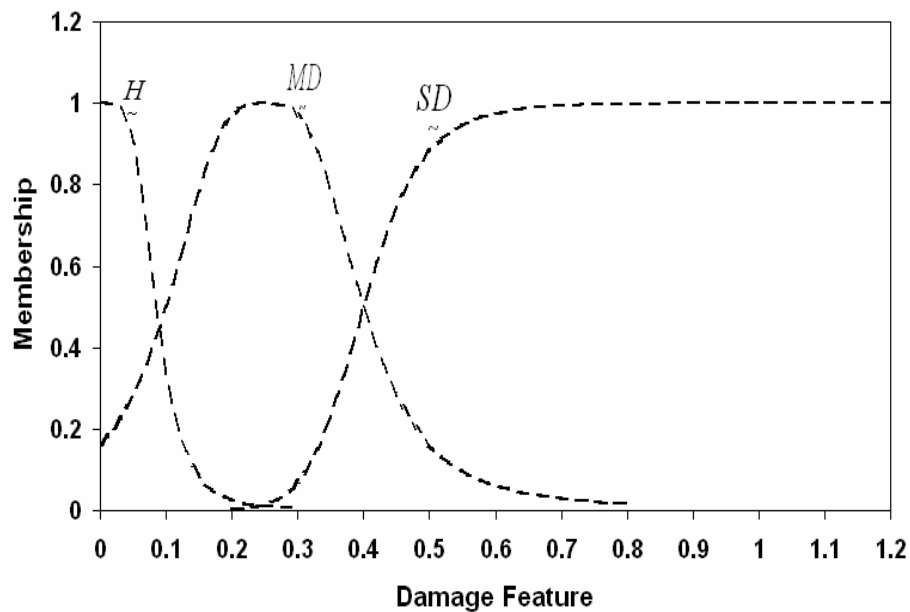
Figure 5-76 Fuzzy sets representing healthy, medium damage and severe damage states of the Tucumcari Bridge.

The process of finding secondary threshold values is based on minimization of entropy function within each class. The secondary threshold values have 0.5 membership value at each new class. This segmentation process can be repeated within each subclass to make even more classes. For Tucumcari Bridge, we stop the segmentation process at this level which classifies the damage feature calculated at the location of Acc.8 into three classes of healthy, medium damage and severe damage.

5.10.4 Damage detection

After the fuzzy sets representing healthy, medium damage and severe damage states are established, two unknown sets of data which are the energy of accelerometer signals in wavelet domain computed from the measurements obtained from Acc 8 on the Tucumcari Bridge are used to confirm the efficiency of the proposed method in identifying unknown

states of the bridge. The first unknown dataset is calculated from the measurements obtained from Acc 8 installed on the Tucumcari Bridge in June 26, 2009 and the second unknown dataset obtained in May 21, 2009. The energy of acceleration signals calculated from these measurements is shown in Table 5-3. Two other energies of acceleration signal at the location of Acc 8 were generated using the FE model were the bridge was damaged at the previously identified location. Two damage datasets represent stiffness reduction of the 35% and 65% respectively. Also, a new set of data from different trucks passing across the bridge for the stiffness reduction of 40% by adding noise to increase the data set at the previously identified damaged location was considered. All these unknown events are presented in Table 5-3.

Table 5-3 Energy of acceleration signal calculated in wavelet domain for unknown datasets obtained from Acc 8 installed on Tucumcari bridge.

Events	λ_8 Unknown 1	λ_8 Unknown 2	λ_8 Unknown 3	λ_8 Unknown 4	λ_8 Unknown 5
1	0.028751	0.038998	0.197615	0.470238	0.183345
2	0.05824	0.001956			0.234567
3	0.031468	0.052005			0.14563
4	0.051837	0.035061			0.175681
5	0.024029	0.019538			0.178943
6	0.063529	0.004446			0.28675
7	0.055835	0.000894			0.21879
8	0.058512	0.019005			0.168976
9	0.047665	0.01922			0.195576
10	0.025344	0.011854			0.265642

171

By calculating the mean value and standard deviation of the unknown datasets presented in Table 5-3 and using "bell shape function" defined in Equation (5.16), the membership function of these unknown datasets can be calculated at any damage feature. Figure 5-77 and Figure 5-78 represent the unknown dataset 1 denoted as A and unknown dataset 2 denoted as B and how they compare to the three fuzzy sets indicating different damage states of the Tucumcari Bridge. Moreover, Figure 5-79 shows the unknown single damage features denoted as C and D, and how they compare to the established fuzzy sets. Figure 5-80 illustrates the unknown dataset 5 denoted as E along with established fuzzy sets.
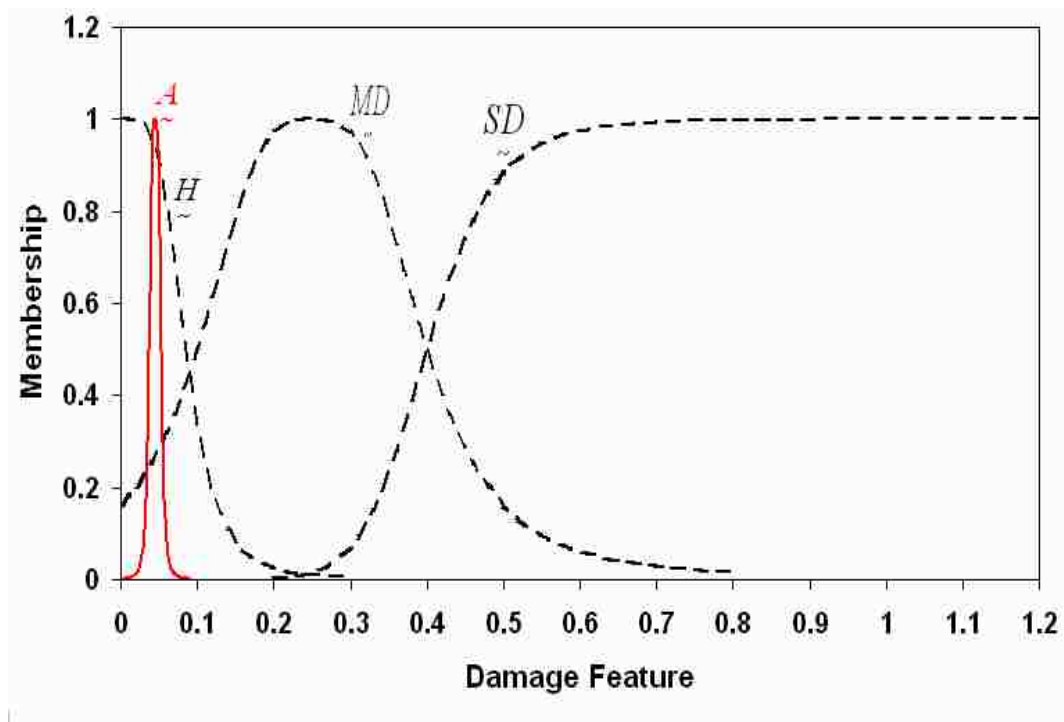
Figure 5-77 Unknown fuzzy set A among the known damage states of the Tucumcari Bridge.

172
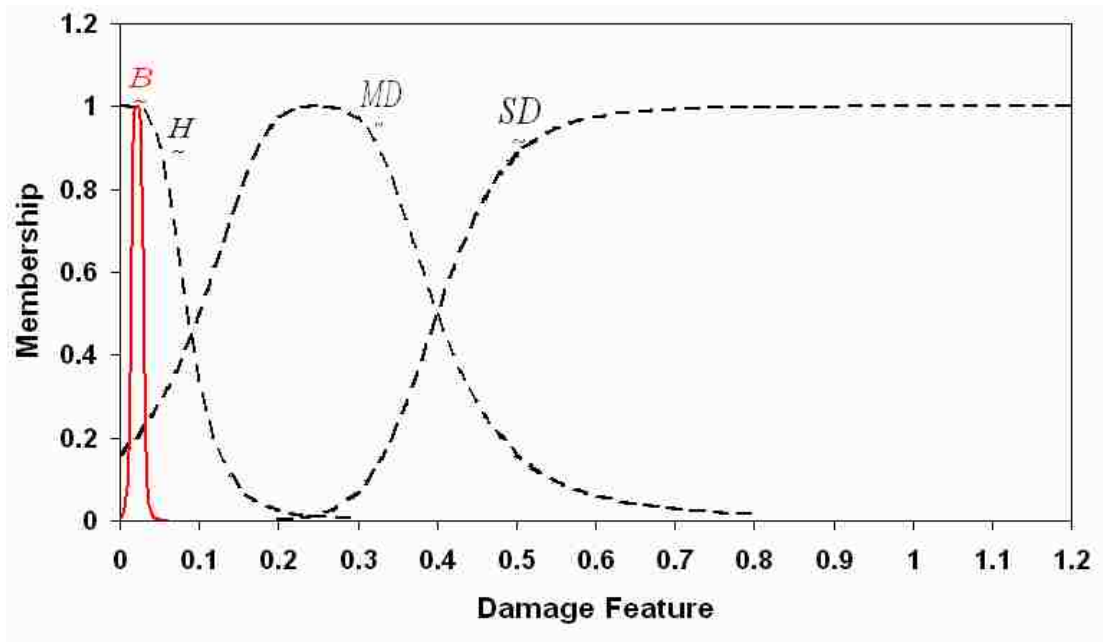
Figure 5-78 Unknown fuzzy set B **among the known damage states of the Tucumcari Bridge.**
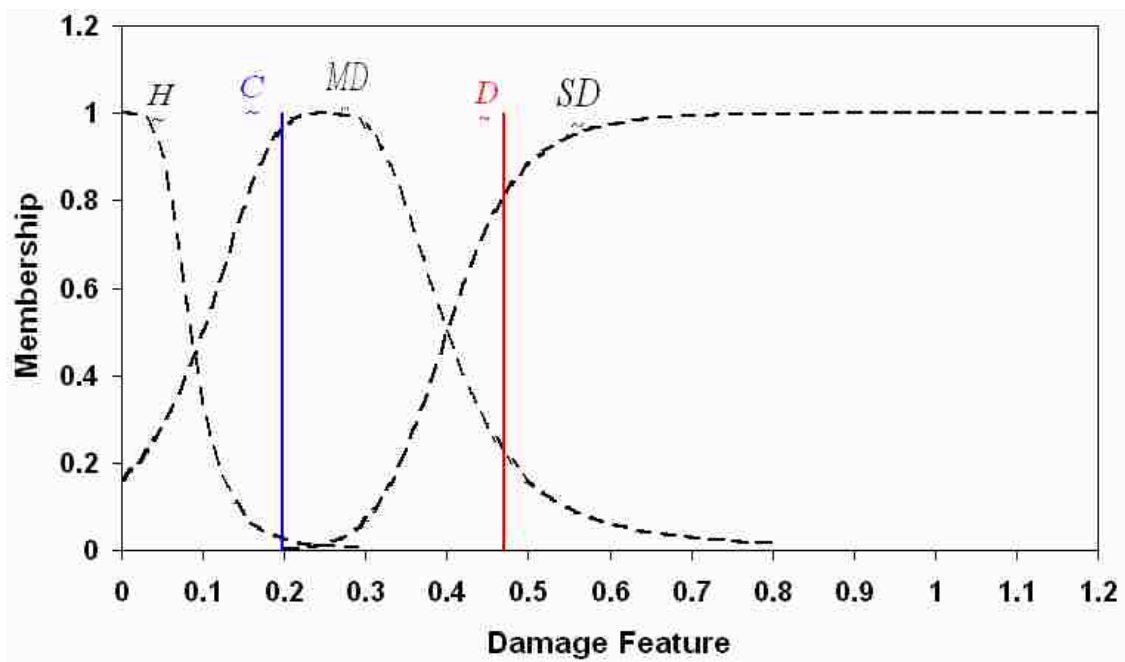
Figure 5-79 Unknown fuzzy sets C **and** D **among the known damage states of the Tucumcari Bridge.**

173
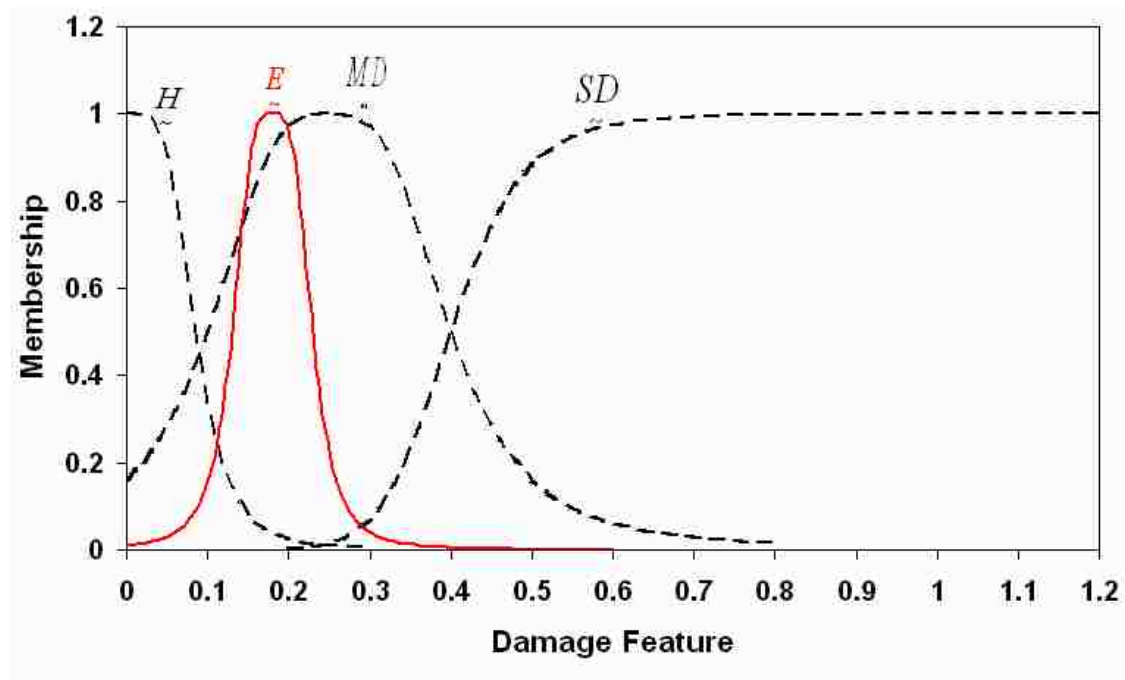
Figure 5-80 Unknown fuzzy set $E \atop \sim$ **among the known damage states of the Tucumcari Bridge.**

Using the similarity degree (*DM*) described by Equation (5.15), the similarity between unknown datasets and established fuzzy damage states of the Tucumcari Bridge can be calculated by the means of fuzzy pattern recognition. Table 5-4 represents the results of the similarity calculation.

174

Table 5-4 Degree of similarity between unknown fuzzy sets and known damage states in Tucumcari bridge.

	H ~	MD ~	SD ~
A ~	**0.95**	0.33	0
B ~	**0.98**	0.24	0
C ~	0.04	**0.97**	0
D ~	0	0.22	**0.85**
E ~	0.27	**0.97**	0.08

Based on the classification presented in Table 5-4, both unknown datasets A and B indicate healthy cases, which is a validation of the ability of the proposed method to classify damage successfully. Both datasets were extracted from the measurements acquired from Tucumcari Bridge in two different dates. The bridge is in its healthy state now; therefore, the proposed approach can classify damage efficiently in the Tucumcari Bridge. Unknown cases C, D and E selected from damaged cases in FE model also, validate the ability of the proposed method in classification unknown cases.

Tucumcari Bridge represents the ability of the inductive reasoning method to establish fuzzy classification of the damage states. The proposed approach enables the use of limited observation SHM data with considerable uncertainty. While the precise damage

175

identification of critical infrastructure is useful, in most cases a warning on departure of normal/acceptable performance is what is needed. The proposed system can be definitely used in providing such warning. A classification of structural performance in the moderate damage category will inform the responsible authorities of the need to conduct maintenance inspection and safety analysis. The proposed method also has the advantage of being independent of the damage feature and not based on a probabilistic assumption and thus does not require specific knowledge about probabilistic characteristics of the damage feature. This enables the use of the proposed approach in many SHM systems.

5.11 Conclusions

In this chapter, an innovative SHM system using Field Programmable Gate Array (FPGA) technology was designed and implemented on a reinforced concrete bridge located at Interstate 40 in New Mexico. This bridge was previously strengthened with Carbon Fiber Reinforced Polymer (CFRP) sheets on one girder at the location of maximum negative moment. The design and necessity of putting CFRP sheets along with field application of the sheets are also shown and validated with a 2D FE model.

The smart SHM system is able to acquire data from different types of sensors including accelerometers, strain gauges and thermocouples installed on the bridge and communicate this data wirelessly via the worldwide web. A friendly web user-interface was designed to give a remote end user control over acquiring data and some essential controls over saving data. The data saved on the smart SHM unit can then be sent to the office using FTP protocol. Two executable graphical user interfaces were made; one to show the raw data from different sensors in time, frequency and wavelet domains and the

other to do data analysis using fast Fourier transform and energy of acceleration signals calculated in wavelet domain. Using training datasets, a new dataset can be compared to the acceptable range of data defined by the mean value plus or minus three times of the standard deviation of the training datasets. Also, the end user is able to compare up to twenty new datasets together to realize changes in the structural performance.

Finally, a 3D FE model was developed and calibrated based on the static field test data. High correlation of acceleration signals between field test and the FE model validate the efficiency of FE model as a good representation of the real bridge. Data measured from sensors installed on the bridge along with data from calibrated and validated FE model were used to calculate the damage features at each sensor. Using the principles of inductive reasoning and information entropy, different fuzzy sets were established to describe different healthy and damaged states of the bridge. After establishing fuzzy sets to describe different states of the bridge, four unknown datasets obtained from accelerometers installed on the bridge were used for calculating damage features and these damage features were compared to the established fuzzy set damage features using fuzzy pattern recognition. The efficiency of the proposed method was confirmed by successfully classifying the unknown datasets.

177

CHAPTER 6 CONCLUSIONS

In this work, different methodologies were investigated to enhance the use of current structural health monitoring (SHM) systems in damage detection process by identifying the optimal sensor networks. Moreover, an innovative SHM system was designed and implemented on a field application of a reinforced concrete (RC) bridge paving the road for field implementation of SHM systems.

To identify the optimal locations of sensors in a sensor network designed for a structure, a probabilistic based method using artificial neural networks (ANN) was developed to enhance the probability of detection (POD) of damage occurrence in a structure. The proposed method was able to efficiently increase the POD compared with uniform distribution of sensors for a prestressed concrete bridge that was damaged in several locations with different damage severities. The finite element (FE) model of the bridge was used as a representation of the real bridge. Since the proposed method has a mathematical concept in allocating sensors on a structure, it can be used with different types of structures, independent of the damage feature. Moreover, the proposed method considers the robustness in designing sensor networks by considering network redundancy. This shall enhance the network performance in field applications. The redundant sensors were added at the location of critical sensors which were identified based on "leave one sensor out" analysis.

178

The proposed probabilistic method can be used for *a priori* known number of sensors. For small structures the total number of sensors can be easily identified, but as the size of structure grows, determining the optimal number of sensors for a sensor network becomes challenging. To overcome this challenge, a multi-objective optimization problem was formulated by considering information entropy as the first objective function while using the cost of the sensor network as the second objective function. The efficiency of combining the probabilistic method with information entropy and solving the multi-objective optimization problem was validated on the Luling Bridge, a cable stayed bridge passing over the Mississippi River. The FE model of this large infrastructure was developed. Considering redundancy to the optimal sensor network, concluded in the design of robust sensor networks for different structures.

Finally, the last part of this dissertation was devoted to design and implementation of an innovative SHM system for monitoring a RC Bridge in Tucumcari, New Mexico. The new SHM system is designed to reduce human intervention and provide continuous monitoring of the structure. This RC bridge was strengthened with carbon fiber reinforced polymer (CFRP) sheets. The design and implementation of the CFRP strengthening system on the bridge was delivered. Part of the monitoring system was to monitor the effectiveness of the CFRP strengthening system. Field Programmable Gate Array (FPGA) technology was used as a major component of the new SHM system. Using FPGA technology, smart data acquisition (SDA) system was developed to obtain the real time data from the structure. Moreover, the SDA system allows communicating the data wirelessly. System design and programming of the SDA system was developed and the effectiveness of the monitoring system was verified on a model truss bridge at the

179

structural health monitoring laboratory at University of New Mexico. The monitoring system was then implemented on the RC bridge in the city of Tucumcari at I-40 about 200 miles east of Albuquerque, New Mexico. The process of installing the monitoring system on the bridge was discussed in detail. Solar panels were designed and used to power the SHM system. The use of solar panels and wireless technology enable the use of such SHM system in remote locations where access to power or the worldwide web is not possible. Design and installation of the solar panel system is explained in details.

The monitoring system was able to send different signals acquired from different sensors such as accelerometers, environmental strain gauges and thermocouples installed on the bridge remotely to the office through the wireless network. The energy of acceleration signals calculated in the wavelet domain was selected as the damage metric and its effectiveness in differentiating between healthy and damaged states of the structure was also validated on the model truss bridge. A web user interface was designed to give the user the ability to view live data from all the sensors installed on the bridge and to control the saving process of data acquired from different sensors. Moreover, two types of software were developed for data analysis: one to visualize the raw data in time, frequency and wavelet domains and the other to perform for damage analysis of the data acquired from the bridge using wavelet and frequency analysis.

To validate the effectiveness of the monitoring system in damage detection of I-40 Bridge, a 3D FE model of the bridge was developed. The 3D model was calibrated using field strain measurements obtained from a field test performed on the bridge. The signals gathered from the calibrated FE model and the signals obtained from sensors installed on the bridge were correlated well. Using principles of inductive reasoning, fuzzy sets

180

describing different states of the bridge structural health were established based on the data obtained from the real bridge and the calibrated FE model. The effectiveness of the monitoring system in detecting damage in the bridge was verified by recognizing unknown cases of healthy and damage performance correctly.

Future Research

- To compare the efficiency of the proposed method in determining optimal sensor location with other methods such as particle filtering that control placing of sensors actively while using large numbers of sensors on the structure.

- To develop an SHM system that can integrate signals from fiber bragg grating (FBG) strain gauge and FBG accelerometer modules with regular electrical strain gauge and piezoelectric accelerometer analogue modules using FPGA technology. Up to now, the FBG sensors need their own data acquisition system that does not take advantage of FPGA technology which makes it possible to program the hardware of the acquisition device.

- Improving the FPGA technology to allow enable performing the data analysis at the bridge site for efficient use of the SHM system and limited data communication.

- To perform prognostic analysis using the data gathered from the bridge. That shall enable establishing rules for performance based maintenance of the bridge instead of prescheduled inspection.

- To develop the proposed FPGA system on other civil and mechanical infrastructures such as pipelines, wind turbines, airplanes, satellites, as well as etc. considering different types of sensors and analogue modules and integrate them into one smart data acquisition system.

182

- To verify different effective damage features for different monitoring applications and to add the damage feature calculations to the smart data acquisition hardware, so instead of acquiring raw data, end user can receive the processed damage features from the monitoring system.

183

REFERNCES

AASHTO (2006). *LRFD Bridge Design Specifications, Manual for Condition Evaluation of Bridges*, 2nd Edn, American Association of State Highway and Transportation Officials, Washington, D.C.

Aberg, M. and Gudmundson, P. (1998). "Optimization of multi-wavelength interdigital dielectrometry instrumentation and algorithms", *IEEE Transaction on Dielectrics and Electrical Insulation*, V. 5, pp. 408–420.

Achenbach, J.D. (2007). "On the Road from Schedule-Based Nondestructive Inspection to Structural Health Monitoring", *Proc. of the 6th International Workshop on Structural Health Monitoring*, Stanford University, Stanford, CA, DEStech Publications, pp. 16–28.

ACI 440 Committee (2002). "Guide for the design and construction of externally bonded FRP systems for strengthened concrete structures", ACI 440.2R-02, American Concrete Institutes, Farmington Hills, Michigan.

Adams, D.E. (2007). *Health Monitoring of Structural Materials and Components*, West Sussex, England, John Wiley & Sons.

Adams, D. E., Farrar, C. R. (2002). "Classifying linear and non-linear structural damage using frequency domain ARX Models", *Smart Systems and Structures*, Vol.1, No.2, pp. 185-201.

Agneni, A., Crema, L.B. and Mastroddi, F. (2000). "Damage Detection from Truncated Frequency Response Functions", *European COST F3 Conference on System Identification and Structural Health Monitoring,* Madrid, Spain, pp. 137–146.

Ahmadian, H., Mottershead, J.E. and Friswell, M.I. (1997). "Substructure Modes for Damage Detection", *Structural Damage Assessment Using Advanced Signal Processing Procedures, Proceedings of DAMAS '97,* University of Sheffield, UK, pp. 257–268.

Allbright, K., Parekh, K., Miller, R. and Baseheart, T.M. (1994). "Modal verification of a destructive test of a damaged prestressed concrete beam", *Experimental Mechanics,* V. 24(4), pp. 389–396.

Altunok, E., Reda Taha, M.M. and Ross, T.J. (2007). "A Possibilistic Approach for Damage Detection in Structural Health Monitoring", *ASCE Journal of Structural Engineering*, V. 133(9), pp. 1247–1256.

Ang, A.H.-S. and Tang, W.H. (2006). *Probability Concepts in Engineering: Emphasis on Applications to Civil and Environmental Engineering,* Hoboken, NJ: Wiley.

Ansari, F. (2004). *Sensing Issues in Civil Structural Health Monitoring,* Edited by Farhad Ansari, Dordrecht, The Netherlands, Springer.

Ansari, F. (2007). "Practical implementation of optical fiber sensors in civil structural health monitoring", *J.,Intel. Mat. Syst. Str.,* V. 18, pp. 879–889.

Applebaum, D. (2003). *Probability and Information: An Integrated Approach*, Cambridge University Press, NY, USA.

Azarbayejani, M., El-Osery, A., Choi, K.–K. and Reda Taha, M.M. (2008). "Probabilistic approach for optimal sensor allocation in structural health monitoring", *Smart Materials and Structures*, V. 17(5), paper # 055019, 2008.

Azarbayejani, M., El-Osery, A. and Reda Taha, M.M. (2009). "Entropy-based optimal sensor networks for structural health monitoring of a cable-stayed bridge", *Smart Structures and Systems*, V. 5(4), pp. 369–379.

Azarbayejani, M., Reda Taha, M.M. and Ross, T.J. (2008). "An inductive fuzzy damage classification approach for structural health monitoring", *Int. J. Materials and Structural Integrity*, V. 2(3), pp. 193–206.

Baker J. (1987). "Reducing bias and inefficiency in the selection algorithm in Genetic Algorithms and Their Applications.", *Proceedings of the 2nd Intl. Conf.*, Ed. J.J. Grefenstette, LEA, Cambridge, MA, pp. 14–21.

Barai, S.V. and Pandey, P.C. (1995). "Vibration Signature Analysis Using Artificial Neural Networks", *ASCE Journal of Computing in Civil Engineering*, V. 9(4), pp. 259–265.

Beard, S., Liu, B., Qing, P. and Zhang, D. (2007). "Challenges in Implementation of SHM", *Proc. of the 6th International Workshop on Structural Health Monitoring*, Stanford University, Stanford, CA, DEStech Publications, pp. 65–81.

Bishop, C.M., (2000). *Neural Networks for Pattern Recognition*, New York: Oxford University Press.

Broek D. (1986). *Elementary engineering fracture mechanics*. Dordrecht: Martinus Nijhoff Publishers.

Brown, S. and Vranesic, Z. (2009). *Fundamentals of Digital Logic with VHDL Design, 3/e*, *McGraw Hill*, Boston.

Browne, M., Shiry, S., Don, M. and Ouellette, R. (2002). "Visual Feature Extraction Via PCA-based Parameterization of Wavelet Density Functions", *In Proceedings of the Third International Symposium on Robots and Automation*, Toluca, Mexico, pp. 398–402.

Browne, M., Dorn, M., Ouellette, R., Christaller, T. and Shiry, S. (2002b). "Wavelet Entropy-based Feature Extraction for Crack Detection in Sewer Pipes", *In Proceedings of the 6th International Conference on Mechatronics Technology*, Kitakyushu, Japan, pp. 202–206.

Bukkapatnam, S.T.S., Kumara S.R.V.T. and Lakhtakia, A. (1999). "Analysis of acoustic emission signals in machining", *ASME Journal of Manufacturing Science and Engineering*, V. 121, pp. 568–576.

Cai, C.S. and Shahawy, M. (2004). "Predicted and measured performance of prestressed concrete bridges", *ASCE Journal of Bridge Engineering*, V. 9(1), pp. 4–13.

Carden, E.P. and Brownjohn, J.M.W. (2008). "Fuzzy Clustering of Stability Diagrams for Vibration-Based Structural Health Monitoring", *Computer-Aided Civil and Infrastructure Engineering*, V. 23, pp. 360–372.

186

Cardini, A.J. and DeWolf J.T. (2009). "Long-term Structural Health Monitoring of a Multi-girder Steel Composite Bridge Using Strain Data", *Structural Health Monitoring,* V. 8(1), pp. 47-58.

Carpinteri, A., Lacidogna, G. and Pugno N. (2005). "Structural damage diagnosis and life-time assessment by acoustic emission monitoring", *Engineering Fracture Mechanics*, V. 74, pp. 273–289.

Carpinteri, A., Cardone, F. and Lacidogna G. (2009). "Energy emissions from failure phenomena: Mechanical, Electromagnetic, Nuclear", *SEM Annual Conference and Exposition on Experimental and Applied Mechanics*, Albuquerque, New Mexico.

Carrasco, C., Osegueda, R., Ferregut, C. and Grygier, M. (1997). "Localization and Quantification of Damage in a Space Truss Model Using Modal Strain Energy", *Smart Systems for Bridges, Structures, and Highways, Proceedings of SPIE,* 3043, pp. 181–192.

CEB-FIP (2001). *Externally Bonded FRP Reinforcement for RC Structures, Technical Report Bulletin 14*. p. 124.

Chacón, R., Guzmán, F., Mirambell, E., Real, E. and Oñate, E. (2009). "Wireless Sensor Networks for Strain Monitoring during Steel Bridges Launching", *Structural Health Monitoring,* V. 8(3), pp. 195–205.

Chandrashekhar, M. and Gangul, R. (2009). "Structural Damage Detection Using Modal Curvature and Fuzzy Logic", *Structural Health Monitoring,* V. 8(4), pp. 267–282.

Chang, C.-C. and Chen, L.-W. (2004). "Damage Detection of Cracked Thick Rotating Blades by a Spatial Wavelet Based Approach", *Applied Acoustics,* V. 65, pp. 1095–1111.

Chang, F.-K. and Markmiller, J.F.C., (2006). "A New Look in Design of Intelligent Structures with SHM", *Proceedings of the Third European Workshop: Structural Health Monitoring*, DEStech Publications, pp.5–20.

Choi, S. and Stubbs, N. (1997). "Nondestructive Damage Detection Algorithms for 2D Plates", *Smart Systems for Bridges, Structures and Highways, Proceedings of SPIE,* 3043, pp. 193–204.

187

Coifman, R. and Wickerhauser, M.V. (1992). "Entropy-based Algorithms for Best Basis Selection", *IEEE Transaction on Information Theory*. V. 38, pp. 713–718.

Cybenko, G. (1989). "Approximation by superpositions of a sigmoidal function", *Mathematics of Control, Signals and Systems,* V. 2, pp. 303-314.

Doebling, S.W., Farrar, C.R. and Prime, M.B. (1998). "A Summary Review of Vibration-based Damage Identification Methods", *The Shock and Vibration Digest*, V. 30(2), pp. 91–105.

Doebling, S.W., Farrar, C.R., Prime, M.B. and Shevitz, D.W. (1996). "Damage Identification and Health Monitoring of Structural and Mechanical Systems from Changes in their Vibration Characteristics: A Literature Review", *Los Alamos National Laboratory Report* LA-13070-MS.

Douka, E., Loutridis, S. and Trochidis, A. (2003). "Crack Identification in Beams Using Wavelet Analysis," *International Journal of Solids and Structures*, V.40(13-14), pp. 3557-3569.

Elms, D. G. (2004). "Structural safety issues and progress", *Progress in Structural Engineering and Materials,* Vol. 6, No. 2, pp. 116-126.

Farrar, C.R., Sohn, H., Hemez, F.M., Anderson, M.C., Bement, M.T., Cornwell, P.J., Doebling, S.W., Lieven, N., Robertson, A.N. and Schultze, J.F. (2004). *Damage Prognosis: Current Status and Future Needs*, Los Alamos National Lab Report, LA-14051-MS.

Farrar, C.R.., Lieven, N.A.J. and Bement, M.T. (2005). *An Introduction to Damage Prognosis. Damage Prognosis for Aerospace, civil and Mechanical Systems,* Edited by D.J.Inman, C.R. Farrar, V.Lopes, Jr. and V. Steffen, Jr., John Wiley and Sons Ltd, West Sussex, England.

Feeney A. and Heit, E. (2007). "*Inductive Reasoning: Experimental, Developmental and Computational* Approach", Cambridge University Press, UK.

Foedinger, R., Rea, D., Sirkis, J., Grande R. and Vandiver, T.L. (1999). "Structural Health Monitoring and Impact Damage Detection for Filament Wound Composite Pressure Vessels", *Structural Health Monitoring,* Stanford University, Palo Alto, California, pp. 159–169.

188

Frangopol, D.M., Neves, L.C. and Petcherdchoo, A. (2004). "Health and safety of civil infrastructures: A unified approach", *In Proceedings of the 2nd International Workshop on Structural Health Monitoring of Innovative Civil Structures,* Winnipeg, Canada, Mufti, A., and Ansari, F. Eds., pp. 253–264.

Friswell, M.I. and Penny, J.E.T. (1997). "Is Damage Location Using Vibration Measurements Practical?", *In Proceedings of the International Workshop: DAMAS 97, Structural Damage Assessment Using Advanced Signal Processing Procedures*, Sheffield, UK.

Fritzen C.-P. and Bohle, K. (2001). "Application of Model-Based Damage Identification to a Seismically Loaded Structure", *Smart Materials and Structures*, V. 10, pp. 452–458.

Gentile, A. and Messina, A. (2003). "On the Continuous Wavelet Transforms Applied to Discrete Vibrational Data for Detecting Open Cracks in Damaged Beams", *Int. Journal of Solids and Structures*, V. 40(2): 295–315.

Giurgiutiu, V. (2007). *Structural Health Monitoring: With Piezoelectric Wafer Active Sensors*. Academic Press.

Gros, X.E., Ogi, K. and Takahashi, K. (1998) "Strain and Damage Monitoring of CFRP Laminates by Means of Electrical Resistance Measurement", *Journal of Reinforced Plastics and Composites*, V. 17(5), pp. 389–405.

Guan, H. and Karbhari, V.M. (2006). "Web-Based Structural Health Monitoring of an FRP Composite Bridge", *Computer-Aided Civil and Infrastructure Engineering*, V. 21, pp. 39–56.

Guratzsch, R.F. and Mahadevan, S. (2005). "SHM Sensor Placement Under Uncertainty", *Proceedings of the 5th International Workshop on Structural Health Monitoring*, Ed. Fu-Kuo Chang, DEStech Publications, pp.1343–1352.

Guratzsch, R.F. and Mahadevan, S. (2006). "Sensor Placement Design for SHM under Uncertainty", *Proceedings of the Third European Workshop: Structural Health Monitoring*, DEStech Publications, pp.1168–1175.

Haykin, S. (1998). *Neural Networks: A Comprehensive Foundation*, 2nd Edition, Prentice Hall.

Helmicki, A., Hunt, V., Shell, M., Lenett, M., Turer, A., Dala, V. and Aktan, A. (1999). "Multidimensional Performance Monitoring of a Recently Constructed Steel-Stringer Bridge", *Proceedings of the 2nd International Workshop on Structural Health Monitoring*, Stanford University, Palo Alto, California, pp. 408–416.

Hemmert, K.S., and Underwood, K.D. (2005). "An analysis of the double-precision floating-point FFT on FPGAs", *In Proceedings of the IEEE Symposium on Field-Programmable Custom Computing Machines*, Napa Valley, CA, April 2005.

Ho, Y.K. and Ewins, D.J. (2000). "On the Structural Damage Identification with Mode Shapes", *European COST F3 Conference on System Identification and Structural Health Monitoring*, Madrid, Spain, pp. 677–686.

Horton, S., Reda Taha, M.M. and Baca, T. J. (2005). "A Neural-Wavelet Damage Detection Module for Structural Health Monitoring", *Proceedings of International Workshop on Structural Health Monitoring*, Stanford, USA, Chang, Fu-Kuo, Ed., pp. 556–564.

Hubbard, B. (1998). *The World According to Wavelets: The Story of a Mathematical Technique in the Making*, AK Peters, Ltd., Second Revised Edition, Wellesley, Massachusetts, USA.

Humar, J. (2002). *Dynamics of Structures*. 2nd Edition, Balkema Publishers, Rotterdam, The Netherlands.

Hung, T.-W, Fang, S.-C., and Nuttle, H. L. W . (2003). "A two-phase approach to fuzzy system identification", *Journal of Systems Science and Systems Engineering*, Vol. 12, No. 4, pp. 408-423.

IEEE Std. 1076 VHDL Language Reference Manual, IEEE VHDL Analysis and Standarization Group.

IEEE Std. 1374 Verilog hardware description language, IEEE Verilog Standarizatino Group.

Iranmanesh, A., Bassam, A. and Ansari, F. (2009). "Post earthquake performance monitoring of a typical highway overpass bridge", *Smart Structures and Systems*, V. 5(4), pp. 495 –505.

Jiang, L.J. and Wang, K.W. (2009). "An experiment-based frequency sensitivity enhancing control approach for structural damage detection", *Smart Materials and Structures*, V. 18, 12 p.

Jonker, P. P., Duin, R. P. W., de Ridder, D., Ligteringen R. and Tax, D. M. J. (1999) *Proc. the First Sino-European Symposium on Quality Control of High-Grade Steel*, China, pp. 38-40.

Karbhari, V.M., Guan, H. and Sikorsky, C. (2003a). "Webbased structural health monitoring of a FRP composite bridge", *Proceedings of the 1st International Conference on Structural Health Monitoring and Intelligent Infrastructure*, Tokyo, Japan, pp. 217–26.

Karbhari, V.M., Guan, H. and Zhao, L. (2003b). "Composite structural systems—from characterization to field implementation", *Proceedings of the 6th International Symposium on Fiber-Reinforced Polymer Reinforcements for Concrete Structures*, Singapore, pp. 1381–90.

Kessler, S.S. (2002). "Piezoelectric-Based In-Situ Damage Detection of Composite Materials for Structural Health Monitoring Systems", *PhD Dissertation*, Department of Aeronautics and Astronautics, Massachusetts Institute of Technology (MIT), Cambridge, USA.

Klir, G.J. and Yuan, B. (1995). *Fuzzy Sets and Fuzzy Logic, Theory and Application*, Prentice Hall, Upper Saddle River, NJ, USA.

Kim, K. and Paik, S.-H. (1997). "Optical Fiber Monitoring System of Bridges in Korea", *Structural Health Monitoring, Current Status and Perspectives,* Stanford University, Palo Alto, California, pp. 555–563.

Kim, C.J., Russell, B.D. (1991). "A learning method for use in intelligent computer relays for high impedance faults", *IEEE Trans. Power Delivery,* V. 6(1), pp. 109–115.

Kim, J-T., Ryu, Y-S., Choi, H-M. and Stubbs, N. (2003). "Damage Identification in Beam-type Structures: Frequency-based Method vs. Mode-shape-based Method", *Engineering Structures*, V. 25, pp. 57–67.

191

Kim, S.D., In, C.W., Cronin, K., Sohn, H. and Harries, K. (2007). "Reference-Free NDT Technique for Debonding Detection in CFRP-Strengthened RC Structures", *J. of Structural Engineering @ ASCE*, V. 130(8), pp. 1080–1091.

Kostopoulos, V., Vavouliotis, A., Karapappas, P., Tsotra P. and Paipetis, A. (2009). "Damage Monitoring of Carbon Fiber Reinforced Laminates Using Resistance Measurements. Improving Sensitivity Using Carbon Nanotube Doped Epoxy Matrix System", *Journal of Intelligent Material Systems and Structures,* V. 20, pp. 1025–1034.

Kumara, S., Suh, J. and Mysore, S.P. (1999). "Machinery fault diagnosis and prognosis: applications of advanced signal processing techniques", *CIRP Annals*, Manufacturing Technology, V. 48(1), pp. 317 –320.

Kwon, S.-J., Soobong, S., Lee, H.S. and Park Y.-H. (2003) "Design of Accelerometer Layout for Structural Monitoring and Damage Detection", *KSCE J. of Civil Engineering*, V. 7(6), pp. 717–724.

Lee, J-R. and Tsuda, H. (2005). "A novel fiber Bragg grating acoustic emission sensor head for mechanical tests", *Scripta Materialia*, V. 53(10), pp. 1181–1186.

Lemaitre, J. and Desmorat, R. (2002). *Engineering Damage Mechanics: Ductile, Creep, Fatigue and Brittle Failures,* Springer, New York.

Li, H., Ou, J., Zhao, X., Zhou, W., Li, H., Zhou, Z. and Yang, Y. (2006). "Structural Health Monitoring System for the Shandong Binzhou Yellow River Highway Bridge", *Computer-Aided Civil and Infrastructure Engineering*, V. 21, pp. 306–317.

Liang, Y., Sun, C. and Ansari, F. (2004). "Acoustic Emission Characterization of Damage in Hybrid Fiber Reinforced Polymer Rods", *Journal for Composites for Construction*, V. 8(1), pp. 70–78.

Liu, M., Frangopol, D.M. and Kim, S. (2009). "Bridge System Performance Assessment from Structural Health Monitoring: A Case Study", *ASCE J. of Structural Engineering,* V. 135(6), pp. 733–742.

Liew, K.M. and Wang, Q. (1998). "Application of Wavelet Theory for Crack Identification in Structures", *Journal of Engineering Mechanics*, V. 124(2), pp. 152–157.

Maeck, J. and De Roeck, G. (1999). "Damage Detection on a Prestressed Concrete Bridge and RC beams Using Dynamic System Identification", *Damage Assessment of Structures, Proc. Of the International Conference on Damage Assessment of Structures* (DAMAS 99), Dublin, Ireland, pp. 320–327.

Masuda, A., Nakaoka, A., Sone, A. and Yamamoto, S. (1995). "Health Monitoring Systems of Structures Based on Orthonormal Wavelet Transform. Seismic Engineering", *Transaction of ASME*, V. 312, pp. 161–167.

McCuskey, M. C. Reda Taha, M. M. Horton S. R. and Baca, T. J. (2006) "Identifying damage in the ASCE benchmark structure using a neural-wavelet module", *Proc. of 6th International Workshop on Structural Health Monitoring,* Granada, Spain, pp. 421-428.

Mehrani, E., Ayoub, A. and Ayoub, A. (2009) "Evaluation of fiber optic sensors for remote health monitoring of bridge structures", *Smart Structures and Systems*, V. 5(4), pp. 381–395.

Metallidis P., Verros, G., Natsiavas, S. and Papadimitriou, C. (2003). "Identification, Fault Detection and Optimal Sensor Location in Vehicle Suspensions", *Journal of Vibration and Control*, V. 9(3-4), pp. 337–359.

Miettinen, K., (1999). *Nonlinear Multi-objective Optimization*, Kluwer, suston.

Moerman, W., Taerwe, L., De Waele, W., Degrieck, J. and Bates, R. (1999). "Remote Monitoring of Concrete Elements by means of Bragg Gratings", *Structural Health Monitoring,* Stanford University, Palo Alto, California, pp. 369–378.

Moria, K., Kasashimaa, N., Yoshiokaa T. and Uenob, Y. (1996). "Prediction of Spalling on a Ball Bearing by Applying the Discrete Wavelet Transform to Vibration Signals", *Wear*, V. 195(1-2), pp. 162–168.

Mosallam, A., Miraj, R. and Abdi, F. (2009) "Diagnostic/prognostic health monitoring system and evaluation of a composite bridge", *Smart Structures and Systems*, V. 5(4), pp. 397–413.

Mufti, A., (2004). *Sensing Issues in Civil Structural Health Monitoring,* Edited by Farhad Ansari, Dordrecht, The Netherlands, Springer.

193

Natke, H.G. and Cempel, C. (1997). "Model-Aided Diagnosis Based on Symptoms", *Structural Damage Assessment Using Advanced Signal Processing Procedures*, Proceedings of DAMAS 97, University of Sheffield, UK, pp. 363–375.

Neild, S.A., McFadden, P.D. and Williams, M.S. (2003). "A review of time-frequency methods for structural vibration analysis", *Engineering Structures*, V. 25, pp. 713–728.

Ntotsios, E., Christodoulou, K. and Papadimitriou, C. (2006). "Optimal Sensor Location Methodology for Structural Identification and Damage Detection.", *Proceedings of the Third European Workshop: Structural Health Monitoring*, DEStech Publications, pp.1160–1167.

Ohtsu, M. (1996). "The history and development of acoustic emission in concrete engineering", *Magazine of Concrete Research*, V. 48, pp. 321–330.

Osyczka, A., (1984). *Multi Criterion Optimization in Engineering,* Ellis Howard Series.

Pandy, A.K., Biswas, M. and Samman, M.M. (1991). "Damage Detection From Changes in Curvature Mode Shapes", *Journal of Sound and Vibration,* V. 145(2), pp. 321-332.

Papadimitriou, C., Beck, J.L., Au, S.-K. (2000). "Entropy-Based Optimal Sensor Location for Structural Model Updating", *Journal of Vibration and Control*, V. 6, pp. 781–800.

Papadimitriou, C. (2004). "Optimal Sensor Placement Methodology for Parametric Identification of Structural Systems", *Journal of Sound and Vibration*, V. 278(4), pp. 923–947.

Pareto, V. (1971). *Manual of Political Economy*, NY.

Parker, D.L., Frazier, W.G., Rinehart, H.S. and Cuevas, P.S. (2006). "Experimental Validation of Optimal Sensor Placement algorithms for Structural Health Monitoring.", *Proceedings of the Third European Workshop: Structural Health Monitoring 2006*, DEStech Publications, pp. 1144–1150.

Prosser, W.H. (1996*).* "Advanced AE Techniques in Composite Materials Research", *Journal of Acoustic Emission*, V. 14(3-4), S1–S11.

Qi, G., Barhorst, A. Hashemi, J. and Kamala, G. (1997). "Discrete wavelet decomposition of acoustic emission signals from carbon-fiber-reinforced composites", *Composites Science and Technology*, V. 57(4), pp. 389-403.

Raich A.M. and Liszkai T.R. (2003). "Multi-Objective Genetic Algorithm Methodology for Optimization Sensor Layouts to Enhance Structural Damage Identification", *Proceedings of the 3rd Structural Health Monitoring*, Ed. Fu-Kuo Chang, DEStech Publications, pp. 650–657.

Read, I., Foote, P. and Murray, S. (2002). "Optical fiber acoustic emission sensor for damage detection in carbon fiber composite structures", *Measurement Science and Technology*, V. 13, N5–N9.

Reda Taha, M.M., Choi, K.K. and Azarbayejani, M. (2007). "Structural analysis and evaluation of Bridges (7930, 7931, 7937, and 7938) in Tucumcari, New Mexico", Technical Report # C04961 submitted to NMDOT.

Reda Taha, M.M. and Lucero, J. (2005). "Damage identification for structural health monitoring using fuzzy pattern recognition", *Engineering Structures,* V. 27(12), pp. 1774–1783.

Reda Taha, M.M., Noureldin, A., Lucero, J.L. and Baca, T.J. (2006). "Wavelet Transform for Structural Health Monitoring: A Compendium of Uses and Features", *Journal of Structural Health Monitoring*, V. 5(3), pp. 267–295.

Reda Taha, M., Noureldin, A., Osman, A. and El-Sheimy, N. (2004). "Introduction to the Use of Wavelet Multi-Resolution Analysis for Intelligent Structural Health Monitoring", *Canadian Journal of Civil Engineering*, V. 31(5), pp. 719-731.

Ren, W.X. and De Roeck, G. (2002). "Structural damage identification using modal data. I: Simulation verification", *ASCE J Structural Engineering,* V. 128(1), pp. 87–95.

Rizkalla, S., Benmokrane, B., and Tadros, G. (2000). "Structural Health Monitoring Bridges with Fiber Optic Sensors", *European COST F3 Conference on System Identification and Structural Health Monitoring,* Madrid, Spain, pp. 501–510.

Robertson, D.C., Camps, O.I., Mayer, J.S. and Gish, W.B. (1996). "Wavelets and Electromagnetic Power System Transients", *IEEE Transaction on Power Delivery*, V. 11(2), pp. 1050–1056.

Ross, T.J. (2004). *Fuzzy Logic with Engineering Applications*, John Wiley and Sons.

Rus, G., Lee, S.-Y., Gallego, R. and Park, T.-H. (2006). "Inverse Problem Filtering for Noise Reduction in QNDE", *Proceedings of the Third European Workshop: Structural Health Monitoring*, DEStech Publications, pp.563–570.

Saltelli, A., Chan, K. and Scott, E. M. (2000). *Sensitivity Analysis,* West Sussex: Wiley.

Schoess, J.N. and Zook, J.D. (1998). "Test results of Resonant Integrated Microbeam Sensor (RIMS) for acoustic emission monitoring", *Proceedings of the SPIE Conference on Smart Electronics and MEMS*, 3328, pp. 326–332.

Schulte, R.T., Bohle, K., Fritzen C.-P. and Schuhmacher, G. (2006). "Optimal Sensor Placement for Damage Identification – An Efficient forward-Backward Selection Algorithm", *Proceedings of the Third European Workshop: Structural Health Monitoring*, DEStech Publications, pp.1151–1159.

Seible, F., Karbhari, V.M. and Burgueno, R. (1999), "Kings Stormwater Channel and I-5/Gilman Bridges, USA", *Structural Engineering International*, V. 9(4): 250–253.

Shannon, C.E. (1948). "A Mathematical Theory of Communication", *Bell System Technical Journal,* V. 27, pp. 379–423.

Sheyka, M. (2008). "Analytical and Experimental Investigations of Photonic Crystals for Sub-Micron Damage Detection", M.Sc. Thesis, Department of Civil Engineering, University of New Mexico, NM, USA.

Shiao, M. (2005). "Risk forecasting and updating for damage accumulation processes with inspections and maintenance', *Proc. of the Structural Health Monitoring Workshop on Structural Health Monitoring*, Stanford, USA, Chang, FK, Ed., pp. 1190-1197.

Shrive, P.L., Brown, T.G. and Shrive, N.G. (2009). "Practicalities of Structural Health Monitoring Systems", *Smart Structures and Systems*, V. 5(4), pp. 357–367.

Shrive, P.L., Newhook, J.P., Brown, T.G., Shrive, N.G., Tadros, G. and Kroman, J. (2003). "Thermal Strains in Steel and Glass Fibre Reinforced Polymer Reinforcement in a Bridge Deck", *Proceedings of the International Conference on Performance of Constriction Materials (ICPCM)*, Cairo, Egypt. El-Dieb et al. Eds., Vol. 1, pp. 429–437.

196

Stanbridge, A.B., Khan, A.Z. and Ewins, D.J. (1997). "Fault Identification in Vibrating Structures Using a Scanning Laser Doppler Vibrometer", *Structural Health Monitoring, Current Status and Perspectives,* Stanford University, Palo Alto, CA, pp.56–65.

Staszewski, W.J. (1998). "Structural and Mechanical Damage Detection Using Wavelets", *The Shock and Vibration Digest*, V. 30(6), pp. 457–472.

Staszewski, W., Boller C. and Tomlinson, G. (2003). *Health Monitoring of Aerospace Structures, Smart Sensor Technologies and Signal Processing.*, John Wiley and Sons Ltd, West Sussex, England.

Strang, G. and Nguyen, T. (1997). *Wavelet and Filter Banks*, Wellesley-Cambridge Press, NY, USA.

Su, Z., Ye, L. and Bua, X. (2002). "A Damage Identification Technique for CF/EP Composite Laminates Using Distributed Piezoelectric Transducers", *Composite Structures*, V. 57(1-4), pp. 465–471.

Su, Z. and Ye, L. (2004). "Lamb wave-based quantitative identification of delamination in CFEP composite structures using artificial neural algorithm", *Composite Structures*, V. 66, pp. 627–637.

Sun, Z., and Chang, C.-C. (2002). "Structural damage assessment based on wavelet packet transform", *ASCE J. Structural Engineering,* 128 :1354–1361.

Swann, C. and Chattopadhyay, A. (2005). "A Stochastic Approach to Optimum Sensor Placement for Damage Detection", *Proceedings of the 5th International Workshop on Structural Health Monitoring*, Ed. Fu-Kuo Chang, DEStech Publications, pp. 871–878.

Täljsten, B. (2002). "CFRP Strengthening and Monitoring of a Box Girder Bridge", *Sensing Issues in Civil Structural Health Monitoring,* Edited by Farhad Ansari, Dordrecht, The Netherlands, Springer.

Talebinejad, I., Fischer, C. and Ansari, F. (2009). "Serially multiplexed FBG accelerometer for structural health monitoring of bridges", *Smart Structures and Systems*, V. 5(4), pp. 345–355.

Tenenbaum, J. B., Griffiths T. L., Kemp, C. (2006). "Theory-based Bayesian models of inductive learning and reasoning", *Trends in Cognitive Science*, Vol. 10, No. 7, pp. 309-318.

Thein, A. (2006). "Pipeline structural health monitoring using macro-fiber composite active sensors", Master Thesis, Department of Mechanical, Industrial, and Nuclear Engineering, University of Cincinnati.

Todd., M.D., Johnson, G. and Vohra, S. (2000). "Civil Infrastructure Monitoring with Fiber Optic Bragg Grating Sensor Arrays", *Structural Health Monitoring,* Stanford University, Palo Alto, CA, pp. 359–368.

Tozser, O. and Elliott, J. (2000). "Continuous Acoustic Monitoring of Prestressed Structures", *3rd Structural Specialty Conference of the Canadian Society of Civil Engineering*, Regina, Saskatchewan, 6 p.

Underwood, K.D. and Hemmert, K.S. (2004). "Closing the gap: CPU and FPGA trends in sustainable floating-point BLAS performance", In *Proceedings of the IEEE Symposium on Field-Programmable Custom Computing Machines*, Napa Valley, CA, April 2004.

USA TODAY (Friday July 25, 2008). "Billions needed to shore up bridges", pp.1 and 10A.

Wang, L. and Yuan, F.G. (2005). "Damage Identification in a Composite Plate using Prestack Reverse-time Migration Technique", *Structural Health Monitoring*, V. 4(3), pp. 195–211.

Wang, M. L., Satpathi, D., and Heo, G. (1997). "Damage Detection of a Model Bridge Using Modal Testing", *Structural Health Monitoring, Current Status and Perspectives,* Stanford University, Palo Alto, California, pp. 589–600.

Williams, E.J. and Messina, A. (1999). "Applications of the Multiple Damage Location Assurance Criterion", *Proceedings of the International Conference on Damage Assessment of Structures (DAMAS '99)*, University College, Dublin, Ireland, pp. 256–264.

Worden, K. and Dulieu-Barton, J.M. (2004). "An Overview of Intelligent Fault Detection in Systems and Structures", *Structural Health Monitoring*, V. 3(1), pp. 85–98.

Yan, B, Goto, S. and Miyamoto, A. (2004). "Time-frequency analysis based on Methods for Modal parameter Identification of Bridge Structure Considering Uncertainty", *In Proceedings of the 2nd International Workshop on Structural Health Monitoring of Innovative Civil Structures*, Mufti, A., and Ansari, F. Eds., Winnipeg, Canada, pp. 453–464.

Yan, Y.J. and Yam, L.H. (2004). "Detection of delamination in composite plates using energy spectrum of structural dynamic responses decomposed by wavelet analysis", *Computers and Structures*, V. 82, pp. 347–358.

Yang D.-M., Stronach A.F. and MacConnell P. (2003). "The Application of Advanced Signal Processing Techniques to Induction Motor Bearing Condition Diagnosis. Meccanica", V. 38(2), pp. 297–308.

Yong, X. (2002). *Condition Assessment of Structures Using Dynamic Data*, Ph.D. Dissertation, School of Civil and Environmental Engineering, Nanyang Technological University, Singapore.

Yu, L., Cheng, L., Yam, L.H., Yan, Y. J. and Jiang, J.S., (2007). "Online damage detection for laminated composite shells partially filled with fluid", *Composite Structures*, V. 80(3), pp. 334–342.

Yu, W. (2005). "State-Space Recurrent Fuzzy Neural Networks for Nonlinear System Identification", *Neural Processing Letters*, 22(3), 391-404.

Zak, A., Krawczuk, M. and Ostachowicz, W. (1999). "Vibration of a Laminated Composite Plate with Closing Delamination", *Structural Damage Assessment Using Advanced Signal processing Procedures, Proceedings of DAMAS '99*, University College, Dublin, Ireland, pp. 17–26.

Zhang, L., Quiong, W. and Link, M. (1998). "A Structural Damage Identification Approach Based on Element Modal Strain Energy", *Proceedings of ISMA23, Noise and Vibration Engineering,* Leuven, Belgium.

Zhang, J., Sato, T., Iai, S. and Hutchinson, T. (2008). "A pattern recognition technique for structural identification using observed vibration signals: Nonlinear case studies", *Engineering Structures*, V. 30(5), pp. 1417–1423.

Zhao, Y. and Ansari, F. (2002). "Embedded fiber optic sensor for characterization of interface strains in FRP composite", *Sensors and Actuators A: Physical*, V. 100, Issues 2-3, pp. 247–251.

Zhou, G. and Sim, L.M. (2002). "Damage detection and assessment in fiber-reinforced composite structures with embedded fiber optic sensors – review", *Smart Materials and Structures*, V. 11, pp. 925–939.

Zhu, X.Q. and Law, S.S. (2007). "Damage Detection in Simply Supported Concrete Bridge Structure Under Moving Vehicular Loads", *Journal of Vibration and Acoustics*, V. 129(1), pp. 58–65.

APPENDICES

A. Factored shear and moment capacity of bridge 7937 from FE model

Positive factored moment and flexural capacity of exterior frame of bridge 7937

Location (m)	Element	Beam thickness (m)	Factored moment-*Strength I* (kNm)	Factored moment-*Strength II* (kNm)	Flexural capacity (kNm)	Shortage of capacity (kNm)
0	1	0.765	0.0	0.0	967.8	-967.8
1	2	0.779	505.3	488.3	990.5	-485.3
2	3	0.807	808.3	769.3	1036.5	-228.2
3	4	0.850	936.4	891.5	1106.8	-170.4
4	5	0.908	924.2	889.8	1203.3	-279.1
5	6	0.984	798.9	761.0	1329.0	-530.1
6	7	1.080	575.8	531.0	1488.2	-912.5
7	8	1.201	269.7	185.1	1688.2	-1418.5
8	9	1.354	-111.3	-197.6	1941.1	-2052.4
9	10	1.554	-565.3	-610.5	2271.6	-2836.9
10	11	1.717	-1095.5	-1092.6	2542.1	-3634.7
11	12	5.449	-1683.8	-1635.2	8712.0	-10347.2
12	13	4.787	-2294.7	-2184.0	7618.5	-9802.5
13	14	4.027	-5232.4	-4998.4	6361.8	-11360.3
14	15	2.952	-4162.1	-3972.3	4583.2	-8555.5
15	16	1.807	-3398.6	-3241.1	2689.8	-5930.9
16	17	1.690	-2549.7	-2448.1	2496.1	-4944.2
17	18	1.597	-1737.0	-1687.3	2342.1	-4029.4
18	19	1.520	-974.6	-973.1	4254.8	-5227.9
19	20	1.456	-263.5	-310.6	4042.7	-4306.2
20	21	1.402	388.5	355.3	3864.1	-3475.5
21	22	1.356	983.4	968.1	3713.9	-2730.5
22	23	1.319	1548.5	1582.0	3588.8	-2006.7
23	24	1.287	2051.4	2157.8	4965.3	-2807.4
24	25	1.263	2480.4	2680.1	4842.3	-2162.1

201

25	26	1.244	2833.5	3156.5	4748.4	-1591.9
26	27	1.230	3107.4	3520.2	4682.3	-1162.0
27	28	1.222	3289.7	3762.0	4642.9	-880.9
28	29	1.220	3377.2	3880.1	4629.9	-749.8
29	30	1.222	3375.3	3878.1	4642.9	-764.8
30	31	1.230	3283.9	3756.2	4682.3	-926.1
31	32	1.244	3098.0	3510.8	4748.4	-1237.6
32	33	1.263	2820.7	3143.6	4842.3	-1698.7
33	34	1.287	2464.4	2664.2	4965.3	-2301.1
34	35	1.319	2032.8	2139.2	3588.8	-1449.6
35	36	1.356	1527.8	1561.3	3713.9	-2152.6
36	37	1.402	961.2	946.0	3864.1	-2902.8
37	38	1.456	365.8	332.6	4042.7	-3676.8
38	39	1.520	-285.7	-332.8	4254.8	-4540.5
39	40	1.597	-995.2	-993.7	2342.1	-3335.8
40	41	1.690	-1754.6	-1704.9	2496.1	-4200.9
41	42	1.807	-2562.5	-2460.9	2689.8	-5150.7
42	43	2.952	-3404.5	-3247.0	4583.2	-7830.2
43	44	4.027	-4158.1	-3968.3	6361.8	-10330.2
44	45	4.787	-2951.4	-2813.9	7618.5	-10432.4
45	46	5.449	-2323.5	-2212.8	8712.0	-10924.8
46	47	1.717	-1698.2	-1649.6	2542.1	-4191.6
47	48	1.554	-1097.2	-1094.2	2271.6	-3365.8
48	49	1.354	-557.6	-602.8	1941.1	-2498.7
49	50	1.201	-97.8	-184.1	1688.2	-1785.9
50	51	1.080	286.4	201.8	1488.2	-1201.8
51	52	0.984	593.5	548.8	1329.0	-735.5
52	53	0.908	816.0	778.1	1203.3	-387.3
53	54	0.850	939.4	905.0	1106.8	-167.4
54	55	0.807	948.6	903.7	1036.5	-87.9
55	56	0.779	816.8	777.9	990.5	-173.7
56	57	0.765	509.7	492.7	967.8	-458.2

Negative factored moment and flexural capacity of exterior frame of bridge 7937

Location (m)	Element	Beam thickness (m)	Factored moment-*Strength I* (kNm)	Factored moment-*Strength II* (kNm)	Flexural capacity (kNm)	Shortage of capacity (kNm)
0	1	0.765	0.0	0.0	-1493.0	-1493.0
1	2	0.779	59.4	4.8	-1530.2	-1535.0
2	3	0.807	63.9	-42.6	-1605.4	-1562.8
3	4	0.850	13.2	-142.5	-1720.6	-1578.1
4	5	0.908	-93.5	-295.4	-1878.7	-1583.2
5	6	0.984	-257.7	-502.6	-2084.4	-1581.9
6	7	1.080	-479.9	-764.9	-2345.2	-1580.3
7	8	1.201	-762.7	-1084.5	-2672.6	-1588.1
8	9	1.354	-1108.0	-1534.7	-3086.7	-1552.0
9	10	1.554	-1520.7	-2170.7	-3627.9	-1457.2
10	11	1.717	-2017.8	-2918.1	-4070.8	-1152.7
11	12	5.449	-2864.1	-3925.8	-14174.0	-10248.2
12	13	4.787	-3822.7	-5058.2	-12383.6	-7325.3
13	14	4.027	-8753.2	-11253.6	-20839.4	-9585.8
14	15	2.952	-7141.3	-9070.7	-14814.2	-5743.5
15	16	1.807	-5948.5	-7458.5	-8400.3	-941.7
16	17	1.690	-4793.0	-5993.8	-7744.1	-1750.2
17	18	1.597	-3707.3	-4621.7	-980.4	**3641.4**
18	19	1.520	-2706.6	-3353.8	-928.5	**2425.3**
19	20	1.456	-1795.5	-2245.7	-885.0	**1360.7**
20	21	1.402	-986.7	-1314.2	-848.4	**465.8**
21	22	1.356	-279.2	-499.1	-817.7	-318.6
22	23	1.319	314.2	128.0	-792.1	-920.1
23	24	1.287	704.1	620.7	-771.1	-1391.8
24	25	1.263	1013.0	952.4	-754.3	-1706.7
25	26	1.244	1262.9	1198.0	-741.5	-1939.4
26	27	1.230	1454.4	1382.7	-732.4	-2115.1
27	28	1.222	1587.7	1511.8	-727.1	-2238.9
28	29	1.220	1661.5	1584.0	-725.3	-2309.2
29	30	1.222	1659.5	1582.0	-727.1	-2309.1
30	31	1.230	1581.9	1506.0	-732.4	-2238.4
31	32	1.244	1444.9	1373.3	-741.5	-2114.7
32	33	1.263	1250.0	1185.1	-754.3	-1939.4

33	34	1.287	997.0	936.5	-771.1	-1707.5
34	35	1.319	685.5	602.1	-792.1	-1394.2
35	36	1.356	293.4	107.3	-817.7	-925.0
36	37	1.402	-301.3	-521.3	-848.4	-327.2
37	38	1.456	-1009.4	-1336.9	-885.0	**451.8**
38	39	1.520	-1817.7	-2267.9	-928.5	**1339.5**
39	40	1.597	-2727.2	-3374.4	-980.4	**2394.0**
40	41	1.690	-3724.8	-4639.3	-7744.1	-3104.7
41	42	1.807	-4805.7	-6006.6	-8400.3	-2393.7
42	43	2.952	-5954.3	-7464.4	-14814.2	-7349.8
43	44	4.027	-7137.3	-9066.7	-20839.4	-11772.7
44	45	4.787	-4974.6	-6330.3	-12383.6	-6053.2
45	46	5.449	-3851.6	-5087.1	-14174.0	-9086.9
46	47	1.717	-2878.5	-3940.2	-4070.8	-130.6
47	48	1.554	-2019.5	-2919.7	-3627.9	-708.1
48	49	1.354	-1513.1	-2163.0	-3086.7	-923.7
49	50	1.201	-1094.5	-1521.2	-2672.6	-1151.4
50	51	1.080	-746.0	-1067.7	-2345.2	-1277.5
51	52	0.984	-462.2	-747.1	-2084.4	-1337.3
52	53	0.908	-240.6	-485.5	-1878.7	-1393.2
53	54	0.850	-78.4	-280.3	-1720.6	-1440.3
54	55	0.807	25.4	-130.3	-1605.4	-1475.2
55	56	0.779	72.5	-34.1	-1530.2	-1496.1
56	57	0.765	63.8	9.2	-1493.0	-1502.2

204

Positive factored shear and shear capacity of exterior frame of bridge 7937

Location (m)	Element	Beam thickness (m)	Factored shear-Strength I (kN)	Factored shear-Strength II (kN)	Shear capacity (kN)	Shortage of capacity (kN)
0	1	0.765	-86.4	-30.4	1058.1	-971.6
1	2	0.779	-31.5	46.0	1065.7	-1019.7
2	3	0.807	64.6	137.2	1081.2	-944.1
3	4	0.850	186.8	245.5	1104.9	-859.4
4	5	0.908	302.8	350.8	1137.5	-786.7
5	6	0.984	412.0	450.1	1179.9	-729.8
6	7	1.080	514.1	549.5	1233.6	-684.0
7	8	1.201	621.4	676.9	1301.0	-624.0
8	9	1.354	737.7	818.3	1386.2	-567.9
9	10	1.554	852.5	956.1	1497.7	-541.6
10	11	1.717	979.4	1072.5	1588.9	-516.4
11	12	5.449	1094.5	1193.2	3669.4	-2476.2
12	13	4.787	1204.3	1329.6	3300.7	-1971.1
13	14	4.027	-1106.6	-1061.5	2876.9	-1770.3
14	15	2.952	-798.9	-762.8	2277.2	-1478.3
15	16	1.807	-769.9	-736.1	1638.7	-868.8
16	17	1.690	-718.9	-687.1	1573.4	-854.5
17	18	1.597	-652.6	-624.0	1521.5	-868.9
18	19	1.520	-585.4	-559.2	1478.7	-893.4
19	20	1.456	-511.5	-487.7	1443.0	-931.5
20	21	1.402	-441.0	-420.3	1412.9	-971.9
21	22	1.356	-364.6	-346.9	1387.5	-1023.0
22	23	1.319	-287.9	-271.1	1366.4	-1078.6
23	24	1.287	-207.1	-191.5	1349.1	-1142.0
24	25	1.263	-124.9	-109.8	1335.3	-1210.4
25	26	1.244	-41.3	-26.1	1324.8	-1283.5
26	27	1.230	43.9	58.6	1317.3	-1258.7
27	28	1.222	132.6	149.9	1312.9	-1163.0
28	29	1.220	220.4	242.6	1311.4	-1068.8
29	30	1.222	309.2	338.6	1312.9	-974.3
30	31	1.230	401.1	439.9	1317.3	-877.4
31	32	1.244	491.5	540.6	1324.8	-784.1
32	33	1.263	582.2	642.7	1335.3	-692.6

33	34	1.287	673.0	750.7	1349.1	-598.4
34	35	1.319	763.7	861.0	1366.4	-505.4
35	36	1.356	851.8	971.2	1387.5	-416.3
36	37	1.402	941.6	1086.8	1412.9	-326.1
37	38	1.456	1024.3	1194.6	1443.0	-248.4
38	39	1.520	1110.8	1310.4	1478.7	-168.3
39	40	1.597	1188.3	1418.5	1521.5	-103.0
40	41	1.690	1263.5	1525.6	1573.4	-47.8
41	42	1.807	1326.9	1616.8	1638.7	-21.9
42	43	2.952	1361.5	1664.8	2277.2	-612.4
43	44	4.027	1723.7	2239.1	2876.9	-637.8
44	45	4.787	-665.1	-636.9	3300.7	-2635.6
45	46	5.449	-589.0	-563.5	3669.4	-3080.5
46	47	1.717	-508.8	-489.7	1588.9	-1080.1
47	48	1.554	-428.2	-407.6	1497.7	-1069.5
48	49	1.354	-338.0	-328.9	1386.2	-1048.2
49	50	1.201	-249.8	-249.4	1301.0	-1051.2
50	51	1.080	-161.4	-169.2	1233.6	-1064.4
51	52	0.984	-70.8	-82.2	1179.9	-1097.7
52	53	0.908	24.3	12.2	1137.5	-1113.2
53	54	0.850	125.1	112.3	1104.9	-979.9
54	55	0.807	234.3	219.4	1081.2	-846.9
55	56	0.779	354.3	337.0	1065.7	-711.5
56	57	0.765	482.6	467.0	1058.1	-575.5

Negative factored shear and shear capacity of exterior frame of bridge 7937

Location (m)	Element	Beam thickness (m)	Factored shear-Strength I (kN)	Factored shear-Strength II (kN)	Shear capacity (kN)	Shortage of capacity (kN)
0	1	0.765	-553.5	-542.5	-1058.1	-504.6
1	2	0.779	-431.0	-416.0	-1065.7	-634.7
2	3	0.807	-315.8	-299.8	-1081.2	-765.5
3	4	0.850	-208.4	-194.9	-1104.9	-896.6
4	5	0.908	-111.1	-98.9	-1137.5	-1026.4
5	6	0.984	-21.3	-9.5	-1179.9	-1158.6
6	7	1.080	63.0	74.6	-1233.6	-1159.0
7	8	1.201	143.2	150.7	-1301.0	-1150.2
8	9	1.354	221.0	219.8	-1386.2	-1165.3
9	10	1.554	298.6	288.1	-1497.7	-1199.1
10	11	1.717	370.7	358.2	-1588.9	-1218.2
11	12	5.449	445.8	428.5	-3669.4	-3223.6
12	13	4.787	516.3	493.3	-3300.7	-2784.5
13	14	4.027	-1640.0	-2156.0	-2876.9	-720.9
14	15	2.952	-1321.2	-1635.7	-2277.2	-641.5
15	16	1.807	-1285.5	-1587.8	-1638.7	-51.0
16	17	1.690	-1226.1	-1501.1	-1573.4	-72.3
17	18	1.597	-1157.0	-1400.7	-1521.5	-120.8
18	19	1.520	-1086.3	-1299.9	-1478.7	-178.8
19	20	1.456	-1008.2	-1190.8	-1443.0	-252.2
20	21	1.402	-933.4	-1090.4	-1412.9	-322.4
21	22	1.356	-852.4	-984.8	-1387.5	-402.7
22	23	1.319	-773.0	-882.5	-1366.4	-483.9
23	24	1.287	-691.2	-780.2	-1349.1	-568.9
24	25	1.263	-609.2	-680.3	-1335.3	-655.0
25	26	1.244	-527.2	-582.5	-1324.8	-742.2
26	27	1.230	-445.3	-490.2	-1317.3	-827.1
27	28	1.222	-361.7	-397.0	-1312.9	-915.9
28	29	1.220	-280.8	-307.7	-1311.4	-1003.7
29	30	1.222	-200.8	-221.1	-1312.9	-1091.8
30	31	1.230	-119.9	-135.5	-1317.3	-1181.8
31	32	1.244	-42.1	-55.3	-1324.8	-1269.5
32	33	1.263	34.5	20.8	-1335.3	-1300.9

207

33	34	1.287	109.6	96.0	-1349.1	-1239.6
34	35	1.319	183.2	169.2	-1366.4	-1183.2
35	36	1.356	253.7	238.8	-1387.5	-1133.8
36	37	1.402	324.1	308.2	-1412.9	-1088.8
37	38	1.456	387.1	368.9	-1443.0	-1055.8
38	39	1.520	453.1	431.9	-1478.7	-1025.6
39	40	1.597	512.3	489.1	-1521.5	-1009.2
40	41	1.690	570.0	544.8	-1573.4	-1003.4
41	42	1.807	619.1	591.6	-1638.7	-1019.6
42	43	2.952	641.7	611.6	-2277.2	-1635.5
43	44	4.027	917.1	878.9	-2876.9	-1959.8
44	45	4.787	-1193.9	-1357.5	-3300.7	-1943.2
45	46	5.449	-1097.8	-1210.8	-3669.4	-2458.6
46	47	1.717	-997.3	-1086.0	-1588.9	-502.9
47	48	1.554	-886.2	-984.1	-1497.7	-513.6
48	49	1.354	-777.3	-863.4	-1386.2	-522.8
49	50	1.201	-669.9	-737.4	-1301.0	-563.5
50	51	1.080	-562.7	-609.2	-1233.6	-624.4
51	52	0.984	-464.0	-492.4	-1179.9	-687.5
52	53	0.908	-370.5	-402.8	-1137.5	-734.7
53	54	0.850	-271.2	-311.8	-1104.9	-793.2
54	55	0.807	-165.8	-216.6	-1081.2	-864.7
55	56	0.779	-54.9	-118.8	-1065.7	-946.9
56	57	0.765	33.1	-36.0	-1058.1	-1022.1

B. Detailed design of photovoltaic system for Tucumcari Bridge

Electrical Load Estimate

In order to design a proper PV system for solar energy, the required energy load for the SDA system on Bridge 7937 was estimated. The PV system needed to support the wireless communication modem, the SDA system, current inverter device and a time controller. Based on the operation requirements of 8 hours of continues energy supply, the following daily energy consumption (E_c) was estimated and shown in Table B.1.

Table B.1 Energy consumption estimation for powering the SHM system at Bridge 7937 in Tucumcari, New Mexico.

Device	Power (W)	Daily Operation time (hr)	Daily Consumption (Whr)
Wireless Modem	4.2	8	33.6
DAQ module	48	8	384
Inverter	7.8	8	62.4
Time controller	1.4	24	33.6
		E_c *(Whr/day)*	**513.6**

Energy Autonomy

The energy source (in this case solar energy) was not available continuously; therefore, an energy autonomy or energy backup method had to be designed. The most

209

common method is an electrical battery system, which will be installed at this project. The battery system had to be able to satisfy all the energy demands in the data acquisition system for some autonomy time required by the specifications of the design. For this particular case, three days of autonomy time were assumed. The battery capacity for holding energy is rated in amp-hours and the energy capacity for the battery system (E_b) can be calculated according to the energy demand as

$$E_b = \frac{E_c \; \varepsilon_1 \quad D_A}{b \; r \; \varepsilon_b \left(1 - \alpha_w\right)} \tag{B.1}$$

Where ε_I is the inverters efficiency, b is the battery system voltage, r is the discharge cycle rate, ε_b is the battery's efficiency, α_w is the wiring losses and D_A is the autonomy time in days. Using the energy consumption data calculated in the electrical load estimation and the battery system parameter specified in Table B.2.

Table B.2 Battery system parameters.

b	12 V
r	60%
ε_b	90%
ε_i	95%
α_w	2%

The energy capacity for different battery systems for different autonomy days can be calculated as

210

$$E_b = \frac{513.6 * 0.95 * 1}{12 * 0.6 * 90 * (1 - 0.2)} = 76.8 \; Ahr \qquad (B.2)$$

PV Array Design

Once the estimation of the energy demand for the system was determined, the photovoltaic arrays characteristics, dimensions and arrangement could be computed to satisfy the energy consumption and backup system. Since PV systems depend on solar energy, the sun hours observed during the day was an essential parameter to calculate the PV array. For this specific system, the location of the system is below the Tucumcari bridge at Latitude: 35° 10' 18" N - Longitude: 103° 43' 27" W in a fixed array configuration experiencing morning shadowing as shown in Figure B.1.
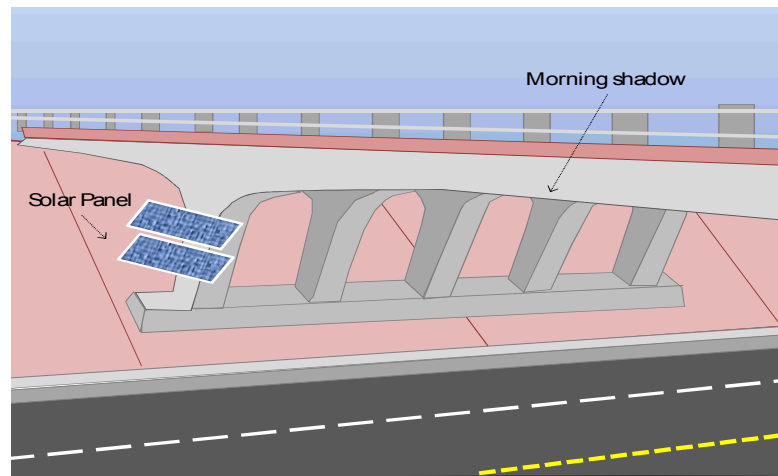

Figure B.1 PV system location (Tucumcari latitude: 35° 10' 18" N - longitude: 103° 43' 27" W) and the proposed location of solar panels to enable SHM power.

Based on an average sun tracking system as shown in Figure B.1, the PV system configuration suggested in Figure B.2 should be able to provide an estimated average peak sun hours (h_s) of 5 hours during the entire year.

211
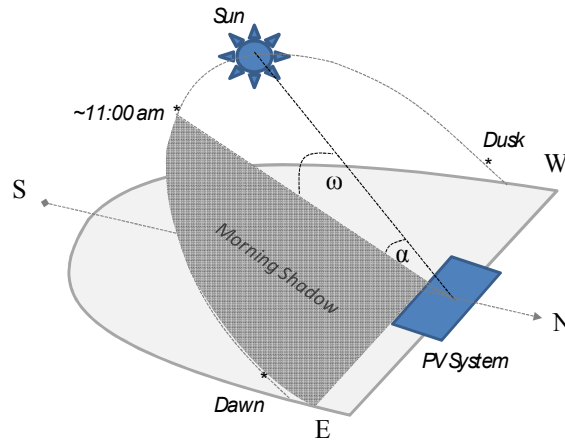
Figure B.2 PV system sun tracking schematic.

The angle α in Figure B.2 represents the altitude of the sun at a specific season of the year expressed in degrees, ψ is the azimuth angle and ω is the time angle expressed in degrees with respect to a specific time/hour of the day. Once the average peak sun hours are estimated for the SHM system, the PV array power required can be computed as

$$P_{array} = \frac{E_b \; b}{h_s \; \alpha_T \; \beta \; \varepsilon_1} \tag{B.3}$$

Where α_T is the temperature loss factor, β is the Derate factor and ε_I is the inverted efficiency factor. The PV array power required to satisfy the different autonomy days can be calculated as

$$P_{array} = \frac{76.8*12}{5*0.88*0.84*0.95} = 262.6 \, W \tag{B.4}$$

Charge Controller

In order to have good management of energy resources in the PV system, a charge controller was incorporated in the system. A charge controller is able to make the system

212

operate at the optimum solar panels energy absorption by performing the maximum power point tracker (MPPT). This controller will also limit the rate at which electrical current is either added to or drawn from the electric batteries. It prevents overcharging and may prevent against over voltage, which can reduce battery performance and/or lifetime.

The adequate charge controller had to be designed according to the PV panel array power and the autonomy battery system previously calculated. These parameters determine the charge controller capacity and parameters that satisfy the system. Based on the PV array power, the solar panel specifications for Kyocera KC130TM 130 Watts Solar Panel and the energy capacity and battery sizing calculated in previous sections, the charge controller should satisfy the energy requirements. The design indicated a 20 controller array Amp and 5.1 controller load Amp.

Time Controller

In PV systems, energy consumption and management is an important issue due to the luck of full accessibility to sun energy radiation. Therefore, energy consumption has to be controlled to avoid energy waste by powering equipment when it is not needed. Programmable time controls are among the most effective energy management devices available. Battery re-chargers and other types of equipment can be effectively managed with time controls.

The SDA system is the main source of the load to be supported by the PV system. Therefore, optimized energy management should be carried out to power the system only when data acquisition is required and avoided when powering equipment is not needed. Programmable time controllers are utilized in the project as a means of energy

213

management device. The time controller used here has the ability to set multiple on/off operations, and includes the ability to have different schedules for each day of the week. Due to the different uploading and downloading of traffic at different times to the wireless communication device, a feasible operation time for the data acquisition system has been determined as shown in Table B.3.

Table B.3 Time controller schedule for the PV system for bridge 7937.

	Monday	Tuesday	Wednesday	Thursday	Friday	Saturday	Sunday
2:00 am	Off	Off	Off	Off	Off	Off	Off
4:00 am	Off	Off	Off	Off	Off	Off	Off
6:00 am	On	On	On	On	On	On	On
8:00 am	On	On	On	On	On	On	On
10:00 am	On	On	On	On	On	On	On
12:00 pm	Off	Off	Off	Off	Off	Off	Off
2:00 am	Off	Off	Off	Off	Off	Off	Off
4:00 pm	Off	Off	Off	Off	Off	Off	Off
6:00 pm	On	On	On	On	On	On	On
8:00 pm	On	On	On	On	On	On	On
10:00 pm	On	On	On	On	On	On	On
12:00 am	Off	Off	Off	Off	Off	Off	Off

214

Based on the respective designs of the various components of the PV system calculated in previous sections, a layout schematic of the proposed PV system could be created. Figure B.3 shows such schematic of the proposed PV system.
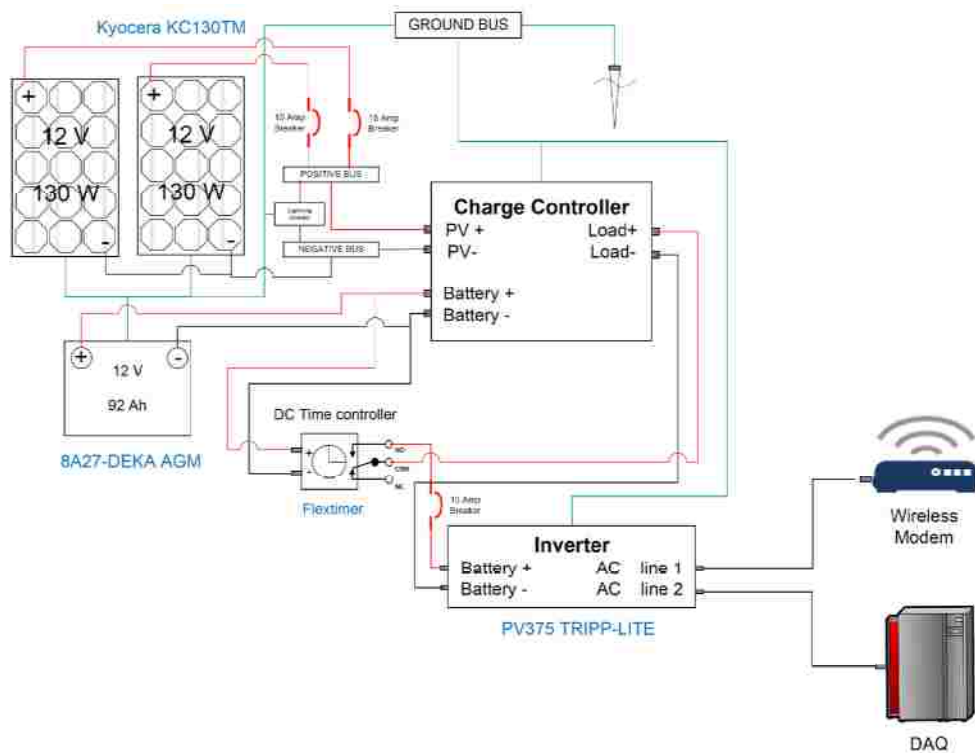
Figure B.3 Schematic of layout of the proposed PV system for 1 day of autonomy.

The different energy demands and PV capacities for the system shown in this schematic can be satisfied with different components. Brands, capacities and qualities vary between different manufacturers and different PV system configurations with distinct components can be found to satisfy the same system capacities in discourse. For this particular case,

215

the system was designed over the inverter type 375 Watt TRIPP-LITE, the battery system utilized battery type 8A27-DEKA AGM, and the PV array utilized the solar panel Kyocera KC130TM. The structural system to support the solar panels and attaching them to the bridge structure is shown in Figure B.4.

Figure B.4 Structural systems to support solar panels and attach them to the bridge.

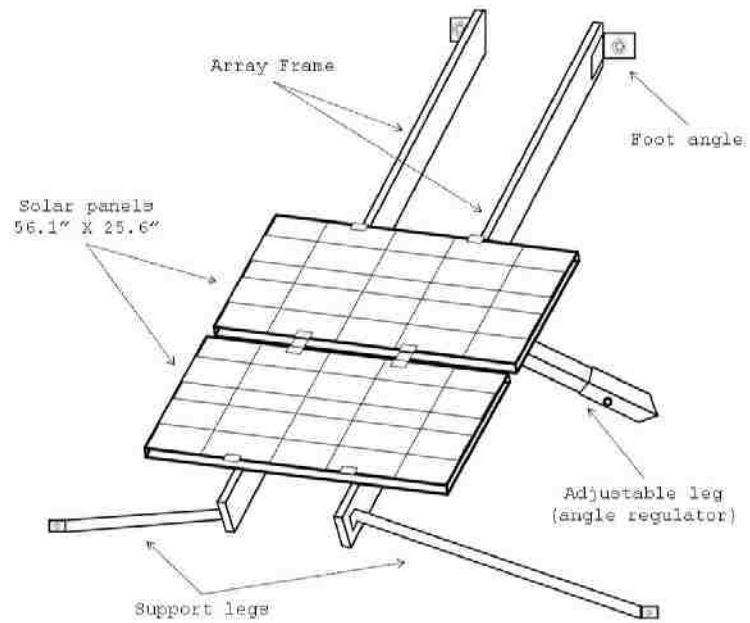# C. Computer code to find the primary and secondary threshold values for establishing fuzzy sets

```matlab
% This code has been written by Mohammad Azarbayejani to calculate the
% threshold values for establishing fuzzy sets for bridge 7937 at
% Tucumcari.

clear all;
close all;
data_nonmdified_1 = [0.026606104 0.602787715 0.041645875 0.07475578
0.059328081 0.024500977 0.031538565 0.043086544 0.048459916
0.207801316]; % Damage feature values
data_nonmdified_2 = [0.216292715 0.194609367 0.19551805 0.198079852
0.199827758 0.221344943 0.276584027]; % Damage feature values

data_1 = sort(data_nonmdified_1);
data_2 = sort(data_nonmdified_2);
Data_1 = sort(data_nonmdified_1, 'descend');
Data_2 = sort(data_nonmdified_2, 'descend');
n1 = size(data_1, 2);
n2 = size(data_2, 2);
x11 = min(data_1);
x12 = min(data_2);
x21 = max(data_1);
x22 = max(data_2);
x1 = min(x11, x12);
x2 = max(x21, x22);
x = x1;
n_1_x = 0;
n_2_x = 0;
N_1_x = 0;
N_2_x = 0;
j = 0;
for x = x1 : 0.01 : x2
    for i = 1 : (n1+n2)
        if(i<=n1)
            if(data_1(1, i)<= x)
                n_1_x = n_1_x + 1;
            else
                N_1_x = N_1_x + 1;
            end
        end
        if(i<=n2)
            if(data_2(1, i)<= x)
                n_2_x = n_2_x + 1;
            else
                N_2_x = N_2_x + 1;
            end
        end
        n_x = n_1_x + n_2_x;
        N_x = N_1_x + N_2_x;
    end
    p_1_x = (n_1_x + 1)/(n_x + 1);
```

217

```matlab
        q_1_x = (N_1_x + 1)/(N_x + 1);
         p_2_x = (n_2_x + 1)/(n_x + 1);
         q_2_x = (N_2_x + 1)/(N_x + 1);
         p_x = n_x / (n1+n2);
         q_x = 1 - p_x;
         S_p_x = -(p_1_x * log(p_1_x) + p_2_x * log(p_2_x));
         S_q_x = -(q_1_x * log(q_1_x) + q_2_x * log(q_2_x));
         j = j+1;
         S(j) = p_x * S_p_x + q_x * S_q_x;
         n_1_x = 0;
         n_2_x = 0;
         N_1_x = 0;
         N_2_x = 0;
end


[s, I] = min(S);
x_PRI_n = x1 + I * 0.01;


data = [data_nonmdified_1, data_nonmdified_2];
data_m = sort(data, 'descend');
n= n1+n2;
for i=1:n;
    if data_m(i)< x_PRI_n
        data_max(i) = data_m(i);
    else
        data_min(i) = data_m(i);
    end
end
data_max_m = sort(data_max,'descend');
data_min_m = sort(data_min);
x_PRI = (data_max_m(1,1)+ data_min_m(1,1))/2


n11 = 0;
n22 = 0;
k = 0;
for i = 1 : n1
    if(data_1(i) <= x_PRI)
        n11 = n11 + 1;
    end
end

for i = 1 : n2
    if(data_2(i) <= x_PRI)
        n22 = n22 + 1;
    end
end

for x = x1 : 0.01 : x_PRI
    for i = 1 : n11
        if(i<=n1)
                if(data_1(1, i)<= x)
                    n_1_x = n_1_x + 1;
                else
                    N_1_x = N_1_x + 1;
                end
```

218

```matlab
            end
        end
        for i = 1 : n22
            if(i<=n2)
                if(data_2(1, i)<= x)
                    n_2_x = n_2_x + 1;
                else
                    N_2_x = N_2_x + 1;
                end
            end
        end
    n_x = n_1_x + n_2_x;
    N_x = N_1_x + N_2_x;

     p_1_x = (n_1_x + 1)/(n_x + 1);
     q_1_x = (N_1_x + 1)/(N_x + 1);
      p_2_x = (n_2_x + 1)/(n_x + 1);
      q_2_x = (N_2_x + 1)/(N_x + 1);
      p_x = n_x / (n11+n22);
      q_x = 1 - p_x;
      S_p_x = -(p_1_x * log(p_1_x) + p_2_x * log(p_2_x));
      S_q_x = -(q_1_x * log(q_1_x) + q_2_x * log(q_2_x));
      k = k + 1;
      S_NG(k) = p_x * S_p_x + q_x * S_q_x;
      n_1_x = 0;
      n_2_x = 0;
      N_1_x = 0;
      N_2_x = 0;
end
%S_NG
[s_NG, I_NG] = min(S_NG);
x_NG_n = x1 + I_NG * 0.01;
for i=1:n;
    if data_m(i)< x_NG_n
        data_max_NG(i) = data_m(i);
    else
        data_min_NG(i) = data_m(i);
    end
end
data_max_NG_m = sort(data_max_NG,'descend');
data_min_NG_m = sort(data_min_NG);
x_NG = (data_max_NG_m(1,1)+ data_min_NG_m(1,1))/2


n111 = 0;
n222 = 0;
l = 0;
for i = 1 : n1
    if(Data_1(i) >= x_PRI)
        n111 = n111 + 1;
    end
end

for i = 1 : n2
    if(Data_2(i) >= x_PRI)
        n222 = n222 + 1;
```

219

www.manaraa.com

```matlab
            end
    end

    for x = x_PRI : 0.01 : x2
        for i = 1 : n111
            if(i<=n1)
                if(Data_1(1, i)>= x)
                    n_1_x = n_1_x + 1;
                else
                    N_1_x = N_1_x + 1;
                end
            end
        end
        for i = 1 : n222
            if(i<=n2)
                if(Data_2(1, i)>= x)
                    n_2_x = n_2_x + 1;
                else
                    N_2_x = N_2_x + 1;
                end
            end
        end
        n_x = n_1_x + n_2_x;
        N_x = N_1_x + N_2_x;

        p_1_x = (n_1_x + 1)/(n_x + 1);
        q_1_x = (N_1_x + 1)/(N_x + 1);
        p_2_x = (n_2_x + 1)/(n_x + 1);
        q_2_x = (N_2_x + 1)/(N_x + 1);
        p_x = n_x / (n111+n222);
        q_x = 1 - p_x;
        S_p_x = -(p_1_x * log(p_1_x) + p_2_x * log(p_2_x));
        S_q_x = -(q_1_x * log(q_1_x) + q_2_x * log(q_2_x));
        l = l + 1;
        S_PO(l) = p_x * S_p_x + q_x * S_q_x;
        n_1_x = 0;
        n_2_x = 0;
        N_1_x = 0;
        N_2_x = 0;
    end
    %S_PO
    [s_PO, I_PO] = min(S_PO);
    x_po_n = x_PRI + (I_PO-1) * 0.01;
    for i=1:n;
        if data_m(i)< x_po_n
            data_max_po(i) = data_m(i);
        else
            data_min_po(i) = data_m(i);
        end
    end
    data_max_po_m = sort(data_max_po,'descend');
    data_min_po_m = sort(data_min_po);
    x_po = (data_max_po_m(1,1)+ data_min_po_m(1,1))/2
```

220